ABSTRACT

TARGET LOCALIZATION IN MIMO RADAR SYSTEMS

by
Hana Godrich

MIMO (Multiple-Input Multiple-Output) radar systems employ multiple antennas to transmit multiple waveforms and engage in joint processing of the received echoes from the target. MIMO radar has been receiving increasing attention in recent years from researchers, practitioners, and funding agencies. Elements of MIMO radar have the ability to transmit diverse waveforms ranging from independent to fully correlated. MIMO radar offers a new paradigm for signal processing research. In this dissertation, target localization accuracy performance, attainable by the use of MIMO radar systems, configured with multiple transmit and receive sensors, widely distributed over an area, are studied. The Cramer-Rao lower bound (CRLB) for target localization accuracy is developed for both coherent and noncoherent processing. The CRLB is shown to be inversely proportional to the signal effective bandwidth in the noncoherent case, but is approximately inversely proportional to the carrier frequency in the coherent case. It is shown that optimization over the sensors' positions lowers the CRLB by a factor equal to the product of the number of transmitting and receiving sensors. The best linear unbiased estimator (BLUE) is derived for the MIMO target localization problem. The BLUE's utility is in providing a closed-form localization estimate that facilitates the analysis of the relations between sensors locations, target location, and localization accuracy. Geometric dilution of precision (GDOP) contours are used to map the relative performance accuracy for a given layout of radars over a given geographic area. Coherent processing advantage for target localization relies on time and phase synchronization between transmitting and receiving radars. An analysis of the sensitivity of the localization performance with respect to the variance of phase synchronization error is provided by deriving the hybrid CRLB. The single target case is extended to the evaluation of multiple target localization performance. Thus far, the

analysis assumes a stationary target. Study of moving target tracking capabilities is offered through the use of the Bayesian CRLB for the estimation of both target location and velocity. Centralized and decentralized tracking algorithms, inherit to distributed MIMO radar architecture, are proposed and evaluated. It is shown that communication requirements and processing load may be reduced at a relatively low performance cost.

TARGET LOCALIZATION IN MIMO RADAR SYSTEMS

by
Hana Godrich

A Dissertation
Submitted to the Faculty of
New Jersey Institute of Technology
in Partial Fulfillment of the Requirements for the Degree of
Doctor of Philosophy in Electrical Engineering

Department of Electrical and Computer Engineering

January 2010

APPROVAL PAGE

TARGET LOCALIZATION IN MIMO RADAR SYSTEMS

Hana Godrich

Dr. Alexander M. Haimovich, Dissertation Advisor   Date
Professor, Department of Electrical and Computer Engineering, NJIT

Dr. Yeheskel Bar-Ness, Committee Member   Date
Distinguished Professor, Department of Electrical and Computer Engineering, NJIT

Dr. Ali Abdi , Committee Member   Date
Associate Professor, Department of Electrical and Computer Engineering, NJIT

Dr. Osvaldo Simeone, Committee Member   Date
Assistant Professor, Department of Electrical and Computer Engineering, NJIT

Dr. Rick S. Blum , Committee Member   Date
Professor, Department of Electrical and Computer Engineering, Lehigh University

BIOGRAPHICAL SKETCH

Author: Hana Godrich

Degree: Doctor of Philosophy

Date: January 2010

Undergraduate and Graduate Education:

- Doctor of Philosophy in Electrical Engineering,
  New Jersey Institute of Technology, Newark, NJ, 2010

- Master of Science in Electrical Engineering,
  Ben-Gurion University, Beer-Sheva, Israel, 1993

- Bachelor of Science in Electrical Engineering,
  Technion Israel Institute of Technology, Haifa, Israel, 1987

Major: Electrical Engineering

Presentations and Publications:

H. Godrich, A. M. Haimovich and R. S. Blum, "Concepts and applications of a MIMO radar system with widely separated antennas," book chapter in *MIMO Radars*, John Wiley, January 2009.

H. Godrich, A. M. Haimovich, and R. S. Blum, "Target localisation techniques and tools for multiple-input multiple-output radar," in *IET Radar, Sonar and Navigation*, Vol.3, August 2009, pp. 314-327.

H. Godrich, A. M. Haimovich, and R. S. Blum, "Target localization accuracy gain in MIMO radar based system," to appear in *IEEE Trans. on Information Theory*.

H. Godrich, A. M. Haimovich, and R. S. Blum, "Target tracking in MIMO radar systems: techniques and performance analysis," submitted to *IEEE Radar Conf.* May, 2010.

H. Godrich, A. M. Haimovich, and H. V. Poor, "An analysis of phase synchronization mismatch sensitivity for coherent MIMO radar systems," to appear in *Proc. of the Third International Workshop on Computational Advances in Multi-Sensor Adaptive Processing (CAMSAP)*, December 2009.

H. Godrich, A. M. Haimovich, and R. S. Blum, "A MIMO radar system approach to target tracking," in *Proc. of 43th Asilomar Conf. Signals, Syst. Comput.*, November 2009.

H. Godrich, A. M. Haimovich, and R. S. Blum, "A comparative study of target localization in MIMO radar systems," in *IEEE Intl. Waveform Diversity and Design Conf.*, February 2009,pp. 124-128.

H. Godrich, A. M. Haimovich, and R. S. Blum, "Target localization accuracy and multiple target localization: tradeoffs in MIMO radars," in *Proc. of 42th Asilomar Conf. Signals, Syst. Comput.*, October 2008, pp. 614-618.

H. Godrich, A. M. Haimovich, and R. S. Blum, "Target localization techniques and tools for MIMO radar," in *IEEE Radar Conf.* , May, 2008, pp. 1-6.

H. Godrich, A. M. Haimovich, and R. S. Blum, "Cramer Rao bound on target localization estimation in MIMO radar systems," in *Proc. of 42nd Annual Conference on information Sciences and Systems (CISS) 2008*, March 2008, pp. 134-139.

Q. He, R. S. Blum, H. Godrich, and A. M. Haimovich, "Cramer-Rao bound for target velocity estimation in MIMO radar with widely separated antennas," in *Proc. of 42nd Annual Conference on information Sciences and Systems (CISS) 2008*, March 2008, pp. 123-127.

Q. He, R. S. Blum, H. Godrich, and A. M. Haimovich, " Target velocity estimation and antenna placement for MIMO radar with widely separated antennas," to appear in *IEEE Journal of Selected Topics in Signal Processing.*

To Kfir, Ran, Dana, and Noa
with Love

ACKNOWLEDGMENT

"Destiny is not a matter of chance, it is a matter of choice;

it is not a thing to be waited for, it is a thing to be achieved."

[Winston Churchill]

To make things happen, one not only needs to take on his own destiny, but also to be blessed with the support of wonderful people along the way. I would like to express my deepest appreciation to my adviser, committee chair, and mentor, Dr. Alexander Haimovich who has opened the doors for me and made all of this possible. Without his confidence, support and inspiration this dissertation would not have been possible. It has been a joy and challenge to work with him in developing the ideas in this thesis. Special thanks to Dr. Rick Blum for partnering with Dr. Alexander Haimovich and me in this research collaboration and for serving on my committee. I would like to thank Dr. Yeheskel Bar-Ness, Dr. Ali Abdi, and Dr. Osvaldo Simeone for serving on my dissertation committee. Extended thanks to Dr. Nikolaus Lehmann for sharing his thoughts, his helpful advice and all the more, for his friendships.

"It is the supreme art of the teacher to awaken joy in creative expression and knowledge." [Albert Einstein]

To the professors at NJIT that have taught me along the way, my sincere gratitude: Dr. Yeheskel Bar-Ness for sharing his extensive knowledge in wireless communication, Dr. Alexander Haimovich for breaking information theory to an understandable level, Dr. Osvaldo Simeone, who makes convex optimization looks so clear and simple - I have put the thing I have learned from him to very good use in this thesis, Dr. Richard Haddad for his inspirational teaching and personality, and Dr. Ali Akansu and Dr. Hongya Ge for providing me with extensive signal processing tools.

TABLE OF CONTENTS

TABLE OF CONTENTS
(Continued)

LIST OF TABLES

LIST OF FIGURES

CHAPTER 1

INTRODUCTION

1.1 MIMO Radar Background

Research in MIMO radar has been growing as evidenced by an increasing body of literature [1–25]. Generally speaking, MIMO radar systems employ multiple antennas to transmit multiple waveforms and engage in joint processing of the received echoes from the target. Two main MIMO radar architectures have evolved: with collocated antennas and with distributed antennas. MIMO radar with collocated antennas makes use of waveform diversity [4,5,13,15,19], while MIMO radar with distributed antenna takes advantage of the spatial diversity supported by the system configuration [1,2,6,14]. MIMO radar systems have been shown to offer considerable advantages over traditional radars in various aspects of radar operation, such as the detection of slow moving targets by exploiting Doppler estimates from multiple directions [17], the ability to identify and separate multiple targets [11, 12], and in the estimation of target parameters, such as direction-of-arrival (DOA) [9, 11], and range-based target localization [18]. In particular, [18] studies target localization with MIMO radar systems utilizing sensors distributed over a wide area.

Conventional localization techniques include time-of-arrival (TOA), time-difference-of-arrival (TDOA), and direction-of-arrival (DOA) based schemes. MIMO radar system with collocated antennas can perform DOA estimation of targets in the far-field, in which case, the received signal has a planar wavefront. Extensive research has focused on waveform optimization. In [8, 15, 19] the signal vector transmitted by a MIMO radar system is designed to minimize the cross-correlation of the signals bounced from various targets to improve the parameter estimation accuracy in multiple target schemes. Some of the waveform optimization techniques suggested in [16] are based on the Cramer-Rao lower bound (CRLB) matrix. The CRLB is known to provide a tight bound on parameter

1

estimation for high signal-to-noise ratio (SNR) [26–28]. Several design criteria are considered, such as minimizing the trace, determinant, and the largest eigenvalue of the CRLB matrix, concluding that minimizing the trace of the CRLB gives a good overall performance in terms of lowering the CRLB. In [10], a CRLB evaluation of the achievable angular accuracy is derived for linear arrays with orthogonal signals. The use of orthogonal signals is shown to provide better accuracy than correlated signals. For low-SNR scenarios, the Barankin bound is derived in [11], demonstrating that the use of orthogonal signals results in a lower SNR threshold for transitioning into the region of higher estimation error. In all, the CRLB is limited to the analysis of the angular accuracy and therefore the results cannot be transformed into an equivalent error in a Cartesian coordinate system.

MIMO radar systems with widely spread antennas take advantage of the geographical spread of the deployed sensors. The multiple propagation paths, created by the transmitted waveforms and echoes from scatterers, support target localization through either direct or indirect multilateration. With direct multilateration, the observations collected by the sensors are jointly processed to produce the localization estimate. With indirect multilateration, the TOAs are estimated first, and the localization is subsequently estimated from the TOAs. The observations and processing of the time delays can be classified as either non-coherent or coherent. Thus, a transmitted signal may have in-phase and quadrature components, yet the localization processing is non-coherent if it utilizes only information in the signal envelope. In the sequel, the performance of localization utilizing both coherent and non-coherent processing is evaluated. The distinction between the two modes, in terms of system requirements, relies on the need for mere time synchronization between the transmitting and receiving radars in the non-coherent case, versus the need for both time and phase synchronization in the coherent case. Note that our coherent/non-coherent terminology is limited to the processing for localization.

MIMO radar systems belongs to the class of active localization systems, where the signal usually travels a round trip, i.e., the signal transmitted by one sensor in a

radar system is reflected by the target, and measured by the same or a different sensor. Traditional single-antenna radar systems, performing active range-based measurements, are well known in literature [29–33]. The target range is computed from the time it takes for the transmitted signal to get to the target, plus the travelling time of the reflected signal back to the sensor. The range estimation accuracy is directly proportional to the mean squared error (MSE) of the time delay estimation and is shown to be inversely proportional to the signal effective bandwidth [29]. A first study of the localization accuracy capability of widely spread MIMO radar systems is provided in [18], where the Fisher information matrix (FIM) is derived for the case of orthogonal signals with coherent processing and widely separated antennas. The CRLB is analyzed numerically, pointing out the dependency of the accuracy on the signal carrier frequency in the coherent case, and its reliance on the relative locations of the target and sensors. In [18], it is observed that the CRLB is a function of the number of transmitting and receiving sensors, however an analytical relation is not developed. The high accuracy capability of coherent processing is illustrated by the use of the ambiguity function (AF). Active range-based target localization techniques are also used in multi-static radar systems, proposed in [34]. The TOA of a signal transmitted by a single transmit radar, reflected by the target and received at multiple receive antennas is used in the localization process. The CRLB is developed for non-coherent processing. It is observed that increasing the number of sensors improves localization performance, yet an exact relation is not specified. In [35] the Bayesian Cramer-Rao bound (BCRB) is developed for the same scheme as in [34]. Simulation-based results show that accuracy performance depends on the geometric setting of the system, nonetheless a notion of this effect is not provided. The multi-static scheme evaluated in [34] and [35] does not deal with the processing of multiple received signals since only one waveform is transmitted. This dissertation addresses deficiencies in the literature by obtaining closed-form expressions of the CRLB for both coherent and non-coherent cases with multiple widely spread transmit and receive radars.

Geolocation techniques have been the subject of extensive research. Geolocation belongs to the class of passive localization systems, where the signal travels one-way. Since these passive measurement systems employ multiple sensors [36–40], further evaluation of existing results for geolocation systems may provide insight for the active case. In wireless communication, passive measurements are used by multiple base stations for localization of a radiating mobile phone. The localization accuracy performance is evaluated in [36, 38]. It is shown that the localization accuracy is inversely proportional to the signal effective bandwidth, as it does in the active localization case. Moreover, the accuracy estimation is shown to be dependent on the sensors/base stations locations. In navigation systems, the target makes use of time-synchronized transmission from multiple Global Positioning Systems (GPS) to establish its location. In [39] and [40], the relation between the transmitting sensors location and the target localization performance is analyzed. GDOP plots are used to demonstrate the dependency of the attainable accuracy on the location of the GPS systems with respect to the target. In an optimal setting of the GPS systems relative to the target position, the best achievable accuracy is shown to be inversely proportional to the square root of the number of participating GPS sensors. In this research work, the GDOP metric is utilized in the evaluation of localization performance of MIMO radar systems.

1.2 Dissertation Main Contributions

The main contributions of this research work are as follows:

1.2.1 Lower Bound on Target Localization

1. The CRLB of the target localization estimation error is developed for the general case of MIMO radar with multiple waveforms with non-coherent and coherent observations. The analytical expressions of the CRLB are derived for the case of orthogonal waveforms (in [3] and [42, 43]).

2. It is shown that the CRLB expressions, for both the non-coherent and coherent cases, can be factored into two terms: a term incorporating the effect of bandwidth, carrier frequency and SNR, and another term accounting for the effect of sensor placement, defined as *spatial advantage*.

3. The CRLB of the standard deviation of the localization estimate with non-coherent observations is shown to be inversely proportional to the signals averaged effective bandwidth. Dramatically higher accuracy can be obtained from processing coherent observations. In this case, the CRLB is inversely proportional to the carrier frequency. This gain is due to the exploitation of phase information, and is referred to as *coherency advantage*.

1.2.2 Spatial Advantage Optimization and Analysis

1. Formulating a convex optimization problem, it is shown that symmetric deployment of transmitting and receiving sensors around a target is optimal with respect to minimizing the trace of the CRLB. The closed-form solution of the optimization problem also reveals that optimally placed M transmitters and N receivers reduce the CRLB on the variance of the estimate by a factor $MN/2$ (in [44] and [45]).

2. A closed-form solution is developed for the best linear unbiased estimator (BLUE) of target localization for coherent and non-coherent MIMO radars. It provides a closed-form solution and a comprehensive evaluation of the performance of the estimator's MSE. This estimator provides insight into the relation between sensor locations, target location, and localization accuracy through the use of the GDOP metric. This metric is shown to represent the spatial advantage of the system. Contour maps of the GDOP, provide a clear understanding of the mutual relation between a given deployment of sensors and the achievable accuracy at various target locations.

3. An evaluation of target localization performances for MIMO radar with coherent processing and single-input multiple-output (SIMO) radar systems, based on the BLUE, is provided. The best achievable accuracy for both configurations is derived. MIMO radar systems with coherent processing are shown to benefit from higher spatial advantage, compared with SIMO systems. The advantage of the MIMO radar scheme over SIMO is evident when considering the achievable accuracy for a radar system with M transmitters and N receivers, rather than 1 transmitter and MN receivers. It is shown that MIMO radar, with a total of $M + N$ sensors, has twice the performance (in terms of localization MSE) of a system with $(MN + 1)$ sensors (in [46]).

1.2.3 CRLB for Multiple Target Localization

1. The localization performance study is extended to the case of multiple targets, with coherent processing. The CRLB for the multiple targets localization problem is derived and analyzed. The localization is shown to benefit from coherency advantage. The trade-off between target localization accuracy and the number of targets that can be localized is shown to be incorporated in the spatial advantage term.

2. An increase in the number of targets to be localized exposes the system to increased mutual interferences. This trade-off depends on the geometric footprint of both the sensors and the targets, and the relative positions of the two. Numerical analysis of some special cases offers an insight to the mutual relation between a given deployment of radars and targets and the spatial advantage it presents (in [47]).

1.2.4 Sensitivity Analysis of Coherent Processing to Phase Synchronization Errors

1. The *hybrid* Cramer-Rao bound (CRB) is developed for target localization, to establish the sensitivity of the estimation mean-square error (MSE) to the level of phase synchronization mismatch in coherent Multiple-Input Multiple-Output (MIMO) radar systems with widely distributed antennas. The lower bound on the MSE is derived for the joint estimation of the vector of unknown parameters, consisting of the target location and the mismatch of the allegedly known system parameters, i.e., phase offsets at the radars.

2. A closed-form expression for the hybrid CRB is derived for the case of orthogonal waveforms. The bound on the target localization MSE is expressed as the sum of two terms – the first represents the CRB with no phase mismatch, and the second captures the mismatch effect. The latter is shown to depend on the phase error variance, the number of mismatched transmitting and receiving sensors and the system geometry.

3. For a given phase synchronization error variance, this expression offers the means to analyze the achievable localization accuracy. Alternatively, for a predetermined localization MSE target value, the derived expression may be used to determine the necessary phase synchronization level in the distributed system (in [48]).

1.2.5 Bayesian Cramer-Rao Bound (BCRB) for Target Tracking

1. The CRLB on target localization is developed in this study for a stationary target whereas the CRLB on target velocity estimation was developed in [49]- [50]. Consequently, our model does not account for Doppler frequency. In practice, a Doppler shift might be introduced and affect the estimation performance. Target tracking involves the joint evaluation of both target parameters.

2. Study of moving target tracking capabilities is offered through the use of the BCRB for the estimation of both target location and velocity in non-coherent MIMO radar systems with widely distributed antennas. It is shown that increasing the number of transmitting and receiving radars provides better tracking performances in terms of higher accuracy gains for target location and velocity estimation. The performance gain is proportional to the increase in the product of the number of transmitting and receiving radars. Wider spread of the radars results in better accuracies.

3. MIMO radar architecture support both centralized and decentralized tracking techniques, inherit to the system nature. Each receiver may contribute to central processing by providing either raw data or partially/fully processed data. It is demonstrated that communication requirements and processing load may be reduced at a relatively low performance cost. Based on mission needs, the system may use either modes of operation: centralized for high accuracy or decentralized resource-aware tracking (in [51] and [52]).

1.3   Dissertation Outline

The dissertation is organized as follows: The localization performance analysis for a single target is developed in Chapter 2. The CRLB is derived for the general case of multiple transmitted waveforms. Analytical expressions are obtained for the cases of non-coherent and coherent observations with orthogonal signals. Optimization of the CRLB as a function of sensor location is provided in the same chapter.

The BLUE is derived and evaluated in Chapter 3 for both coherent and non-coherent processing. To establish a better understanding of the relations between the radar geographical spread and the target location, the GDOP metric is introduced in this chapter and GDOP based analysis is provided for MIMO and SIMO radar configurations.

The CRLB for Multiple targets localization is developed in Chapter 4. Establishing the feasibility of the coherent processing method, sensitivity analysis of coherent target localization estimation error to phase synchronization errors is provided in Chapter 5.

Target tracking model for MIMO radar system with non-coherent processing is introduced in Chapter 6. The theoretical performance bound is set through the use of the BCRB and centralized and decentralized algorithms are proposed. While the first provides high accuracy, the later incorporate resource saving at relatively low performance loss. Finally, conclusions and discussion of future work is provided in Chapter 7.

CHAPTER 2

TARGET LOCALIZATION IN MIMO RADAR

2.1 Introduction

In radar systems, bandwidth plays an important role in determining range resolution, i.e., it is inversely proportional to the signal bandwidth [29]. By exploiting the spatial dimension, coherent MIMO radar with widely separated antennas may overcome bandwidth limitations and support high resolution target localization. The distinction between noncoherent and coherent applications relies on the need for merely time synchronization between the transmitting and receiving radars vs. the need for phase synchronization. The MIMO radar architecture with coherent processing exploits knowledge of the phase differences measured at the receive antennas to produce a high accuracy target location estimate.

In this Chapter, localization performances of coherent and noncoherent processing are evaluated. The distinction between the two modes, in terms of system requirements, relies on the need for mere time synchronization between the transmitting and receiving radars in the noncoherent case, versus the need for both time and phase synchronization in the coherent case.

2.2 System Model

Widely distributed MIMO radar systems with M transmitting radars and N receiving radars are considered. The receiving radars may be collocated with the transmitting ones or individually positioned. The transmitting and receiving radars are located in a two dimensional plane (x, y). The M transmitters are arbitrarily located at coordinates $T_k = (x_{tk}, y_{tk})$, $k = 1, \ldots, M$, and the N receivers are similarly arbitrarily located at coordinates $R_\ell = (x_{r\ell}, y_{r\ell})$, $\ell = 1, \ldots, N$. The set of transmitted waveforms in lowpass equivalent

form is $s_k(t)$, $k = 1, \ldots, M$, where $\int_{\mathcal{T}} |s_k(t)|^2 dt = 1$, and $\mathcal{T}$ is the common duration of all transmitted waveforms. The power of the transmitted waveforms is normalized such that the aggregate power transmitted by the sensors is constant, irrespective of the number of transmit sensors. To simplify the notation, the signal power term is embedded in the noise variance term, such that the SNR at the transmitter, denoted SNR_t and defined as the transmitted power by a sensor divided by the noise power at a receiving sensor, is set at a desired level. Let all transmitted waveforms be narrowband signals with individual effective bandwidth β_k defined as $\beta_k^2 = \left[\left(\int_{W_k} f^2 |S_k(f)|^2 df \right) / \left(\int_{W_k} |S_k(f)|^2 df \right) \right]$, where the integration is over the range of frequencies with non-zero signal content W_k [29]. Further define the signals' averaged effective bandwidth or rms bandwidth as $\beta^2 = \frac{1}{M} \sum_{k=1}^{M} \beta_k^2$, and the normalized bandwidth terms as $\beta_{R_k} = \beta_k / \beta$. The signals are narrowband in the sense that for a carrier frequency of f_c, the narrowband signal assumption implies $\beta_k^2 / f_c^2 \ll 1$ and $\beta^2 / f_c^2 \ll 1$.

The target model developed here generalizes the model in [29] to a near-field scenario and distributed sensors. In Skolnik's model [29], the returns of individual point scatterers have fixed amplitude and phase, and are independent of angle. For a moving target, the composite return fluctuates in amplitude and phase due to the relative motion of the scatterers. When the motion is slow, and the composite target return is assumed to be constant over the observation time, the target conforms to the classical Swerling case I model. This model is generalize to a target observed by a MIMO radar with distributed sensors. Assume an extended target, composed of a collection of Q individual point scatterers located at coordinates $X_q = (x_q, y_q)$, $q = 1, \ldots, Q$, concentrated in a circle centered at $X\prime = (x\prime, y')$, with an area smaller than the signal wavelength. The amplitudes ζ_q of the point scatterers are assumed to be mutually independent. The pathloss and phase of a signal reflected by a scatterer, when measured with respect to a transmitted signal $s_k(t)$, are functions of the path transmitter-scatterer-receiver. Let $\tau_{\ell k}(X_q)$ denote the propagation

time from transmitter k, to scatterer q, to receiver ℓ,

$$\tau_{\ell k}\left(X_q\right) = \frac{1}{c}\left(\sqrt{\left(x_{tk}-x_q\right)^2 + \left(y_{tk}-y_q\right)^2} + \sqrt{\left(x_{r\ell}-x_q\right)^2 + \left(y_{r\ell}-y_q\right)^2}\right), \quad (2.1)$$

where c is the speed of light. Our signal model assumes that the sensors are located such that variations in the signal strength due to different target to sensor distances can be neglected, i.e., the model accounts for the effect of the sensors/target localizations only through time delays (or phase shifts) of the signals. The common path loss term is embedded in ζ_q. The baseband representation for the signal received at sensor ℓ is:

$$r_\ell\left(t\right) = \sum_{k=1}^{M}\sum_{q=1}^{Q}\zeta_q \exp\left(-j2\pi f_c \tau_{\ell k}\left(X_q\right)\right) s_k\left(t - \tau_{\ell k}\left(X_q\right)\right) + w_\ell(t), \quad (2.2)$$

where the term $2\pi f_c \tau_{\ell k}\left(X_q\right)$ is the phase of a signal transmitted by sensor k, reflected by scatterer q located at X_q, and received by sensor ℓ. Phases are measured relative to a common phase reference assumed to be available at the transmitters and receivers. The term $w_\ell\left(t\right)$ is circularly symmetric, zero-mean, complex Gaussian noise, spatially and temporally white with autocorrelation function $\sigma_w^2\delta\left(\tau\right)$. The noise term is set $\sigma_w^2 = 1/\text{SNR}_t$, where SNR_t is measured at the transmitter. SNR_t is normalized such that the aggregate transmitted power is independent of the number of transmitting sensors. The SNR at the receiver, due to a scatterer with amplitude ζ_q, is $\text{SNR}_r = |\zeta_q|^2\text{SNR}_t$. Signals reflected from the target combine at each of the receive antennas. For example, the resultant signal at receive antenna ℓ is given by

$$s_r\left(t\right) \approx s_k\left(t - \tau_{\ell k}\left(X'\right)\right)\sum_{q=1}^{Q}\zeta_q \exp\left(-j2\pi f_c \tau_{\ell k}\left(X_q\right)\right). \quad (2.3)$$

In obtaining (2.3), the narrowband assumption is invoked $s_k\left(t - \tau_{\ell k}\left(X_q\right)\right) \approx s_k\left(t - \tau_{\ell k}\left(X'\right)\right)$, for all scatterers, namely that the change in the lowpass equivalent signals across the target is negligible. In [29] it is shown that a complex target defined by (2.3) may be written as:

$$s_r\left(t\right) \approx s_k\left(t - \tau_{\ell k}\left(X'\right)\right)\zeta' \exp\left(-\gamma'\right), \quad (2.4)$$

where ζ' is the amplitude given by

$$\zeta' = \left[\left(\sum_{q=1}^{Q} \zeta_q \cos \left(2\pi f_c \tau_{\ell k} \left(X_q \right) \right) \right)^2 + \left(\sum_{q=1}^{Q} \zeta_q \sin \left(2\pi f_c \tau_{\ell k} \left(X_q \right) \right) \right)^2 \right]^{1/2}, \quad (2.5)$$

and γ' is

$$\gamma' = \arctan \frac{\sum_{q=1}^{Q} \zeta_q \cos \left(2\pi f_c \tau_{\ell k} \left(X_q \right) \right)}{\sum_{q=1}^{Q} \zeta_q \sin \left(2\pi f_c \tau_{\ell k} \left(X_q \right) \right)}. \quad (2.6)$$

The targets are concentrated in a small area, such that the viewing angles on path ℓk for all Q targets are approximately the same, i.e. $\cos \left(2\pi f_c \tau_{\ell k} \left(X_q \right) \right) \approx \cos \left(2\pi f_c \tau_{\ell k} \left(X' \right) \right)$ and $\sin \left(2\pi f_c \tau_{\ell k} \left(X_q \right) \right) \approx \sin \left(2\pi f_c \tau_{\ell k} \left(X' \right) \right)$ for all $q = 1, ... Q$. It follows from this discussion that the extended target is represented by a point scatterer of amplitude $\zeta' = \sum_{q=1}^{Q} \zeta_q$ and time delays $\tau_{\ell k} \left(X' \right)$, where all the quantities are unknown.

While this target model is completely adequate for our needs, it is possible to extend it slightly, at little cost. Assume a constant time offset error $\Delta\tau$ at the receivers. Further, assume that the error is small such that it does not impact the signal envelope, but it does impact the phase. Then the time delays can be written as $\tau_{\ell k} \left(X' \right) = \tau_{\ell k} \left(X \right) + \Delta\tau$ for some location $X = (x, y)$. The target model (2.3) can now be expressed

$$\zeta' s_k \left(t - \tau_{\ell k} \left(X' \right) \right) \exp \left(-j 2\pi f_c \tau_{\ell k} \left(X' \right) \right) \approx \zeta s_k \left(t - \tau_{\ell k} \left(X \right) \right) \exp \left(-j 2\pi f_c \tau_{\ell k} \left(X \right) \right),$$

$$(2.7)$$

where $\zeta = \zeta' e^{-j 2\pi f_c \Delta\tau}$ and the narrowband assumption was invoked once more. The composite target of (2.3) is then equivalent to a point scatterer of complex amplitude ζ and time delays $\tau_{\ell k} \left(X \right)$. For simplicity, the following notation is used: $\tau_{\ell k} = \tau_{\ell k} \left(X \right)$. The signal model (2.2) becomes

$$r_{\ell} (t) = \sum_{k=1}^{M} \zeta \exp \left(-j 2\pi f_c \tau_{\ell k} \right) s_k \left(t - \tau_{\ell k} \right) + w_{\ell}(t). \quad (2.8)$$

The vector of received signals is defined as $\mathbf{r} = [r_1, r_2, ..., r_N]^T$, for later use. The radar system's goal is to estimate the target location $X = (x, y)$. The target location can be

estimated directly, for example by formulating the maximum likelihood estimate (MLE) associated with (2.8). Alternatively, an indirect method is to estimate first the time delays $\tau_{\ell k}$. Subsequently, the target location can be computed from the solution to a set of equations of the form (2.1), (see Figure 2.1) viz.,

$$\tau_{\ell k} = \frac{1}{c} \left(\sqrt{(x_{tk} - x)^2 + (y_{tk} - y)^2} + \sqrt{(x_{r\ell} - x)^2 + (y_{r\ell} - y)^2} \right). \qquad (2.9)$$

The unknown complex amplitude ζ is treated as a nuisance parameter in the estimation problem.
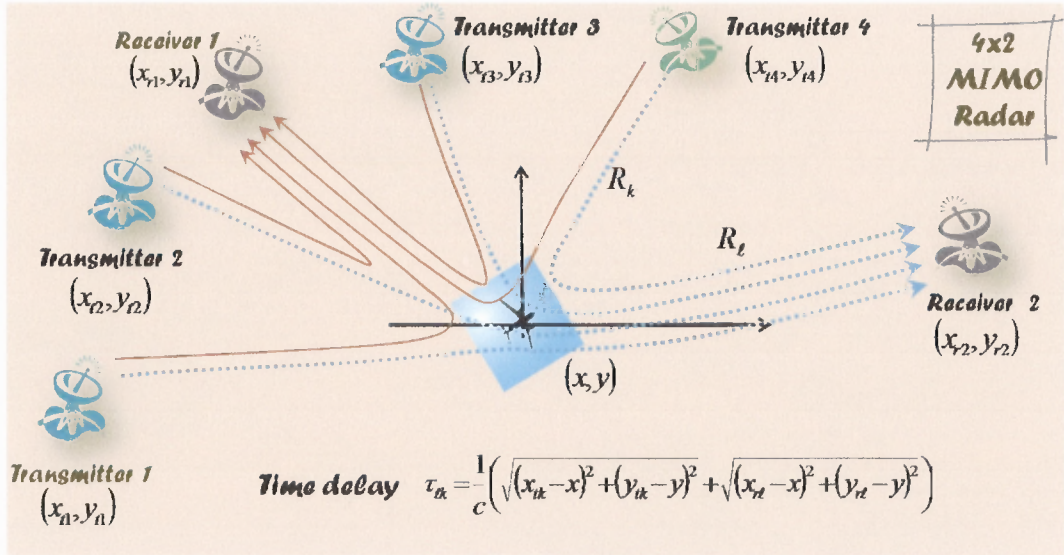
Figure 2.1 System Layout.

Let the unknown target location $X = (x, y)$, unknown time delays delays $\tau_{\ell k}$, and unknown target complex amplitude $\zeta = \zeta^R + j\zeta^I$, where the notation specifies the real and imaginary components of ζ.

Target location estimation process may be referred as *noncoherent* or *coherent*. The received signal introduced in (2.8) is adequate for the coherent case, where the transmitting and receiving radars are assumed to be both time and phase-synchronized. As such, the time delays information, $\tau_{\ell k}$, embedded in the phase terms may be exploited in the estimation

process by matching both amplitude and phase at the receiver end. In contrast, noncoherent processing estimates the time delays $\tau_{\ell k}$ from variations in the envelope of the transmitted signals $s_k(t)$. A common time reference is required for all the sensors in the system. In this case, the transmitting radars are not phase-synchronized and therefore the received signal model is of the form:

$$r_\ell(t) = \sum_{k=1}^{M} \alpha_{\ell k} s_k(t - \tau_{\ell k}) + w_\ell(t), \tag{2.10}$$

where the complex amplitude terms $\alpha_{\ell k}$ integrate the effect of the phase offsets between the transmitting and receiving sources and the target impact on the phase and amplitude of the transmitted signals. These elements are treated as unknown complex amplitudes, where $\alpha_{\ell k} = \alpha_{\ell k}^R + j\alpha_{\ell k}^I$. The following vector notations are defined:

$$\alpha = [\alpha_{11}, \alpha_{12}, ..., \alpha_{\ell k}, ..., \alpha_{MN}]^T, \tag{2.11}$$

$$\alpha^R = Re(\alpha); \quad \alpha^I = Im(\alpha),$$

where $Re(\cdot)$ and $Im(\cdot)$ denote the real and imaginary parts of a complex-valued vector/matrix.

2.3 Localization CRLB

The CRLB provides a lower bound for the MSE of any unbiased estimator for an unknown parameter(s). Given a vector parameter θ, constituted of elements θ_i, the unbiased estimate $\widehat{\theta}_i$ satisfies the following inequality [26]:

$$var\left(\widehat{\theta}_i\right) \geq \left[\mathbf{J}^{-1}(\theta)\right]_{ii}, \quad i = 1, 2, ... \tag{2.12}$$

where $[\mathbf{J}^{-1}(\theta)]_{ii}$ are the diagonal elements of the Fisher Information matrix (FIM) $\mathbf{J}(\theta)$. The FIM is given by:

$$\mathbf{J}(\theta) = E_{\mathbf{r}|\theta}\left\{\left[\frac{\partial}{\partial\theta}\log p(\mathbf{r}|\theta)\right]\left[\frac{\partial}{\partial\theta}\log p(\mathbf{r}|\theta)\right]^{T}\right\}, \qquad (2.13)$$

where $p(\mathbf{r}|\theta)$ is the joint probability density function (pdf) of $\mathbf{r}$ conditioned on θ and $E_{\mathbf{r}|\theta}\{\cdot\}$ is the conditional expectation of $\mathbf{r}$ given θ.

The CRLB is then defined:

$$\mathbf{C}_{CRLB} = [\mathbf{J}(\theta)]^{-1}. \qquad (2.14)$$

Sometime, it is easier to compute the FIM with respect to another vector ψ, and apply the chain rule to derive the original $\mathbf{J}(\theta)$. In our case, since the received signals in both (2.8) and (2.10) are functions of the time delays, $\tau_{\ell k}$, and the complex amplitudes, by the chain rule, $\mathbf{J}(\theta)$ can be expressed in the alternative form [26]:

$$\mathbf{J}(\theta) = \mathbf{P}\mathbf{J}(\psi)\mathbf{P}^{T}, \qquad (2.15)$$

where ψ is a vector of unknown parameters, and it incorporates the time delays. Matrix $\mathbf{J}(\psi)$ is the FIM with respect to ψ, and matrix $\mathbf{P}$ is the Jacobian:

$$\mathbf{P} = \frac{\partial\psi}{\partial\theta}. \qquad (2.16)$$

From this point onward, the CRLB is developed for the case of noncoherent and coherent processing, separately.

2.3.1 Noncoherent Processing CRLB

For noncoherent processing, there is no common phase reference among the sensors. Consequently, the complex-valued terms α_{lk} incorporate phase offsets among sensors and the effect of the target on the phase and complex amplitude, following the definitions in (2.11). The vectors of unknown parameters is defined:

$$\theta_{nc} = \left[x, y, \alpha^R, \alpha^I \right]^T . \tag{2.17}$$

The process of localization by noncoherent processing depends on time delay estimation of the signals observed at the receive sensors and also on the location of the sensors. To gain insight into how each of the factors affects the performance of localization, the form of the FIM given in (2.15) is utilized. The vector of unknown parameters is defined by:

$$\psi_{nc} = \left[\tau, \alpha^R, \alpha^I \right]^T , \tag{2.18}$$

where α is given in (2.11) and $\tau = [\tau_{11}, \tau_{12}, ..., \tau_{\ell k}, ..., \tau_{MN}]^T$. Only estimates of x and y are of interest, while α^R, α^I act as nuisance parameters in the estimation problem.

Given a set of known transmitted waveforms $s_k (t - \tau_{\ell k})$ parameterized by the unknown time delays $\tau_{\ell k}$, which in turn are a function of the unknown target location $X = (x, y)$, the conditional, joint pdf of the observations at the receive sensors, given by (2.10), is then:

$$p\left(\mathbf{r} | \psi_{nc} \right) \propto \exp \left\{ -\frac{1}{\sigma_w^2} \sum_{\ell=1}^{N} \int_T \left| r_\ell(t) - \sum_{k=1}^{M} \alpha_{\ell k} s_k \left(t - \tau_{\ell k} \right) \right|^2 dt \right\} . \tag{2.19}$$

The matrix $\mathbf{P}_{nc}$ for (2.17) and (2.18), to be used in (2.15), is defined as:

$$
\mathbf{P}_{nc} = \frac{\partial \psi_{nc}}{\partial \theta_{nc}} = \begin{bmatrix} \frac{\partial}{\partial x}\tau^T & \frac{\partial}{\partial x}\left(\alpha^R\right)^T & \frac{\partial}{\partial x}\left(\alpha^I\right)^T \\[6pt] \frac{\partial}{\partial y}\tau^T & \frac{\partial}{\partial y}\left(\alpha^R\right)^T & \frac{\partial}{\partial y}\left(\alpha^I\right)^T \\[6pt] \frac{\partial \tau}{\partial \alpha^R} & \frac{\partial \alpha^R}{\partial \alpha^R} & \frac{\partial \alpha^I}{\partial \alpha^R} \\[6pt] \frac{\partial \tau}{\partial \alpha^I} & \frac{\partial \alpha^R}{\partial \alpha^I} & \frac{\partial \alpha^I}{\partial \alpha^I} \end{bmatrix}_{(2MN+2)\times 3MN} , \tag{2.20}
$$

where $\frac{\partial}{\partial x}\tau$ is standard notation for taking the derivative with respect to x of each element of τ, and $\dfrac{\partial \tau}{\partial \alpha^R}$ denotes the Jacobian of the vector τ with respect to the vector α^R. The subscript denotes the matrix dimensions.

It is not too difficult to show that using (2.9), the matrix $\mathbf{P}_{nc}$ can be expressed in the form:

$$
\mathbf{P}_{nc} = \begin{bmatrix} \mathbf{H}_{2\times MN} & \mathbf{0}_{2\times 2MN} \\[6pt] \mathbf{0}_{2MN\times MN} & \mathbf{I}_{2MN\times 2MN} \end{bmatrix} , \tag{2.21}
$$

where $\mathbf{0}$ is the all zero matrix, $\mathbf{I}$ is the identity matrix, and $\mathbf{H} \in R^{2\times MN}$ incorporates the derivatives of the time delays in (2.9) with respect to the x and y parameters. These derivatives result in cosine and sine functions of the angles the transmitting and receiving radars create with respect to the target, incorporating information on the sensors and target locations as follows:

$$
\mathbf{H} = -\frac{1}{c}\begin{bmatrix} a_{tx_1} + a_{rx_1} & a_{tx_1} + a_{rx_2} & \cdots & a_{tx_M} + a_{rx_N} \\[6pt] b_{tx_1} + b_{rx_1} & b_{tx_1} + b_{rx_2} & \cdots & b_{tx_M} + b_{rx_N} \end{bmatrix} . \tag{2.22}
$$

The elements of $\mathbf{H}$ are given by:

$$a_{tx_k} = \cos \phi_k; \quad b_{tx_k} = \sin \phi_k; \quad k = 1, .., M,$$

$$a_{rx_\ell} = \cos \varphi_\ell; \quad b_{rx_\ell} = \sin \varphi_\ell; \quad \ell = 1, .., N, \tag{2.23}$$

$$\phi_k = \tan^{-1}\left(\frac{y - y_{tk}}{x - x_{tk}}\right); \quad \varphi_\ell = \tan^{-1}\left(\frac{y - y_{r\ell}}{x - x_{r\ell}}\right),$$

where the phase ϕ_k is the bearing angle of the transmitting sensor k to the target measured with respect to the x axis; the phase φ_ℓ is the bearing angle of the receiving radar ℓ to the target measured with respect to the x axis. See illustration in Figure 2.2. For later use, the following notations are defined: $\phi = [\phi_1, \phi_2, ..., \phi_M]^T$, $\varphi = [\varphi_1, \varphi_2, ..., \varphi_N]^T$, $\mathbf{a}_{tx} = [a_{tx_1}, a_{tx_2}, ..., a_{tx_M}]^T$, $\mathbf{a}_{rx} = [a_{rx_1}, a_{rx_2}, ..., a_{rx_N}]^T$, $\mathbf{b}_{tx} = [b_{tx_1}, b_{tx_2}, ..., b_{tx_M}]^T$ and $\mathbf{b}_{rx} = [b_{rx_1}, b_{rx_2}, ..., b_{rx_M}]^T$.
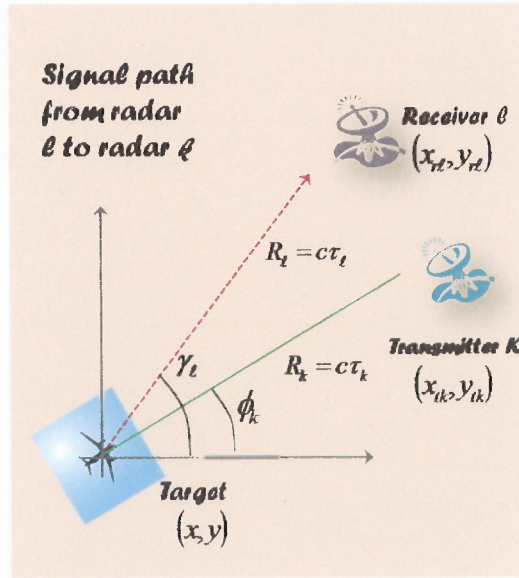
Figure 2.2 Transmiter - receiver path.

An expression for the FIM $\mathbf{J}(\psi_{nc})$, is derived in Appendix A, yielding:

$$\mathbf{J}(\psi_{nc}) = \frac{2}{\sigma_w^2} \begin{bmatrix} \mathbf{S}_{nc} & \mathbf{V}_{nc} \\ \mathbf{V}_{nc}^T & \mathbf{\Lambda}_\alpha \end{bmatrix}_{(3MN) \times (3MN)}, \tag{2.24}$$

with the block matrices $\mathbf{S}_{nc}$, $\mathbf{\Lambda}_{\alpha}$, and $\mathbf{V}_{nc}$ terms defined in the Appendix A in (A.2), (A.3)-(A.4) and (A.5)-(A.6) respectively.

In order to determine the value of $\mathbf{J}\left(\theta_{nc}\right)$, (2.15) and (2.21) are used in (2.24), to obtain the following CRLB matrix:

$$\mathbf{C}_{CRLB_{nc}} = \mathbf{J}^{-1}\left(\theta_{nc}\right) = \frac{c^2}{2/\sigma_w^2} \begin{bmatrix} \mathbf{HS}_{nc}\mathbf{H}^T & \mathbf{HV}_{nc} \\ \mathbf{V}_{nc}^T\mathbf{H}^T & \mathbf{\Lambda}_{\alpha} \end{bmatrix}^{-1}. \tag{2.25}$$

The CRLB matrix is related to the sensor and target locations through the matrix $\mathbf{H}$, and to the received waveforms correlation functions and its derivatives through the $\mathbf{S}_{nc}$ and $\mathbf{V}_{nc}$ matrices.

Orthogonal Waveforms When the waveforms are orthogonal, the block matrices $\mathbf{S}_{nc}$, $\mathbf{\Lambda}_{\alpha}$, and $\mathbf{V}_{nc}$ simplify to (A.7) in Appendix A. This simplification enables to compute the CRLB (2.25) in closed-form. This calculation is performed next.

While the CRLB expresses the lower bound on the variance of the estimate of $\theta_{nc} = \left[x, y, \alpha^R, \alpha^I\right]^T$, only the estimation of x and y is of interest. The amplitude terms α^R and α^I serve as nuisance parameters. For the variances of the estimates of x and y, it is sufficient to derive the 2×2 upper left submatrix $[\mathbf{C}_{CRLB_{nc}}]_{2\times 2} = \left[\left(\mathbf{J}\left(\theta_{nc}\right)\right)^{-1}\right]_{2\times 2}$.

The CRLB submatrix $[\mathbf{C}_{CRLB_{nc}}]_{2\times 2}$ for target localization in the *noncoherent* case with orthogonal signals is:

$$[\mathbf{C}_{CRLB_{nc}}]_{2\times 2} = \frac{c^2}{2/\sigma_w^2}\left(\mathbf{HS}_{nc}\mathbf{H}^T\right)^{-1}. \tag{2.26}$$

Proof: From (A.7) in Appendix A, terms (2.25) is:

$$\mathbf{S}_{nc} = 4\pi^2\beta^2 \left[diag(\alpha)\mathbf{B}diag(\alpha^*) \right], \tag{2.27}$$

$$\mathbf{V}_{nc} = \mathbf{0},$$

$$\mathbf{\Lambda}_\alpha = \mathbf{I}_{2MN \times 2MN}.$$

In (2.27), $diag(\alpha)$ denotes a diagonal matrix with the elements of vector α. Matrix $\mathbf{B} = diag\left(\mathbf{1}\left[\beta_{R_1}^2, \beta_{R_2}^2, ..., \beta_{R_M}^2\right]\right)$, with β_{R_k} denoting the normalized elements $\beta_{R_k} = \beta_k/\beta$, and $\mathbf{1} = [1, 1, ...1]^T$, $\mathbf{1} \in R^{N \times 1}$. Using (2.27) in (2.25), it is easy to see that

$$[\mathbf{C}_{CRLB_{nc}}]_{2 \times 2} = \frac{c^2}{2/\sigma_w^2} \left(\mathbf{HS}_{nc}\mathbf{H}^T\right)^{-1} \tag{2.28}$$

$$= \frac{\eta_{nc}}{g_{x_{nc}}g_{y_{nc}} - h_{nc}^2} \begin{bmatrix} g_{x_{nc}} & h_{nc} \\ h_{nc} & g_{y_{nc}} \end{bmatrix},$$

where:

$$\eta_{nc} = \frac{c^2}{8\pi^2\beta^2/\sigma_w^2},$$

$$g_{x_{nc}} = \sum_{k=1}^{M}\sum_{\ell=1}^{N} |\alpha_{\ell k}|^2 \beta_{R_k}^2 \left(b_{tx_k} + b_{rx_\ell}\right)^2,$$

$$g_{y_{nc}} = \sum_{k=1}^{M}\sum_{\ell=1}^{N} |\alpha_{\ell k}|^2 \beta_{R_k}^2 \left(a_{tx_k} + a_{rx_\ell}\right)^2, \tag{2.29}$$

$$h_{nc} = -\sum_{k=1}^{M}\sum_{\ell=1}^{N} |\alpha_{\ell k}|^2 \beta_{R_k}^2 \left(a_{tx_k} + a_{rx_\ell}\right)\left(b_{tx_k} + b_{rx_\ell}\right).$$

This concludes the proof of the proposition. ∎

It follows that the lower bound on the variance for estimating the x coordinate of the target is given by

$$\sigma_{x_{nc}CRB}^2 = \eta_{nc}\frac{g_{x_{nc}}}{g_{x_{nc}}g_{y_{nc}} - h_{nc}^2}. \tag{2.30}$$

Similarly, for the y coordinate,

$$\sigma_{y_{nc}CRB}^2 = \eta_{nc}\frac{g_{y_{nc}}}{g_{x_{nc}}g_{y_{nc}} - h_{nc}^2}. \tag{2.31}$$

The terms $g_{x_{nc}}$, $g_{y_{nc}}$, and h_{nc} are summations of a_{tx_k}, a_{rx_ℓ}, b_{tx_k} and b_{rx_ℓ} terms that represent sine and cosine expressions of the angles ϕ and φ, and therefore relate to the radars and target geometric layout. It is apparent that for the noncoherent case, the lower bounds on the variances (2.30) and (2.31) are inversely proportional to the averaged effective bandwidth β^2, and $SNR = 1/\sigma_w^2$ (see expression for η_{nc} in (2.29)). It is interesting to note that η_{nc} is actually the CRLB for range estimation in a single antenna radar, based on the one-way time delay between the radar and the target (see for example [26]). The other terms in (2.30) and (2.31) incorporate the effect of the sensor locations.

2.3.2 Coherent Processing CRLB

Recall that in the signal model Section, the complex amplitude $\alpha_{\ell k}$ i s associated with the path transmitter $k \to$ target $\to$ receiver ℓ. In the noncoherent case, the complex amplitude is a nuisance parameter in estimating the target location x, y. In the coherent case, the transmitting and receiving radars are assumed to be phase-synchronized. By eliminating the phase offsets, the signal model in (2.8) applies, and the nuisance parameter role is left to the complex target amplitude $\zeta = \zeta^R + j\zeta^I$. The coherent approach to localization seeks to exploit the target location information embedded in the phase terms $\exp\left(-2\pi f_c \tau_{\ell k}\right)$ that depend on the delays $\tau_{\ell k}$, which in turn are function of the target coordinates x, y.

Define the vector of unknown parameters:

$$\theta_c = \left[x, y, \zeta^R, \zeta^I\right]^T. \tag{2.32}$$

As before, define a second vector of unknown parameters in terms of the time delays τ (rather then the target location),

$$\psi_c = \left[\tau, \zeta^R, \zeta^I\right]^T, \tag{2.33}$$

to be used in (2.15) to derive the CRLB. In comparing the coherent case in (2.33) with the noncoherent counterpart in (2.18), note that ψ_{nc} incorporates the vectors α^R and α^I, while ψ_c is a function of the scalars ζ^R and ζ^I. The reduction in the number of unknown parameters is made possible through the measurement of the phase terms of α^R and α^I.

For coherent observations, the conditional, joint pdf of the observations at the receive sensors, given by (2.8), is of the form:

$$
p\left(\mathbf{r}|\psi_c\right) \propto \exp\left\{ -\frac{1}{\sigma_w^2}\sum_{\ell=1}^{N} \int_T \left| r_\ell(t) - \sum_{k=1}^{M} \zeta \exp\left(-j2\pi f_c \tau_{\ell k}\right) s_k\left(t - \tau_{\ell k}\right) \right|^2 dt \right\}. \quad (2.34)
$$

Following a process similar to the one in Section 2.3.1, the CRLB is derived for the coherent case, based on the relation in (2.15). The matrix $\mathbf{P}_c$ takes the form:

$$
\mathbf{P}_c = \frac{\partial \psi_c}{\partial \theta_c} = \begin{bmatrix} \mathbf{H} & \mathbf{0}_{MN\times 2} \\ \mathbf{0}_{2\times MN} & \mathbf{I}_{2\times 2} \end{bmatrix}_{4\times(MN+2)}, \quad (2.35)
$$

where matrix $\mathbf{H}$ has the same form as in (2.22), since it is independent of the nuisance parameters in both cases.

An expression for the FIM matrix, $\mathbf{J}\left(\psi_c\right)$, is derived in Appendix B, yielding:

$$
\mathbf{J}(\psi_c) = \frac{2}{\sigma_w^2} \begin{bmatrix} \mathbf{S}_c & \mathbf{V}_c \\ \mathbf{V}_c^T & \mathbf{\Lambda}_{\alpha c} \end{bmatrix}_{(MN+2)\times(MN+2)}, \quad (2.36)
$$

where the elements of the submatrices are found in Appendix B as follows: $\mathbf{S}_c$ in (B.4), $\mathbf{\Lambda}_{\alpha c}$ in (B.5)-(A.5), and $\mathbf{V}_c$ in (B.7)-(B.9).

The CRLB matrix for the coherent case is then found substituting (2.35) and (2.36) in (2.15) and (2.14), obtaining:

$$\mathbf{C}_{CRLB_c} = \frac{c^2}{2/\sigma_w^2} \begin{bmatrix} \mathbf{HS}_c\mathbf{H}^T & \mathbf{HV}_c \\ \mathbf{V}_c^T\mathbf{H}^T & \mathbf{\Lambda}_{\alpha c} \end{bmatrix}^{-1}. \tag{2.37}$$

As in Section 2.3.1, the closed-form solution to the CRLB matrix in (2.37) is reduced to the case of orthogonal waveforms. Since only the lower bound on the variances of the estimates of x and y, is of interest, the submatrix $[\mathbf{C}_{CRLB_c}]_{2\times 2} = \left[(\mathbf{J}_c(\theta))^{-1}\right]_{2\times 2}$ is derived and evaluated next.

Orthogonal Waveform   The CRLB 2×2 submatrix for the *coherent* case and orthogonal waveforms is:

$$[\mathbf{C}_{CRLB_c}]_{2\times 2} = \frac{c^2}{2/\sigma_w^2} \left(\mathbf{HS}_c\mathbf{H}^T - \mathbf{HV}_c\mathbf{\Lambda}_{\alpha c}^{-1}\mathbf{V}_c^T\mathbf{H}^T\right)^{-1}. \tag{2.38}$$

Proof: From (B.11) in Appendix B the values of the matrices $\mathbf{S}_c$, $\mathbf{\Lambda}_{\alpha c}$, and $\mathbf{V}_c$ are obtained for orthogonal waveforms. Using this and $\mathbf{H}$ defined in (2.22) in (2.37), the CRLB matrix $\mathbf{C}_{CRLB_{cor}}$ is obtained. Consequently, the submatrix $[\mathbf{C}_{CRLB_c}]_{2\times 2}$ is computed, resulting in the form given in (2.38).

This completes the proof of the proposition.   ∎

From (2.38) and (B.11), it can be shown that $[\mathbf{C}_{CRLB_c}]_{2\times 2}$ can be expressed as:

$$[\mathbf{C}_{CRLB_c}]_{2\times 2} = \frac{\eta_c}{g_{x_c}g_{y_c} - h_c^2} \begin{bmatrix} g_{x_c} & h_c \\ h_c & g_{y_c} \end{bmatrix}, \tag{2.39}$$

where the various quantities are as follows:

$$\eta_c = \frac{c^2}{8\pi^2 f_c^2 \left(|\zeta|^2/\sigma_w^2\right)},$$

$$g_{x_c} = \sum_{k=1}^{M}\sum_{\ell=1}^{N} f_{R_k} \left(b_{tx_k} + b_{rx_\ell}\right)^2 - \frac{1}{MN} \left(\sum_{k=1}^{M}\sum_{\ell=1}^{N} \left(b_{tx_k} + b_{rx_\ell}\right)\right)^2,$$

$$g_{y_c} = \sum_{k=1}^{M}\sum_{\ell=1}^{N} f_{R_k} \left(a_{tx_k} + a_{rx_\ell}\right)^2 - \frac{1}{MN} \left(\sum_{k=1}^{M}\sum_{\ell=1}^{N} \left(a_{tx_k} + a_{rx_\ell}\right)\right)^2, \qquad (2.40)$$

$$h_c = -\sum_{k=1}^{M}\sum_{\ell=1}^{N} f_{R_k} \left(a_{tx_k} + a_{rx_\ell}\right)\left(b_{tx_k} + b_{rx_\ell}\right)$$

$$+ \frac{1}{MN}\sum_{k=1}^{M}\sum_{\ell=1}^{N} \left(a_{tx_k} + a_{rx_\ell}\right) \sum_{k=1}^{M}\sum_{\ell=1}^{N} \left(b_{tx_k} + b_{rx_\ell}\right).$$

The lower bound on the error variance is provided by the diagonal elements of the $\left[\mathbf{C}_{CRLB_{cor}}\right]_{2\times2}$ submatrix and are of the form:

$$\sigma^2_{x_cCRB} = \eta_c \frac{g_{x_c}}{g_{x_c}g_{y_c} - h_c^2}, \qquad (2.41)$$

$$\sigma^2_{y_cCRB} = \eta_c \frac{g_{y_c}}{g_{x_c}g_{y_c} - h_c^2}.$$

The terms g_{x_c}, g_{y_c}, and h_c are summations of a_{tx_k}, a_{rx_ℓ}, b_{tx_k} and b_{rx_ℓ} that represent sine and cosine expressions of the angles ϕ and φ, and therefore relate to the radars and target geometric layout, multiplied by the ratio terms $f_{R_k} = \left(1 + \frac{\beta_k^2}{f_c^2}\right)$. Invoking the narrowband signals assumption $\beta_k^2/f_c^2 \ll 1$, it follows that $f_{R_k} \simeq 1$. These terms have some additional elements when compared with the noncoherent case. It is apparent that for the coherent case, the variances of the target location estimates in (2.41) are inversely proportional to the carrier frequency f_c^2.

2.3.3 Discussion

The following observations are made:

- The lower bound on the variance in the noncoherent case is inversely proportional to the averaged effective bandwidth β. For the coherent case, with narrowband signals, where $\beta_k^2/f_c^2 \ll 1$, the localization accuracy is inversely proportional to the carrier frequency f_c and independent of the signal individual effective bandwidth, due to the use of the phase information across the different paths. It is apparent that coherent processing offers a target localization precision gain (i.e., reduction of the localization root mean-square error) of the order of f_c/β, refer to as *coherency gain*. Designing the ratio f_c/β to be in the range 100-1000, leads to dramatic gains.

- The term η_c in (2.40) is the range estimate based on one-way time delay with coherent observations for a radar with a single antenna [53].

- The CRLB terms are strongly reliant on the relative geographical spread of the radar systems vs. the target location. This dependency is incorporated in the terms g_{x_{nc}/x_c}, g_{y_{nc}/y_c} and $h_{nc/c}$. It is apparent from (2.41), (2.30) and (2.31) that there is a trade-off between the variances of the target location computed horizontally and vertically. A set of sensor locations that minimizes the horizontal error, may result in a high vertical error. For example, spreading the transmitting and receiving radars in an angular range of $-(\pi/10)$ to $+(\pi/10)$ radians with respect to the target, will result in high horizontal error while providing low vertical error, as intuitively expected. This is caused by the fact that the terms $g_{x_{nc}}/g_{x_c}$ are summations of sine functions and $g_{y_{nc}}/g_{y_c}$ are summation of cosine functions of the same set of angles. In order to truly determine the minimum achievable localization accuracy in both x and y axis, the *over-all* accuracy, defined as the total variance $\sigma_c^2 = \left(\sigma_{x_cCRB}^2 + \sigma_{y_cCRB}^2\right)$ needs to be minimized.

- The message of dramatic improvement in localization accuracy needs to be moderated with the observation that the CRLB is a bound of *small errors*. As such, it ignores effects that could lead to *large errors*. For example, MIMO radar with distributed sensors and coherent observations is subject to high sidelobes [1]. These topics are outside the scope of this paper, but they should be kept in perspective.

- *Phase synchronization:* The coherent scheme promises of higher accuracy performances involve the challenge of distributed carrier phase synchronization. The synchronization complexity in distributed and autonomous sensors/platforms is common to widely spread MIMO radar systems, wireless sensor networks and cooperative wireless communication. In the latter two, some of the proposed solutions make use of a reference signal [54–57] provided by one of the sensors. These schemes mainly focus on master/slave strategies where one sensor is chosen to be the master and broadcasts a sinusoidal reference signal to all slaves. Carrier phase synchronization is also established using an external beacon in the form of a GPS or a ground communication broadcasting station [58–61]. These highly stable broadcasting sources continuously transmit a reference signal to be used at each sensor node, where more than one beacon may be used for higher accuracy. In all of these synchronization methods, a periodic re-synchronization is necessary to avoid unacceptable levels of phase drift. The increasing interest in distributed phase synchronization and vibrant research activity set the ground for promising progress.

- *Doppler shift:* The CRLB on target localization is developed for a stationary target whereas the CRLB on target velocity estimation is developed in [50]. Consequently, the model in (2.8) does not account for Doppler frequency. In practice, a Doppler shift might be introduced and affect the estimation performance with coherent processing. To evaluate the affect of such a Doppler shift on the CRLB the following

signal model adaptation is applied [31]:

$$r_\ell(t) \approx \sum_{k=1}^{M} \zeta \exp\left(-j2\pi f_c \tau_{\ell k}\right) s_k\left(t - \tau_{\ell k}\right) \exp\left(j2\pi f_{d_{\ell k}} t\right) + w_\ell(t), \qquad (2.42)$$

where $f_{d_{\ell k}}$ is the Doppler frequency and $\frac{f_c}{f_{d_{\ell k}}} \ll 1$ is assumed. Without loss of generality, the transmitted waveforms are time-delayed such that they add coherently in the center of a given search cell $\left[x_o \pm \frac{c}{\beta}, y_o \pm \frac{c}{\beta}\right]$. For a slow moving target, i.e. $\frac{f_{d_{\ell k}}}{\beta} \ll 1$, the Doppler term $\exp\left(j2\pi f_{d_{\ell k}} t\right) \approx 1$ and therefore the Doppler shift does not affect the localization performance as shown in this section. If the latter does not apply, the off-diagonal elements of matrix $\mathbf{S}_c$ are non-zero and therefore introduce an estimation error. A current research effort is focused on the extension of the current model to a Bayesian CRLB that accounts for both target location and velocity estimation.

- *Orthogonality:* The CRLB is developed for a general set of waveforms $\{s_k(t)\}$. The general solution in (2.25) and (2.37) is later given in closed-form for the special case of orthogonal signals. Albeit the design of such signal sets is beyond the framework of this paper, elaboration as for some possible schemes is provided. Attaining a set of orthogonal waveforms that follow the requirement of $\int s_k(\nu) s_{k'}^*(\nu - \Delta\tau_{\ell k,\ell k'}) d\nu = 0$ over all cross-elements, $k \neq k'$, and any $\Delta\tau_{\ell k,\ell k'} = \tau_{\ell k} - \tau_{\ell k'}$, is a challenging task. Accomplishing full orthogonality under these conditions is very demanding. A practical way to address this problem is by relaxing the design criteria to low cross-correlation, i.e., $\left|\int s_k(\nu) s_{k'}^*(\nu - \Delta\tau_{\ell k,\ell k'}) d\nu\right| < \epsilon$, where ϵ is chosen such that the estimation MSE performance penalty, with respect to fully orthogonal sets, in minimized. This offers a reasonable way to generate approximate-orthogonal waveforms for some range of delays or what is defined in [62] as *quasi-orthogonal* waveforms. Such an alternative is presented in [50]. Some other design possibilities are provided in [21–23,62]. The extension of the radar AF to the MIMO radar case in [24, 25] offers design tools for such quasi-orthogonal waveforms. The CRLB

analytical expressions provided in Appendix A and Appendix B could than be used for a comparative evaluation of the CRLB performance for a given quasi-orthogonal set vs. a fully orthogonal set of waveforms.

- The lower bound as expressed by the CRLB, provides a tight bound at high SNR, while at low SNR, the CRLB is not tight [28]. As the ambiguity problems are usually addressed through the signal waveform design, a more rigid bound needs to be found for the localization variance in the low-SNR case.

The coherency gain obtained with coherent processing makes it advantageous over noncoherent processing. All the same, the contribution of the product terms g_{x_c}, g_{y_c} and h_c needs further evaluation. The following sections focus on elucidating the role of these terms for coherent processing.

2.4   Effect of Sensor Locations

The CRLB for target localization with coherent MIMO radar shows a gain, i.e., reduction in the standard deviation of the localization estimate, of f_c/β compared to noncoherent localization. Yet, the CRLB is strongly dependent on the locations of the transmitting and receiving sensors relative to the target location, through the terms g_{x_{nc}/x_c}, g_{y_{nc}/y_c} and $h_{nc/c}$. To gain a better understanding of these relations, and set a lower bound on the CRLB over all possible sensor placements, further analysis is developed in this section.

The following general notation are introduced: for any given set of vectors $\xi = (\xi_1, \xi_2, ..., \xi_L)$ and $\kappa = (\kappa_1, \kappa_2, ..., \kappa_L)$:

$$
\begin{aligned}
T(\xi) &= \tfrac{1}{L}\sum_{i=1}^{L}\xi_i \\
T(\xi^2) &= \tfrac{1}{L}\sum_{i=1}^{L}\xi_i^2 \\
T(\xi\kappa) &= \tfrac{1}{L}\sum_{i=1}^{L}\xi_i\kappa_i.
\end{aligned}
\tag{2.43}
$$

2.4.1 Optimization Problem

The terms g_{x_c} and g_{y_c} in (2.29) can be expressed using the conventions defined in (2.43) and terms defined in Section 2.3.2, viz.:

$$g_{x_c} = MN \left[T \left(\mathbf{b}_{tx}^2 \right) + T \left(\mathbf{b}_{rx}^2 \right) - \left[T \left(\mathbf{b}_{tx} \right) \right]^2 - \left[T \left(\mathbf{b}_{rx} \right) \right]^2 \right], \qquad (2.44)$$

and

$$g_{y_c} = MN \left[T \left(\mathbf{a}_{tx}^2 \right) + T \left(\mathbf{a}_{rx}^2 \right) - \left[T \left(\mathbf{a}_{tx} \right) \right]^2 - \left[T \left(\mathbf{a}_{rx} \right) \right]^2 \right], \qquad (2.45)$$

where the narrowband signals assumption is applied. Similarly, the term h_c in (2.40) can be expressed:

$$h_c = -MN \left[T \left(\mathbf{a}_{tx} \mathbf{b}_{tx} \right) + T \left(\mathbf{a}_{rx} \mathbf{b}_{rx} \right) \qquad (2.46)$$

$$-T \left(\mathbf{a}_{tx} \right) E \left(\mathbf{b}_{tx} \right) - T \left(\mathbf{a}_{rx} \right) T \left(\mathbf{b}_{rx} \right) \right].$$

Since $a_{tx_k}^2 + b_{tx_k}^2 = \cos^2 \phi_k + \sin^2 \phi_k = 1$ and $a_{rx_\ell}^2 + b_{rx_\ell}^2 = \cos^2 \varphi_\ell + \sin^2 \varphi_\ell = 1$, the following conditions apply:

$$\begin{aligned}
T \left(\mathbf{a}_{tx}^2 \right) + T \left(\mathbf{b}_{tx}^2 \right) &= 1 \\
T \left(\mathbf{a}_{rx}^2 \right) + T \left(\mathbf{b}_{rx}^2 \right) &= 1 \\
0 \le \left[T \left(\mathbf{a}_{tx} \right) \right]^2 \le 1; \quad 0 &\le \left[T \left(\mathbf{a}_{rx} \right) \right]^2 \le 1 \\
0 \le \left[T \left(\mathbf{b}_{tx} \right) \right]^2 \le 1; \quad 0 &\le \left[T \left(\mathbf{b}_{rx} \right) \right]^2 \le 1 \\
0 \le T \left(\mathbf{a}_{tx}^2 \right) \le 1; \quad 0 &\le T \left(\mathbf{a}_{rx}^2 \right) \le 1 \\
0 \le T \left(\mathbf{b}_{tx}^2 \right) \le 1; \quad 0 &\le T \left(\mathbf{b}_{rx}^2 \right) \le 1.
\end{aligned} \qquad (2.47)$$

Seeking to find sets of angles ϕ^* and φ^*, that yield sets of cosine and sine expressions $\mathbf{a}_{tx}^*, \mathbf{a}_{rx}^*, \mathbf{b}_{tx}^*, \mathbf{b}_{rx}^*$ for which the values of the Cramer-Rao bounds for localization along the x and y axes ($\sigma_{x_cCRB}^2$ and $\sigma_{y_cCRB}^2$, respectively) are jointly minimized,

$$\underset{\mathbf{a}_{tx},\mathbf{a}_{rx},\mathbf{b}_{tx},\mathbf{b}_{rx}}{\text{minimize}} \left(\sigma_{x_cCRB}^2 + \sigma_{y_cCRB}^2 \right). \tag{2.48}$$

This is equivalent to minimizing the trace of the CRLB submatrix $[\mathbf{C}_{CRLB_c}]_{2\times 2}$. The explicit minimization problem is formulated introducing the objective function f_0:

$$\underset{\mathbf{a}_{tx},\mathbf{a}_{rx},\mathbf{b}_{tx},\mathbf{b}_{rx}}{\text{minimize}} \quad f_0\left(\mathbf{a}_{tx},\mathbf{a}_{rx},\mathbf{b}_{tx},\mathbf{b}_{rx}\right) = \eta_c \frac{g_{x_c}+g_{y_c}}{g_{x_c}g_{y_c}-h_c^2}$$

$$\text{subject to constraints (2.47).} \tag{2.49}$$

This representation of the problem is not a convex optimization problem.[1] The next steps are undertaken in order to formulate a convex optimization problem equivalent to (2.49), i.e., a convex optimization problem that can be solved through routine techniques and from whose solution it is readily possible to find the solution to (2.49).

In [39], it is shown that for a given positive definite matrix, in our case $[\mathbf{C}_{CRLB_c}]_{2\times 2}$, and its inverse matrix $\mathbf{F}$, in this case:

$$\mathbf{F} = \frac{1}{\eta_c} \begin{bmatrix} g_{yc} & -h_c \\ -h_c & g_{xc} \end{bmatrix}, \tag{2.50}$$

the following relation exists between the diagonal elements of these matrices:

$$[\mathbf{C}_{CRLB_c}]_{ii} \geq \frac{1}{[\mathbf{F}]_{ii}}; \quad i = 1,2. \tag{2.51}$$

---

[1] A convex optimization problem in *standard form* is [63]

$$\begin{aligned} \text{minimize} \quad & f_0\left(x\right) \\ \text{subject to} \quad & f_i\left(x\right) \leq 0 \\ & \sum_j a_j x_j = 0 \end{aligned}$$

for some constants a_i, i, j, $i = 1,...,m$, $j = 1,...,p$, and where $f_0,...,f_m$ are convex functions.

Equality conditions apply for all i iff $\mathbf{F}$ is a diagonal matrix, i.e., $h_c = 0$. Enforcing this condition later on guarantees that $\min\left(\sum_i \frac{1}{[\mathbf{F}]_{ii}}\right) = \min\left(\sum_i [\mathbf{C}_{CRLB_c}]_{ii}\right)$. Now, observe that the inverse of the elements on the diagonal of $\mathbf{F}$ lower bound the elements on the diagonal of the matrix $\mathbf{C}_{CRLB_c}$ for any $\mathbf{a}_{tx}, \mathbf{a}_{rx}, \mathbf{b}_{tx}, \mathbf{b}_{rx}$. The following objective function is defined $\overline{f_0}\left(\mathbf{a}_{tx}, \mathbf{a}_{rx}, \mathbf{b}_{tx}, \mathbf{b}_{rx}\right)$, and the optimization problem,

$$\min \overline{f_0}\left(\mathbf{a}_{tx}, \mathbf{a}_{rx}, \mathbf{b}_{tx}, \mathbf{b}_{rx}\right) = \frac{1}{\eta_c}\left(\frac{1}{g_{x_c}} + \frac{1}{g_{y_c}}\right) \tag{2.52}$$

subject to (2.47).

The new objective function and the original objective function are related as $f_0\left(\mathbf{a}_{tx}, \mathbf{a}_{rx}, \mathbf{b}_{tx}, \mathbf{b}_{rx}\right) \geq \overline{f_0}\left(\mathbf{a}_{tx}, \mathbf{a}_{rx}, \mathbf{b}_{tx}, \mathbf{b}_{rx}\right)$, with equality for $h_c = 0$. Substitute the values of g_{x_c} and g_{y_c} from (2.44) and (2.45) in the objective function of (2.52) to obtain

$$\overline{f_0}\left(\mathbf{a}_{tx}, \mathbf{a}_{rx}, \mathbf{b}_{tx}, \mathbf{b}_{rx}\right) = \frac{1/\left(\eta_c MN\right)}{2 - T\left(\mathbf{b}_{tx}^2\right) - T\left(\mathbf{b}_{rx}^2\right) - \left[T\left(\mathbf{a}_{tx}\right)\right]^2 - \left[T\left(\mathbf{a}_{rx}\right)\right]^2} \tag{2.53}$$
$$+ \frac{1/\left(\eta_c MN\right)}{T\left(\mathbf{b}_{tx}^2\right) + T\left(\mathbf{b}_{rx}^2\right) - \left[T\left(\mathbf{b}_{tx}\right)\right]^2 - \left[T\left(\mathbf{b}_{rx}\right)\right]^2}.$$

It is apparent that the denominator of the first summand is bounded by:

$$0 \leq 2 - T\left(\mathbf{b}_{tx}^2\right) - T\left(\mathbf{b}_{rx}^2\right) - \left[T\left(\mathbf{a}_{tx}\right)\right]^2 - \left[T\left(\mathbf{a}_{rx}\right)\right]^2 \leq 2 - T\left(\mathbf{b}_{tx}^2\right) - T\left(\mathbf{b}_{rx}^2\right), \quad (2.54)$$

and the denominator of the second summand is bounded by:

$$0 \leq T\left(\mathbf{b}_{tx}^2\right) + T\left(\mathbf{b}_{rx}^2\right) - \left[T\left(\mathbf{b}_{tx}\right)\right]^2 - \left[T\left(\mathbf{b}_{rx}\right)\right]^2 \leq T\left(\mathbf{b}_{tx}^2\right) + T\left(\mathbf{b}_{rx}^2\right). \tag{2.55}$$

Denote $T\left(\mathbf{b}_{tx}^2\right) + T\left(\mathbf{b}_{rx}^2\right) = \mu$, and let $T\left(\mathbf{a}_{tx}\right) = T\left(\mathbf{a}_{rx}\right) = T\left(\mathbf{b}_{tx}\right) = T\left(\mathbf{b}_{rx}\right) = 0$. Then, from (2.53)-(2.55) and (2.52), the following problem is obtained:

$$\begin{aligned}
\underset{\mu}{\text{minimize}} \quad & \overline{f_0}\left(\mu\right) = \frac{1}{2-\mu} + \frac{1}{\mu} \\
\text{subject to} \quad & \mu - 2 \leq 0 \\
& -\mu \leq 0.
\end{aligned} \tag{2.56}$$

The objective function $\overline{f_0}\left(\mu\right) = \frac{2}{\mu(2-\mu)}$ is convex since $g(\mu) = \mu(2-\mu)$ is a concave function and $\overline{f_0}\left(\mu\right) = h\left(g(\mu)\right) = \frac{1}{g(\mu)}$ is a convex and nondecreasing function [63]. The inequality constraint functions are convex as well. Therefore, the problem described in (2.56) is a convex optimization problem. The *epigraph form* is a way to introduce a linear (and convex) objective t, while the original objective f_0 is incorporated into a new constraint $\overline{f_0} - t \leq 0$ [63]. The key point here is that the inequality constraint function $\overline{f_0} - t \leq 0$ can be transformed to a linear convex form [64].

An equivalent epigraph form of the convex optimization problem given in (2.56) may be expressed by using two variables, t_1 and t_2, after rewriting the objective function as $\overline{f_0}\left(\mu\right) = \overline{f_{01}}\left(\mu\right) + \overline{f_{02}}\left(\mu\right)$, where $\overline{f_{01}}\left(\mu\right) = \frac{1}{2-\mu}$ and $\overline{f_{02}}\left(\mu\right) = \frac{1}{\mu}$. Two new inequality constraint functions are introduced: $\frac{1}{2-\mu} - t_1 \leq 0$ and $\frac{1}{\mu} - t_2 \leq 0$. After some simple algebraic manipulations, the epigraph form turns into the following convex optimization problem:

$$\begin{aligned}
\underset{\mu, t_1, t_2}{\text{minimize}} \quad & \left(t_1 + t_2\right) \\
\text{subject to} \quad & \\
& \mu t_1 - 2t_1 + 1 \leq 0 \\
& 1 - \mu t_2 \leq 0 \\
& \mu - 2 \leq 0; \quad -\mu \leq 0 \\
& -t_1 \leq 0; \quad -t_2 \leq 0.
\end{aligned} \tag{2.57}$$

A convenient way to solve this convex optimization problem is to employ the concept of Lagrange duality and exploit the sufficiency of the *Karush-Kuhn-Tucker* (KKT) conditions [63]. The Lagrangian of the problem in (2.57) is given by:

$$L(\mu, t_1, t_2, \lambda) = t_1 + t_2 + \lambda_1 \left(\mu t_1 - 2t_1 + 1\right) + \lambda_2 \left(1 - \mu t_2\right) + \lambda_3 \left(\mu - 2\right) - \lambda_4 \mu - \lambda_5 t_1 - \lambda_6 t_2,$$

$$(2.58)$$

where λ_i, $i = 1, .., 4$ is the *Lagrange multiplier* associated with the ith inequality constraint $f_i\left(\mu, t_1, t_2\right) \leq 0$.

The KKT conditions state that the optimal solution for the primal problem (minimization of $t_1 + t_2$ in (2.57)) is given by the solution to the set of equations:

$$\frac{\partial L(\mu, t_1, t_2, \lambda)}{\partial \mu} = 0 \qquad (2.59)$$

$$\frac{\partial L(\mu, t_1, t_2, \lambda)}{\partial t_1} = 0; \quad \frac{\partial L(\mu, t_1, t_2, \lambda)}{\partial t_2} = 0$$

$$f_i(\mu, t_1, t_2) \leq 0; \quad i = 1, .., 6$$

$$\lambda_i \geq 0; \quad i = 1, .., 6$$

$$\lambda_i f_i(\mu, t_1, t_2) = 0; \quad i = 1, .., 6.$$

Applied to (2.57) and (2.58), these equations specialize to

$$\lambda_1 t_1 - \lambda_2 t_2 + \lambda_3 - \lambda_4 = 0 \quad ; \quad \lambda_3 \left(\mu - 2\right) = 0$$

$$1 - \lambda_1 \left(\mu - 2\right) - \lambda_5 = 0 \quad ; \quad -\lambda_4 \mu = 0$$

$$1 - \lambda_2 \mu - \lambda_6 = 0 \quad ; \quad -\lambda_5 t_1 = 0$$

$$\lambda_1 \left(\mu t_1 - 2t_1 + 1\right) = 0 \quad ; \quad -\lambda_6 t_2 = 0$$

$$\lambda_2 \left(1 - \mu t_2\right) = 0 \qquad .$$

It is not difficult to show that the solution to this system is given by

$$\mu^* = 1$$
$$t_1^* = t_2^* = 1$$
$$\lambda_1^* = \lambda_2^* = 1$$
$$\lambda_3^* = \lambda_4^* = \lambda_5^* = \lambda_6^* = 0$$

(2.60)

Recalling that $\mu = T\left(\mathbf{b}_{tx}^2\right) + T\left(\mathbf{b}_{rx}^2\right)$, the optimal solution can be rewritten as:

$$\mu^* = T\left(\mathbf{b}_{tx}^{*2}\right) + T\left(\mathbf{b}_{rx}^{*2}\right) = 1.$$

(2.61)

In addition to (2.61), $\mathbf{a}_{tx}^*, \mathbf{a}_{rx}^*, \mathbf{b}_{tx}^*, \mathbf{b}_{rx}^*$ have to satisfy the relations (2.47), and the equality conditions for (2.51), (2.54) and (2.55), viz.,

$$T\left(\mathbf{a}_{tx}^{*2}\right) + T\left(\mathbf{a}_{rx}^{*2}\right) = 1$$
$$T\left(\mathbf{b}_{tx}^*\right) = 0; \ T\left(\mathbf{b}_{rx}^*\right) = 0$$
$$T\left(\mathbf{a}_{tx}^*\right) = 0; \ T\left(\mathbf{a}_{rx}^*\right) = 0$$
$$T\left(\mathbf{a}_{tx}^*\mathbf{b}_{tx}^*\right) + T\left(\mathbf{a}_{rx}^*\mathbf{b}_{rx}^*\right) = 0.$$

(2.62)

Substituting these results in (2.44) and (2.45), computes the optimum $g_{x_c}^*$ and $g_{y_c}^*$,

$$g_{x_c}^* = g_{y_c}^* = MN.$$

It follows that the minimum value of the trace of the Cramer-Rao matrix $\left[\mathbf{C}_{CRLB_{cor}}\right]_{2\times2}$, f_0 in (2.49), is given by:

$$f_0\left(\mathbf{a}_{tx}^*, \mathbf{a}_{rx}^*, \mathbf{b}_{tx}^*, \mathbf{b}_{rx}^*\right) = \frac{2\eta_c}{MN}.$$

(2.63)

The final step in determining the effect of sensor locations on the localization CRLB is to recall that the multivariable argument of f_0 in (2.63) is actually a function

of the transmitting sensors angles ϕ_k, $k = 1, \ldots, M$, and receiving sensors angles φ_ℓ, $\ell = 1, \ldots, N$ (see definitions in the previous section). What are then the optimal sets ϕ^* and φ^* that minimize the variance of the localization error? The optimal angles can be found from the relations (2.62). For example, for the cosine of the transmitters bearings $T\left(\mathbf{a}_{tx}^*\right) = 0$,

$$\frac{1}{M} \sum_{k=1}^{M} \cos \phi_k^* = 0. \tag{2.64}$$

A symmetrical set of angles of the form $\phi^* = \left\{\phi_i^* \mid \phi_i^* = \phi_0 + \frac{2\pi(i-1)}{M}; i = 1, .., M; M \geq 2\right\}$, is a solution to (2.64) for any arbitrary ϕ_0. The same solution is obtained for the sines, $T\left(\mathbf{b}_{tx}^*\right) = 0$. The relations $T\left(\mathbf{a}_{rx}^*\right) = 0$, $T\left(\mathbf{b}_{rx}^*\right) = 0$ lead to a solution constituted by a symmetrical set of angles φ^* of the same form as ϕ^*. The relation $T\left(\mathbf{a}_{tx}^* \mathbf{b}_{tx}^*\right) + T\left(\mathbf{a}_{rx}^* \mathbf{b}_{rx}^*\right) = 0$ expressed in terms of angles is

$$\frac{1}{M} \sum_{k=1}^{M} \cos \phi_k^* \sin \phi_k^* + \frac{1}{N} \sum_{\ell=1}^{N} \cos \varphi_\ell^* \sin \varphi_\ell^* = 0. \tag{2.65}$$

It can be shown that (2.65) is met by angles ϕ_k^* and φ_ℓ^* symmetrically distributed around the unit circle, but the number of sensors has to meet $M \geq 3$, $N \geq 3$. The condition $T\left(\mathbf{b}_{tx}^{*2}\right) + T\left(\mathbf{b}_{rx}^{*2}\right) = 1$ in (2.62), expressed in its explicit form, is

$$\frac{1}{M} \sum_{k=1}^{M} \cos^2 \phi_k^* + \frac{1}{N} \sum_{\ell=1}^{N} \cos^2 \varphi_\ell^* = 1. \tag{2.66}$$

The symmetrical set of angles that meet (2.64) and (2.65) provide $\frac{1}{M} \sum_{k=1}^{M} \cos^2 \phi_k^* = \frac{1}{N} \sum_{\ell=1}^{N} \cos^2 \varphi_\ell^* = \frac{1}{2}$ and therefore meet the requirement of (2.66). The same applies to $T\left(\mathbf{a}_{tx}^{*2}\right) + T\left(\mathbf{a}_{rx}^{*2}\right) = 1$, where $\frac{1}{M} \sum_{k=1}^{M} \sin^2 \phi_k^* = \frac{1}{N} \sum_{\ell=1}^{N} \sin^2 \varphi_\ell^* = \frac{1}{2}$.

It can be concluded that $M \geq 3$ transmitting, and $N \geq 3$ receiving sensors, symmetrically placed on a circle around the target at angular spacings of $2\pi/M$ and $2\pi/N$, respectively, lead to the lowest value of the localization CRLB.

This result can be extended by noticing that relations (2.62) also hold for any *superposition* of symmetrical sets containing no less than 3 transmitting and/or receiving sensors. Therefore, the complete set of optimal points is given by:

$$\phi^* = \left\{ \phi_k^* \left| \left(\phi_k^* = \phi_v + \tfrac{2\pi(z-1)}{Z_v} \right) \right|_{z=1,..,Z_v} ; Z_v \geq 3; \underset{v=1}{\overset{V}{}} Z_v = M \right\}$$
$$\varphi^* = \left\{ \varphi_\ell^* \left| \left(\varphi_\ell^* = \varphi_u + \tfrac{2\pi(z-1)}{Z_u} \right) \right|_{z=1,..,Z_u} ; Z_u \geq 3; \underset{u=1}{\overset{U}{}} Z_u = N \right\},$$

(2.67)

where the total number of transmitting (M) and receiving (N) radars may be divided into V and U sets of symmetrically placed radars, each set consists of Z_v and Z_u radars, respectively. The angles ϕ_v and φ_u are an initial arbitrary rotation of the symmetric sets Z_v and Z_u, correspondingly.

As a special case, it is interesting to evaluate the CRLB in (2.39) with 1 transmitter and MN receivers, i.e., a Single-Input Multiple-Output (SIMO) system. This scheme makes use of $(MN+1)$ radars instead of $(M+N)$ radars used in a MIMO system with M transmitters and N receivers. From (2.67) it is apparent the this case does not provide optimality since the number of transmitters is smaller than 3. To evaluate $\sigma_{x_cCRB}^2 + \sigma_{y_cCRB}^2$ for this setting assume 1 transmitter is located at an arbitrary angle ϕ_1 with respect to the target, and a set of MN receivers are located symmetrically around the target, at angles φ^* that follow the condition in (2.67). The expressions in (2.44), (2.45), and (2.46) reduce to the form:

$$g_{x_c} = MN \left[T \left(\mathbf{b}_{rx}^2 \right) - [T \left(\mathbf{b}_{rx} \right)]^2 \right] = \tfrac{1}{2} MN, \tag{2.68}$$
$$g_{y_c} = MN \left[T \left(\mathbf{a}_{rx}^2 \right) - [T \left(\mathbf{a}_{rx} \right)]^2 \right] = \tfrac{1}{2} MN,$$
$$h_c = MN \left[T \left(\mathbf{a}_{rx} \mathbf{b}_{rx} \right) - T \left(\mathbf{a}_{rx} \right) E \left(\mathbf{b}_{rx} \right) \right] = 0,$$

and the trace of the CRLB submatrix $[\mathbf{C}_{CRLB_c}]_{2\times2}$, defined by $f_0\left(\mathbf{a}_{tx},\mathbf{a}_{rx},\mathbf{b}_{tx},\mathbf{b}_{rx}\right) = \sigma^2_{x_cCRB} + \sigma^2_{y_cCRB} = \eta_c\frac{g_{x_c}+g_{y_c}}{g_{x_c}g_{y_c}-h_c^2}$, is

$$f_0\left(\mathbf{a}_{tx},\mathbf{a}_{rx},\mathbf{b}_{tx},\mathbf{b}_{rx}\right) = \frac{4\eta_c}{MN}. \tag{2.69}$$

This result expresses an increase in the estimation error by a factor of 2 when compared with M transmitters and N receivers given in (2.63).

2.4.2 Discussion

The following comments are intended to provide further insight into the results obtained in this section.

- From (2.63), the lowest CRLB for target localization utilizing phase information is given by $2\eta_c/\left(MN\right)$. The reduction in the CRLB by the factor $MN/2$ compared to a single antenna range estimation given by, η_c ia referred as a *MIMO radar gain*. This gain reflects two effects: (1) the gain due to the system footprint; (2) the advantage of using M transmitters and N receivers, rather than, for example, 1 transmitter and MN receivers. The latter gain is apparent when $MN \gg (M+N)$.

- The CRLB obtained through the use of a single transmit antenna and MN receive antennas in (2.69) is $4\eta_c/\left(MN\right)$. It follows that MIMO radar, with a total of $M+N$ sensors, has twice the performance (from the point of view of localization CRLB) of a system with a single transmit antenna and MN receive antennas.

- The best accuracy is obtained when the transmitting and receiving radars are located on a virtual circle, centered at the target position, with uniform angular spacings of $2\pi/M$ and $2\pi/N$, respectively, or any *superposition* of such sets.

- The optimization analysis presented in this section is intended to provide insight into the effect the sensor locations have on the CRLB. Naturally, in practice, it is not possible to control in real time the location of the sensors relative to a

target. However, the results here teach us that selecting among the sensors those who are most symmetrical with respect to the target may lead to the most accurate localization.

So far the focus was on the theoretical lower bound of the localization error. In the next section, specific techniques for target localization and their performance as a function of sensor locations are discussed. For this purpose, the GDOP metric and GDOP contour mapping tools are introduced.

CHAPTER 3

METHODS FOR TARGET LOCALIZATION

The lower bound on the variance of target localization estimate was formulated in Chapter 2. The MLE [65], developed in [18], does not lend itself to a closed-form expression, and numerical methods need to be used to solve it. A closed-form solution to the target localization can be obtained by application of the BLUE. The later, allows the use of the GDOP metric for a more comprehensive understanding of the relation between the target and the sensor locations.

3.1   BLUE for Noncoherent and Coherent Target Localization

To formulate the BLUE, it is necessary to have an observation model in which observations change linearly with the target location coordinates. That is because it is inherent to the BLUE that the estimate is *linear*. To this end, a model is formulated in which the time delays are "observable." In practice, the time delays are not directly observable. Rather, they are estimated, for example by maximum likelihood, from the received signals. Then, the term $\epsilon_{\ell k}$ is the time delay estimation error. Our BLUE estimation problem of the target location should not be confused with the estimation of the time delays. The estimation of the time delays is just a preparatory step in setting up the "observations" of the BLUE model. Once, the observation model has been set up, it is necessary to ensure that the model between the time delays and target location is linear. Setting the origin of the coordinate system at some nominal estimate of the target location $X_c = (x_c, y_c)$ and preserving only linear terms of the Taylor expansion of expressions such as in (2.9), the time delays introduced by a target may be introduced as linear functions of x and y,

$$\widetilde{\tau}_{\ell k} \approx -\frac{x}{c}\left(\cos\phi_k + \cos\varphi_\ell\right) - \frac{y}{c}\left(\sin\phi_k + \sin\varphi_\ell\right), \tag{3.1}$$

where the angles ϕ_k and φ_ℓ are the bearings that the transmitting sensor k and receiving sensor ℓ, respectively, subtend with the reference axis (with the origin at the nominal estimate of the target location). The vertex of the angles is an arbitrary point in the neighborhood of the true target location.

The linear model may be simplified as,

$$\widetilde{\tau}_{\ell k} = -\frac{x}{c}\left(a_{tx_k} + a_{rx_\ell}\right) - \frac{y}{c}\left(b_{tx_k} + b_{rx_\ell}\right). \tag{3.2}$$

Let the observed time delay associated with a transmitter-receiver pair be $\mu_{\ell k}$, then

$$\mu_{\ell k} = \widetilde{\tau}_{\ell k} + \epsilon_{\ell k}, \qquad \forall k = 1,..,M, l = 1,..,N, \tag{3.3}$$

where $\epsilon_{\ell k}$ is the "observation noise." The following linear model is postulated between the observable time delays $\mu = [\mu_{11}, \mu_{12}, ..., \mu_{NM}]^T$ and the vector of unknown parameters θ:

$$\mu = \mathbf{D}\theta + \epsilon, \tag{3.4}$$

where the matrix $\mathbf{D}$ defined the linear relation between $\widetilde{\tau}$ and the vector of unknowns θ. The vector $\epsilon = [\epsilon_{11}, \epsilon_{12}, ..., \epsilon_{NM}]^T$ is the $MN \times 1$ measurement noise vector. According to (3.4), the BLUE's "observations" are in the form of time delays. So an intermediate step of time delay estimation is implied.

For the linear and Gaussian model in (3.4), the BLUE is computed from the Gauss-Markov theorem [26] that states the BLUE of the unknown vector θ is given by the expression:

$$\widehat{\theta}_{BLUE} = \left(\mathbf{D}^T\mathbf{C}_\epsilon^{-1}\mathbf{D}\right)^{-1}\mathbf{D}^T\mathbf{C}_\epsilon^{-1}\mu. \tag{3.5}$$

where $\mathbf{C}_\epsilon$ is the covariance matrix characterizing the "noise" terms $\epsilon_{\ell k}$.

The theorem also determines the error covariance matrix for the estimator $\widehat{\theta}_{BLUE}$ to be

$$\mathbf{C}_{BLUE} = \left(\mathbf{D}^T \mathbf{C}_\epsilon^{-1} \mathbf{D}\right)^{-1}. \tag{3.6}$$

From this point onward, the BLUE is developed for the case of noncoherent and coherent processing, separately.

3.1.1 BLUE for Noncoherent Processing

Recall that in signal model Section, the complex amplitude $\alpha_{\ell k}$ associated with the path transmitter k → target → receiver ℓ in the received signal model given in (2.10) was defined. In the noncoherent case, the complex amplitude is a nuisance parameter in estimating the target location x, y. There is no common phase reference among the sensors and phase information is not exploited in the estimation process. Consequently, the time observation, evaluated using noncoherent processing, are not affected by phase/time bias. In this case, the vector of unknown parameters is defined as $\theta_{nc} = [x, y]^T$ and the the time measurements are modeled as:

$$\mu_{nc_{\ell k}} \approx -\frac{1}{c}\left[x\left(a_{tx_k} + a_{rx_\ell}\right) + y\left(b_{tx_k} + b_{rx_\ell}\right)\right] + \epsilon_{nc_{lk}}. \tag{3.7}$$

The relation in (3.7) can be written as:

$$\mu_{nc} = \mathbf{D}_{nc}\theta_{nc} + \epsilon_{nc}, \tag{3.8}$$

where the observable time delays $\mu_{nc} = [\mu_{nc11}, \mu_{nc12}, ..., \mu_{ncNM}]^T$ are derived incoherently by the MLE as follows:

$$\mu_{nc_{\ell k}} = \arg\max_v \left| \int r_\ell(t) s_k^*(t - v)\, dt \right|, \qquad (3.9)$$

where v is a dummy variable for the time delay. Matrix $\mathbf{D}_{nc}$ is defined as:

$$\mathbf{D}_{nc} = -\frac{1}{c} \begin{bmatrix} a_{tx_1} + a_{rx_1} & b_{tx_1} + b_{rx_1} \\ ... & ... \\ a_{tx_M} + a_{rx_N} & b_{tx_M} + b_{rx_N} \end{bmatrix}_{NM \times 2}. \qquad (3.10)$$

It is shown in Appendix C that the maximum likelihood time delay estimates $\mu_{nc_{\ell k}}$ are unbiased observations, where the measurement errors $\epsilon_{nc} = [\epsilon_{nc11}, \epsilon_{nc12}, ..., \epsilon_{ncNM}]^T$ have Gaussian distribution with zero mean and an error covariance matrix of the form

$$\mathbf{C}_{\epsilon_{nc}} = \frac{1}{8\pi^2 snr} diag \left(\frac{1}{\beta_{R_1}}, \frac{1}{\beta_{R_1}}, ..., \frac{1}{\beta_{R_M}} \right)_{NM \times NM}. \qquad (3.11)$$

with $\beta_{R_k} = \frac{\beta^2 \overline{|\alpha|^2}}{\beta_k^2 |\alpha_{\ell k}|^2}$ and $snr = \frac{\overline{|\alpha|^2}}{\sigma_w^2}$.

The following estimate for the target localization with noncoherent processing is obtained:

$$\begin{bmatrix} \widehat{x} \\ \widehat{y} \end{bmatrix} = \begin{bmatrix} \widehat{\theta}_{nc} \end{bmatrix} = -\frac{8\pi^2 \beta^2 snr}{c} \mathbf{C}_{Bnc} \begin{bmatrix} \sum_{k=1}^{M}\sum_{\ell=1}^{N} \beta_{R_k} SNR_{lk} (a_{tx_k} + a_{rx_\ell}) \mu_{nc_{\ell k}} \\ \sum_{k=1}^{M}\sum_{\ell=1}^{N} \beta_{R_k} SNR_{lk} (b_{tx_k} + b_{rx_\ell}) \mu_{nc_{\ell k}} \end{bmatrix}, \qquad (3.12)$$

where $\mu_{nc_{\ell k}}$ are the time observations, and matrix $\mathbf{C}_{Bnc}$ is the estimation error covariance matrix of the form:

$$\mathbf{C}_{Bnc} = \frac{\eta_{nc}}{\left(g_{B1nc} g_{B2nc} - h_{Bnc}^2 \right)} \begin{bmatrix} g_{B1nc} & h_{Bnc} \\ h_{Bnc} & g_{B2nc} \end{bmatrix}. \qquad (3.13)$$

and

$$\eta_{nc} = \frac{c^2}{8\pi^2\beta^2 snr},$$

$$g_{B1_{nc}} = \sum_{k=1}^{M}\sum_{\ell=1}^{N}\beta_{R_k}\left(b_{tx_k} + b_{rx_\ell}\right)^2,$$

$$g_{B2_{nc}} = \sum_{k=1}^{M}\sum_{\ell=1}^{N}\beta_{R_k}\left(a_{tx_k} + a_{rx_\ell}\right)^2,$$

$$h_{B_{nc}} = -\sum_{k=1}^{M}\sum_{\ell=1}^{N}\beta_{R_k}\left(a_{tx_k} + a_{rx_\ell}\right)\left(b_{tx_k} + b_{rx_\ell}\right). \tag{3.14}$$

Using these results in (3.13) provides the MSE for the BLUE as follows:

$$\sigma_{x,B_{nc}}^2 = \frac{c^2}{8\pi^2\beta^2 snr}\left(\frac{g_{B1_{nc}}}{g_{B1_{nc}}g_{B2_{nc}} - h_{B_{nc}}^2}\right), \tag{3.15}$$

for the estimation of the x coordinate, and

$$\sigma_{y,B_{nc}}^2 = \frac{c^2}{8\pi^2\beta^2 snr}\left(\frac{g_{B2_{nc}}}{g_{B1_{nc}}g_{22} - h_{B_{nc}}^2}\right), \tag{3.16}$$

for the estimation of the y coordinate.

3.1.2 BLUE for Coherent Processing

In the coherent case, the transmitting and receiving radars are assumed to be both time and phase-synchronized. The target reflectivity parameter $\zeta = r_\zeta \exp\left(j2\pi\phi_\zeta\right)$, results in a common unknown time delay nuisance parameter $\Delta_\tau = \phi_\zeta/f_c$ for the signal model given in (2.8), where ζ is replaced by $r_\zeta \exp\left(j2\pi f_c\Delta_\tau\right)$. The time delay observations in coherent MIMO radars are therefore of the form:

$$\mu_{c_{\ell k}} \approx -\frac{1}{c}x\left(a_{tx_k} + a_{rx_\ell}\right) - \frac{1}{c}y\left(b_{tx_k} + b_{rx_\ell}\right) - \Delta_\tau + \epsilon_{c_{\ell k}}, \tag{3.17}$$

where the vector of unknowns is $\theta_c = [x, y, \Delta_\tau]^T$. The linear observation model is represented through:

$$\mu_c = \mathbf{D}\theta_c + \epsilon_c, \tag{3.18}$$

where $\mu_c = [\mu_{c_{11}}, \mu_{c_{12}}, ..., \mu_{c_{MN}}]^T$, and $\epsilon_c = [\epsilon_{c_{11}}, \epsilon_{c_{12}}, ..., \epsilon_{c_{MN}}]^T$ is the $MN \times 1$ observation noise vector.

To reiterate, a key difference between the MLE and BLUE models is that the MLE target localization is carried out utilizing signal observations (which are not linear in x, y), while according to (3.18), the BLUE's "observations" are in the form of time delays. So an intermediate step of time delay estimation is implied. In this case, the MLE computational effort is focused on estimating the time delays. For the BLUE, the estimation is based on a linearized time delay model and therefore its performance is asymptotically optimal, i.e., for a nominal position arbitrarily close to the target location. The time delays estimates used as observations $\mu_{c_{\ell k}}$ can be derived for example by MLE as follows:

$$\mu_{c_{\ell k}} = \arg\max_v \left[\exp\left(j2\pi f_c v\right) \int r_\ell(t) s_k^*(t - v) dt \right], \quad (3.19)$$

where v is a dummy variable for the time delay. Matrix $\mathbf{D}_c$ is defined as:

$$\mathbf{D}_c = -\frac{1}{c} \begin{bmatrix} a_{tx_1} + a_{rx_1} & b_{tx_1} + b_{rx_1} & 1 \\ ... & ... & ... \\ a_{tx_M} + a_{rx_N} & b_{tx_M} + b_{rx_N} & 1 \end{bmatrix}_{NM \times 3}. \quad (3.20)$$

Additional characterization of the "noise" terms $\epsilon_{c_{\ell k}}$ are needed. It is shown in Appendix C, that the maximum likelihood time delay estimates asymptotic error covariance matrix is

$$\mathbf{C}_{\epsilon_c} = \frac{1}{8\pi^2 f_c^2 snr} diag\left(\frac{1}{f_{R_1}}, \frac{1}{f_{R_1}}, ..., \frac{1}{f_{R_M}} \right)_{NM \times NM}, \quad (3.21)$$

where previous definitions of the various quantities apply and $f_{R_k} = \left(1 + \frac{\beta_k^2}{f_c^2} \right)$.

Using the time error covariance matrix $\mathbf{C}_{\epsilon_c}$ and the linear transformation matrix $\mathbf{D}$ in (3.20), the following estimate for $\widehat{\theta}_B$ is obtained:

$$
\begin{bmatrix} \widehat{x} \\ \widehat{y} \\ \Delta_\tau \end{bmatrix} = \left[\widehat{\theta}_{nc} \right] = \left(\mathbf{D}_c^T \mathbf{D}_c \right)^{-1} \mathbf{D}_c^T \mu_c.
\tag{3.22}
$$

The error covariance matrix for $(\widehat{x}, \widehat{y})$ is derived using (3.20) and (3.21) in (3.22) and calculating the 2×2 upper left submatrix, resulting with

$$
[\mathbf{C}_B]_{2\times 2} = \frac{\eta_c}{\left(g_{B1_c} g_{B2_c} - h_{B_c}^2 \right)} \begin{bmatrix} g_{B1_c} & h_{B_c} \\ h_{B_c} & g_{B2_c} \end{bmatrix},
\tag{3.23}
$$

The elements of matrix $\mathbf{G}_B$ are:

$$
\eta_c = \frac{c^2}{8\pi^2 f_c^2 snr}
$$

$$
g_{B1_c} = \sum_{k=1}^{M}\sum_{\ell=1}^{N} f_{R_k} \left(b_{tx_k} + b_{rx_\ell} \right)^2 - \frac{1}{MN} \left(\sum_{k=1}^{M}\sum_{\ell=1}^{N} \left(b_{tx_k} + b_{rx_\ell} \right) \right)^2,
$$

$$
g_{B2_c} = \sum_{k=1}^{M}\sum_{\ell=1}^{N} f_{R_k} \left(a_{tx_k} + a_{rx_\ell} \right)^2 - \frac{1}{MN} \left(\sum_{k=1}^{M}\sum_{\ell=1}^{N} \left(a_{tx_k} + a_{rx_\ell} \right) \right)^2,
\tag{3.24}
$$

$$
h_{B_c} = -\sum_{k=1}^{M}\sum_{\ell=1}^{N} f_{R_k} \left(\left(a_{tx_k} + a_{rx_\ell} \right) \left(b_{tx_k} + b_{rx_\ell} \right) \right)
$$

$$
+ \frac{1}{MN} \sum_{k=1}^{M}\sum_{\ell=1}^{N} \left(a_{tx_k} + a_{rx_\ell} \right) \sum_{k=1}^{M}\sum_{\ell=1}^{N} \left(b_{tx_k} + b_{rx_\ell} \right).
$$

Using these results in (3.23) provides the MSE for the BLUE as follows:

$$
\sigma_{x,B_c}^2 = \frac{c^2}{8\pi^2 f_c^2 snr} \left(\frac{g_{B1_c}}{g_{B1_c} g_{B2_c} - h_{B_c}^2} \right),
\tag{3.25}
$$

for the estimation of the x coordinate, and

$$
\sigma_{y,B_c}^2 = \frac{c^2}{8\pi^2 f_c^2 snr} \left(\frac{g_{B2_c}}{g_{B1_c} g_{B2_c} - h_{B_c}^2} \right),
\tag{3.26}
$$

for the estimation of the y coordinate.

3.1.3 Discussion

The following points are worth noting:

- The BLUE estimator are provided in closed-form for coherent and noncoherent processing. This allows for an analytical analysis of the MSE performance using the GDOP metric that presents a performance study tool for a given layout of sensors. Nonetheless, it does not eliminate the complex computational effort involved in the intermediate step of time delays estimation.

- In general, the variances (3.15), (3.16), (3.25) and (3.26) have similar functional dependencies on the carrier frequency and on the sensor deployment as the CRLB. The terms a_{tx_k}, a_{rx_ℓ}, b_{tx_k} and b_{rx_ℓ} embedded in (3.14) and (3.24) relate the sensors layout to the variance of the BLUE.

- For a target located arbitrarily close to the nominal position, the linearization error is negligible and the bearing angles of the transmit and receive radars, with respect to the target and the nominal position, are approximately the same. In this case, the BLUE performance is determined by the asymptotic characteristics of the time delays estimates used as observations, and derived by the MLE in (3.11) and (3.21). In [66, 67], MLE of the time delays is shown to approach the CRLB arbitrarily close at high-SNR. In this region, the time delays estimation error asymptotic covariance matrices, given by (3.11) and (3.21), are valid. Consequently, the BLUE estimator coefficients, $g_{B1_{nc/c}}$, $g_{B2_{nc/c}}$, and $h_{B_{nc/c}}$ in (3.14) and (3.24), approximate the CRLB terms given in Chapter (2), Section (2.3), and the BLUE asymptotically reach the CRLB.

- The BLUE estimator variance in (3.25) and (3.26) are provided in closed-form. This allows for an analytical analysis of the MSE performance using the GDOP metric that presents a performance study tool for a given layout of sensors. Nonetheless, it does not eliminate the complex computational effort involved in the intermediate step of time delays estimation.

From the expressions of the variance of the BLUE, one can not readily visualize the effect of the sensors layout. A mapping method, acting as a design and decision making tool for MIMO radar systems, is proposed and evaluated later in this Chapter.

3.2 Generalization for MIMO and SIMO Coherent Localization

The BLUE was derived in the previous section for MIMO target localization using noncoherent and coherent processing. Herein, the derivation for the coherent case is generalized for MIMO and SIMO system, such that a comparision between the performance of these two systems may be provided.

3.2.1 MIMO Radar

In the coherent case, the linear relation given in (3.17) are represented through matrix $\mathbf{D}_{mimo}$, as defined in (3.20), resulting into

$$\mathbf{D}_{mimo} = -\frac{1}{c} \left[\begin{array}{cc} \mathbf{H}_{rx_m} + \mathbf{H}_{tx_m} & 1 \end{array} \right]_{NM \times 3}, \tag{3.27}$$

where the matrix $\mathbf{H}_{rx_m}$ is defined as:

$$\mathbf{H}_{rx_m} = \left[\begin{array}{ccc} \mathbf{H}_{rx} & \cdots & \mathbf{H}_{rx} \end{array} \right]^T \tag{3.28}$$

and the matrix $\mathbf{H}_{tx_m}$ as:

$$\mathbf{H}_{tx_m} = \begin{bmatrix} a_{tx_1}\mathbf{1} & \cdots & a_{tx_M}\mathbf{1} \\ b_{tx_1}\mathbf{1} & \cdots & b_{tx_M}\mathbf{1} \end{bmatrix}^T .$$
(3.29)

Matrices $\mathbf{H}_{rx}$ and $\mathbf{H}_{tx}$ are defined for later use,

$$
\begin{aligned}
\mathbf{H}_{rx} &= \begin{bmatrix} \mathbf{a}_{rx} & \mathbf{b}_{rx} \end{bmatrix}_{MN \times 2}, \\
\mathbf{H}_{tx} &= \begin{bmatrix} \mathbf{a}_{tx} & \mathbf{b}_{tx} \end{bmatrix}_{MN \times 2}.
\end{aligned}
$$
(3.30)

Using the time error covariance matrix $\mathbf{C}_{\epsilon_c}$ in (3.21), and the linear transformation matrix $\mathbf{D}_{mimo}$ in (3.20), the BLUE covariance matrix for (x, y) is computed,

$$
\begin{aligned}
[\mathbf{C}_{\theta_{mimo}}]_{2\times2} &= \eta_f \Big[(\mathbf{H}_{rx_m} + \mathbf{H}_{tx_m})^T \\
&\quad \cdot \Big(\mathbf{I} - \frac{1}{MN}\mathbf{1}\mathbf{1}^T \Big) (\mathbf{H}_{rx_m} + \mathbf{H}_{tx_m}) \Big]^{-1},
\end{aligned}
$$
(3.31)

where η_f is

$$\eta_f = \frac{c^2}{8\pi^2 f_c^2 SNR}.$$

The diagonal elements of $[\mathbf{C}_{\theta_{mimo}}]_{2\times2}$ are the target location (x, y) estimation MSE, (σ_x^2, σ_y^2). Applying some algebraic manipulation to (3.31), it results in

$$[\mathbf{C}_{\theta_{mimo}}]_{2\times2} = \eta_f \mathbf{H}_{mimo},$$
(3.32)

where $\mathbf{H}_{mimo}$ is

$$\mathbf{H}_{mimo} = \left[M\mathbf{H}_{rx}^T \left(\mathbf{I} - \mathbf{1}\mathbf{1}^T\right) \mathbf{H}_{rx} + N\mathbf{H}_{tx}^T \left(\mathbf{I} - \mathbf{1}\mathbf{1}^T\right) \mathbf{H}_{tx} \right]^{-1}.$$
(3.33)

The covariance matrix $[\mathbf{C}_{\theta_{mimo}}]_{2\times2}$ is a product of the *coherency advantage* η_f (see discussion in Chapter 2), and a matrix $\mathbf{H}_{mimo}$, incorporating the effect of the geometric

spread of the system through the elements a_{tx_k}, b_{tx_k}, a_{rx_ℓ} and b_{rx_ℓ}. Matrix $\mathbf{H}_{mimo}$ is defined as the spatial matrix and its trace is defined as the *spatial advantage*.

In Chapter 2, the CRLB (Cramer-Rao lower bound) on the localization accuracy is derived for coherent MIMO radar systems, showing that the lowest MSE is obtained when the transmitting and receiving radars are placed with uniform angular spacings of $2\pi/M$ and $2\pi/N$, respectively, around the target position, or any *superposition* of such sets. The optimization holds for MIMO systems with at least 3 transmitting and 3 receiving radars, i.e. $M \geq 3$ and $N \geq 3$. Applying this scenario to the BLUE MSE given in (3.32), the values of sub-matrices in (3.33) are computed,

$$
\begin{aligned}
\mathbf{H}_{rx}^T \mathbf{H}_{rx} &= \frac{N}{2}\mathbf{I} \\
\mathbf{H}_{tx}^T \mathbf{H}_{tx} &= \frac{M}{2}\mathbf{I} \\
\mathbf{H}_{rx}^T \left(\mathbf{1}\mathbf{1}^T\right) \mathbf{H}_{rx} &= \mathbf{H}_{tx}^T \left(\mathbf{1}\mathbf{1}^T\right) \mathbf{H}_{tx} = 0.
\end{aligned}
\tag{3.34}
$$

Applying (3.34) to (3.33), the lowest MSEs $\sigma_{x_{min}}^2$ and $\sigma_{y_{min}}^2$ are computed,

$$
[\mathbf{C}_{\theta_{mimo}}]_{2\times2} (opt) = \eta_f \frac{1}{MN}\mathbf{I}.
\tag{3.35}
$$

It follows that the spatial advantage is given by $tr(\mathbf{H}_{mimo}) = \frac{2}{MN}$ (where $tr(\circ)$ stands for the trace of the matrix).

3.2.2 SIMO Radar

The SIMO radar case is equivalent to the a MIMO system with one transmitter, and therefore the appropriate matrix $\mathbf{D}$ is defined as:

$$
\mathbf{D}_{simo} = -\frac{1}{c} \left[\mathbf{H}_{rx} + \mathbf{H}_{tx1}; \quad \mathbf{1} \right]_{NM \times 3},
\tag{3.36}
$$

where $\mathbf{H}_{rx}$ follows the definition in (3.30) with $\ell = 1, .., MN$. The matrix $\mathbf{H}_{tx1}$ is:

$$\mathbf{H}_{tx1} = \begin{bmatrix} a_{tx_1}\mathbf{1} & b_{tx_1}\mathbf{1} \end{bmatrix}_{NM \times 2}. \tag{3.37}$$

Using the time delay estimation error covariance matrix in (3.21) and the linear transformation matrix $\mathbf{D}$ in (3.36), the following covariance matrix is computed:

$$[\mathbf{C}_{\theta_{simo}}]_{2\times2} = \eta_f \left[(\mathbf{H}_{rx} + \mathbf{H}_{tx1})^T \right. \tag{3.38}$$
$$\left. \cdot \left(\mathbf{I} - \frac{1}{MN}\mathbf{1}\mathbf{1}^T \right) (\mathbf{H}_{rx} + \mathbf{H}_{tx1}) \right]^{-1}.$$

With some algebraic manipulation, the expression in (3.38) reduces to:

$$[\boldsymbol{\Sigma}_{\theta_s}]_{2\times2} = \eta_f \mathbf{H}_{simo}^{-1}, \tag{3.39}$$

where $\mathbf{H}_{simo}$ is

$$\mathbf{H}_{simo} = \mathbf{H}_{rx}^T \left(\mathbf{I} - \mathbf{1}\mathbf{1}^T \right) \mathbf{H}_{rx}. \tag{3.40}$$

The spatial matrix in the SIMO case, $\mathbf{H}_{simo}$, is independent of the transmitting sensor location. It is apparent that the spatial advantage is solely reliant on the spread of the receiving radars with respect to the target.

Using the same optimal sensor placement scheme as in the MIMO case for the receiving radars, the sub-matrices in (3.40) are computed,

$$\mathbf{H}_{rx}^T \mathbf{H}_{rx} = \frac{NM}{2}\mathbf{I} \tag{3.41}$$
$$\mathbf{H}_{rx}^T \left(\mathbf{1}\mathbf{1}^T \right) \mathbf{H}_{rx} = 0.$$

Applying (3.41) to (3.39), the minimal MSEs $\sigma_{x_{min}}^2$ and $\sigma_{y_{min}}^2$ are defined by the diagonal elements in,

$$[\mathbf{C}_{\theta_{mimo}}]_{2\times2} (opt) = \eta_f \frac{2}{MN}\mathbf{I}, \tag{3.42}$$

offering a spatial advantage of $tr(\mathbf{H}_{simo}) = \frac{4}{MN}$.

3.2.3 Discussion

The covariance matrix for the target localization was derived, and the minimal MSEs were calculated and given in (3.35) and (3.42). The following features of coherent MIMO and SIMO localization are worth noting:

- The spatial advantage is determined by the footprint of the multiple sensor system relative to the target location. A MIMO system with $M \geq 3$ transmitters and $N \geq 3$ receivers, positioned optimally with respect to the target, has twice the spatial advantage of a SIMO system with 1 transmitter and MN receivers.

- The MIMO system has a considerable advantage by employing $K = M+N$ sensors, whereas the SIMO system employs $K = (MN + 1)$ sensors. This gain becomes significant for a large number of sensors, where $(M + N) \ll MN$.

The effect of the sensors and the target positions on the expressions in (3.32) and (3.39) for other than optimal setting cannot be intuitively identified. A more suitable method to express these relations is employed in the next section. These evaluation tools incorporate the mapping of spatial advantage over a given geographical area, using the GDOP metric.

3.3 GDOP

In Chapter 2 Section 2.4, optimal sensor location that minimize the CRLB was discussed . In practice, radars deployment is a given one. The question si - what is the localization accuracy performance of an existing radars spread and a specific target location? GDOP is a metric that addresses this question. The GDOP is commonly used in GPS systems for mapping the attainable localization accuracy for a given layout of GPS satellites positions

[39, 40]. The GDOP metric emphasizes the effect of sensor locations by normalizing the localization error with the term contributed by the range estimate.

3.3.1   GDOP for MIMO

The GDOP metric is commonly defined as:

$$\text{GDOP} = \frac{1}{\sigma_R} tr\left(cov(X)\right) \tag{3.43}$$

where σ_R^2 is the range (delay) measurements error, defined by standard deviation of the time delays $c^2 \sigma_\epsilon^2$. $cov(X)$, where $cov(\circ)$ stands for the covariance matrix. For the two dimensional case, where $X = (x, y)$, it is:

$$\text{GDOP} = \sqrt{\frac{\sigma_x^2 + \sigma_y^2}{c^2 \sigma_\epsilon^2}}, \tag{3.44}$$

where σ_x^2 and σ_y^2 are the variances of localization on the x and y axis, respectively. A one dimensional metric is defined: the horizontal x-axis DOP (HxDOP) and horizontal y-axis DOP (HyDOP), as:

$$\text{HxDOP} = \sqrt{\frac{\sigma_x^2}{c^2 \sigma_\epsilon^2}}, \tag{3.45}$$

$$\text{HyDOP} = \sqrt{\frac{\sigma_y^2}{c^2 \sigma_\epsilon^2}}. \tag{3.46}$$

The BLUE MSEs given in (3.15), (3.16), (3.25) and (3.26), are used together with the time delay variances in (3.11) and (3.21), to evaluate the GDOP metric for MIMO radar

systems with noncoherent and coherent processing. The following GDOP expression is obtained for noncoherent processing,

$$\text{GDOP}_{B\_nc} = \sqrt{\frac{g_{1B_{nc}} + g_{2B_{nc}}}{\left(g_{1B_{nc}}g_{2B_{nc}} - h_{nc}^2\right)}}, \tag{3.47}$$

where it is assumed $SNR_{\ell k} = SNR_{\zeta} = SNR_o$, $\beta_{R_k}^2 \simeq 1$ and therefore, $\sigma_{\epsilon_{nc}}^2 = \frac{1}{8\pi^2\beta^2 SNR_o} = \frac{\eta_{nc}}{c^2}$. In this case, the GDOP metric isolates the effect of the sensors and target locations on the MIMO gain performance.

For coherent processing case,

$$\text{GDOP}_{B\_c} = \sqrt{\frac{g_{1B_c} + g_{2B_c}}{\left(g_{1B_c}g_{2B_c} - h_c^2\right)}}, \tag{3.48}$$

where $\sigma_{\epsilon_c}^2 = \frac{1}{8\pi^2 f_c^2 SNR_o} = \frac{\eta_c}{c^2}$.

In the GDOP expressions in (3.47) and (3.48), the sensors' locations are embedded in the terms a_{tx_k}, a_{rx_ℓ}, b_{tx_k} and b_{rx_ℓ}. The GDOP reduces the combined effect of the locations to a single metric. In this case, the metric is a representation of the MIMO gain. Once the values are mapped, the actual localization overall accuracy σ_{xy}^2 is easily derived by multiplying the GDOP value by $c\sigma_\epsilon$, and for either the x or y coordinates accuracy, by multiplying the HxDOP and HyDOP by $c\sigma_\epsilon$.

Contour plots of the GDOP values are presented in Figures 3.1 and 3.2, for the case of noncoherent and coherent processing, respectively, with $M = N = 4$ radars positioned symmetrically on the $M + N$ vertices of a polygon centered at the origin. The radars are all transmitting orthogonal signals and perform time delay estimations. The GDOP value for a target located at the origin is the same in both plots. This value is consistent with the results indicated in the previous section, i.e., the minimal achievable overall MSE is equal to $\left[\sigma_{xy,c}^2\right]_{c\_opt\_set} = \frac{c^2}{8\pi^2 f_c^2 SNR_o}\frac{2}{MN} = c^2\sigma_\epsilon^2 GDOP_{B\_c\_opt}^2$ and, therefore, $GDOP_{B\_c\_opt} = \sqrt{\frac{2}{MN}}$. In Figure 3.2, The GDOP value for a target located at the origin follows the

analytical result with $GDOP_{B\_c\_opt} = \sqrt{\frac{2}{16}} = 0.35355$. It is noticeable that while this value is minimal for coherent processing, this is not the case for noncoherent processing, where curves indicating GDOP values of 0.32 and 0.34 may be found in Figure 3.1. The distribution of the GDOP values has different characteristics for each case. In the coherent case, targets located inside the virtual $(N + M)$-sided polygon formed by the sensors locations demonstrate lower GDOP values than targets located outside the footprint of the polygon. In particular, the best localization is obtained for a target at the center of the system. The increase in GDOP values from the center to the polygon perimeter is slow. Outside the footprint, the GDOP values increase rather rapidly (as manifested by the density of contours). In the noncoherent case, the lowest GDOP values are obtained at the perimeter of the virtual $(N + M)$-sided polygon. The distribution of the GDOP value inside the virtual polygon footprint is almost uniform. Outside the system footprint, a slow increase in the GDOP values is observed.
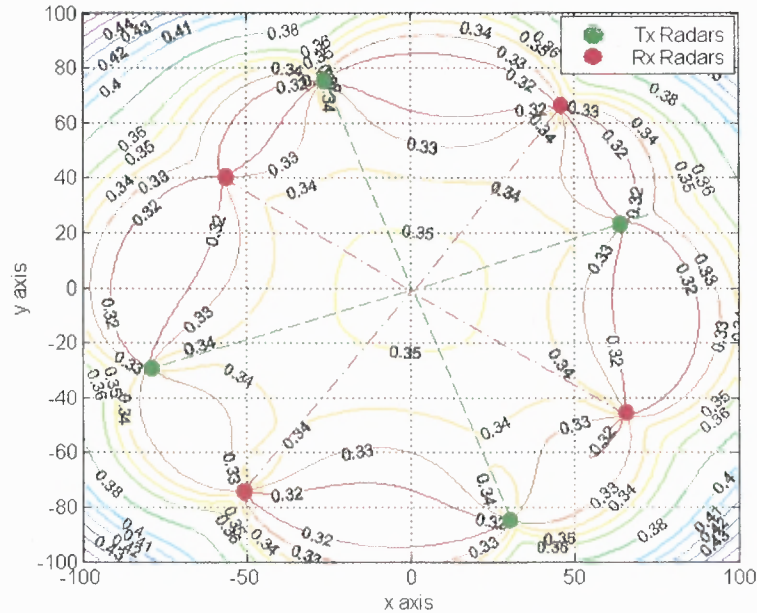
Figure 3.1 Noncoherent GDOP contours with M=N=4.

Contour maps of the HxDOP and HyDOP are presented in Figure 3.3 and Figure 3.4, respectively. The radars are located in a similar manner to the one given in Figures 3.1 and 3.2. The trade-off between the accuracy gains achievable in either the x and y coordinates is demonstrated. In Figure 3.3, the curves with the lowest HxDOP values, ranging from $0.24 - 0.25$, are obtained in the upper and lower most part of the map. Similarly, in Figure 3.4, the lower HyDOP curves, within the same range, are obtained in the right and left most part of the map. With both metric, a target located at the origin benefits from low HxDOP and HyDOP values (of the order 0.25). In the case when better accuracy is required on a single coordinate, the HxDOP and HyDOP maps may serve in the decision making.
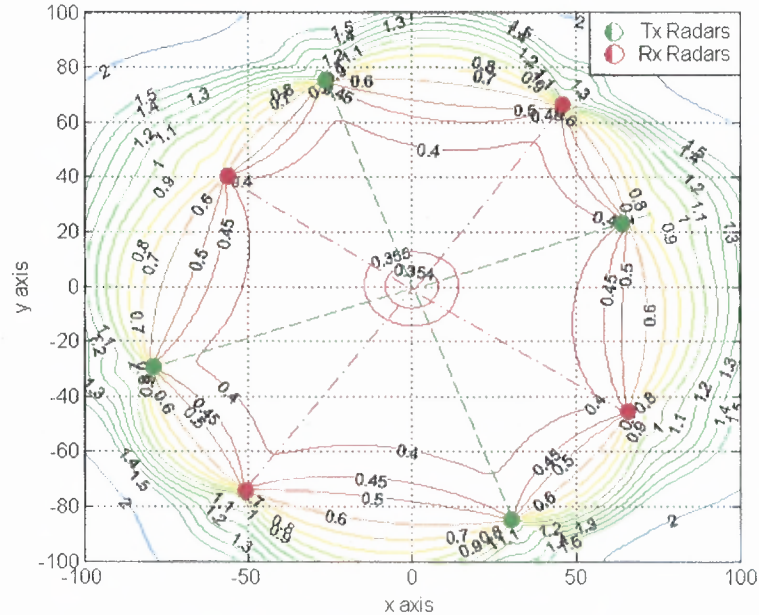
Figure 3.2 Coherent GDOP contours with M=N=4.

In Figures 3.5 and 3.6 contours of $M = N = 4$ of non-symmetrically positioned radars are drawn for noncoherent and coherent processing. When the radars are not spread around the target there is a marked degradation in areas with good measurement accuracy with coherent processing, as demonstrated in Figure 3.6. These examples show that a symmetrical deployment of sensors around the target yields better GDOP values
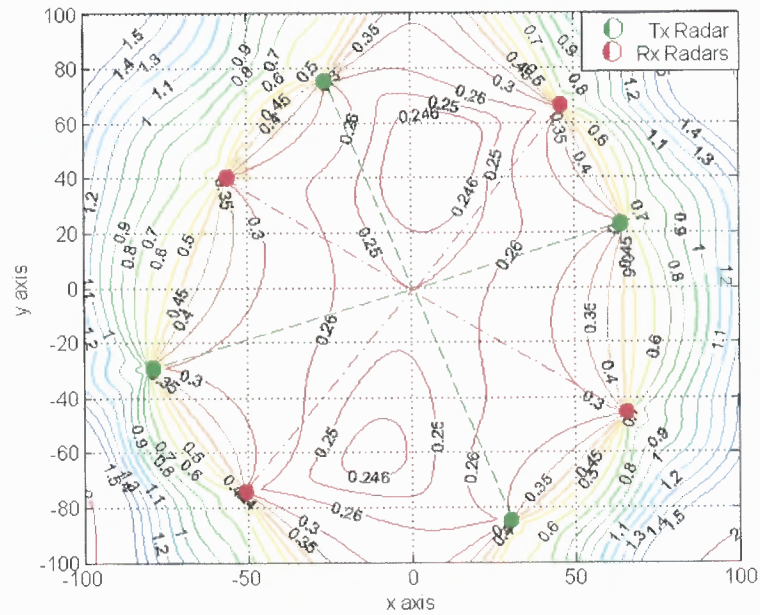
Figure 3.3 Coherent HxDOP contours with M=N=4.
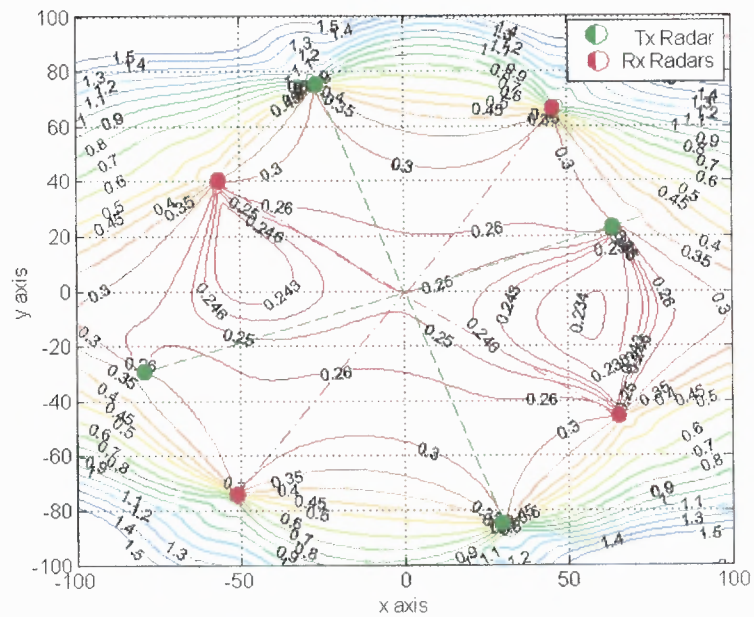
Figure 3.4 Coherent HyDOP contours with M=N=4.

for coherent processing. Noncoherent processing (Figure 3.5) does not show significant degradation with asymmetric placement, though the distribution of lower GDOP curves is different compared with the one observed in Figure 3.1.
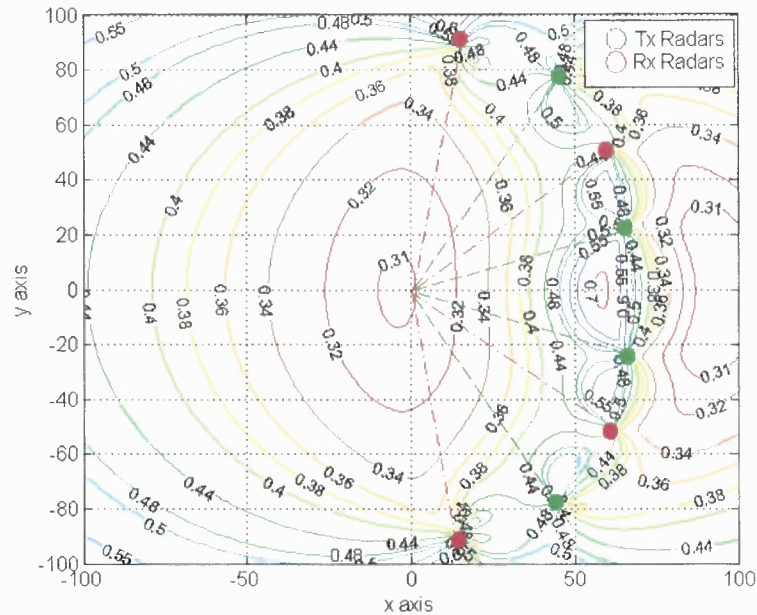
Figure 3.5 Noncoherent GDOP contours with M=N=4 - asymmetrical placement of radars.

Plots of GDOP provide a clear view of high accuracy areas for a given set of radar locations. These plots could also serve as a tool for choosing favorable radar locations to cover a given target area.

3.3.2 GDOP for SIMO

The BLUE MSEs, σ_x^2 and σ_y^2, given by the diagonal elements in (3.32) and (3.39), together with the time delay variance in (3.21) may be used to evaluate the GDOP metric for the MIMO and SIMO radar systems and passive systems. The expression for the GDOP is as follows:
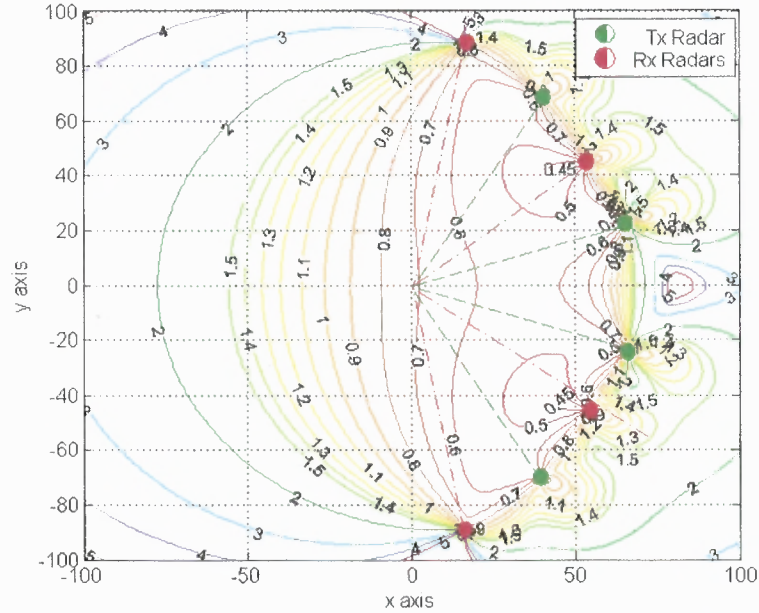
Figure 3.6 Coherent GDOP contours with M=N=4 - asymmetrical placement of radars.

$$\text{GDOP}_m = \sqrt{tr\left(\mathbf{H}_{mimo}\right)} \qquad (3.49)$$

$$\text{GDOP}_s = \sqrt{tr\left(\mathbf{H}_{simo}\right)}. \qquad (3.50)$$

The GDOP reduces the combined effect of the locations to a single metric. In this case, the metric is a representation of the square root of the spatial advantage, exemplified through the trace of matrices $\mathbf{H}_{mimo}$ and $\mathbf{H}_{simo}$. Once the values are mapped, the actual localization overall accuracy $\sqrt{\sigma_x^2 + \sigma_y^2}$ is easily derived by multiplying the GDOP value by $c\sigma_\varepsilon$.

In Figure 3.7 contour plots of the GDOP values are presented for a coherent MIMO radar system with $M = 3$ and $N = 5$ transmit and receive radars, respectively, positioned symmetrically on the $K = M + N = 8$ vertices of a polygon centered at the origin. In Figure 3.8, GDOP plots for a coherent SIMO radar system with one transmitter, $M = 1$, and $N = 15$ receivers are drawn, where the radars are positioned symmetrically on the
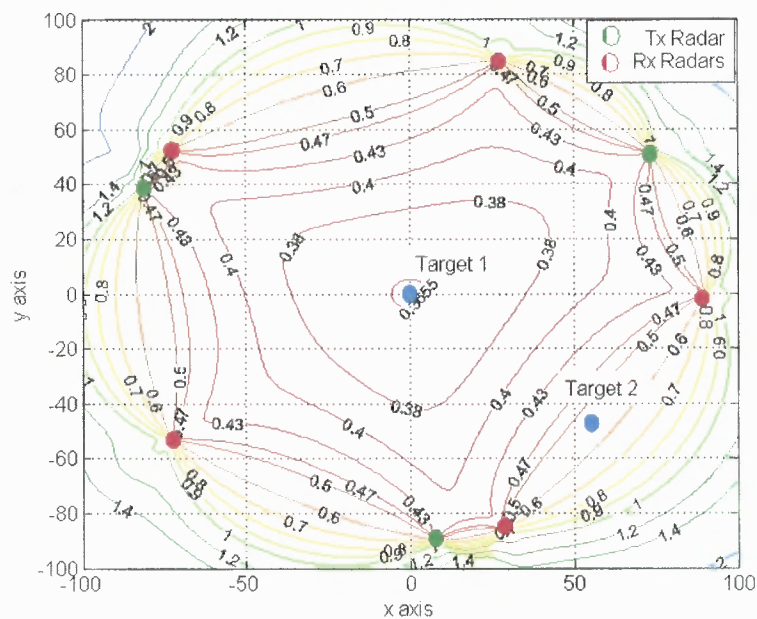
Figure 3.7 GDOP contour maps for coherent MIMO radar with $M = 3$ transmitters and $N = 5$ receivers - case I.
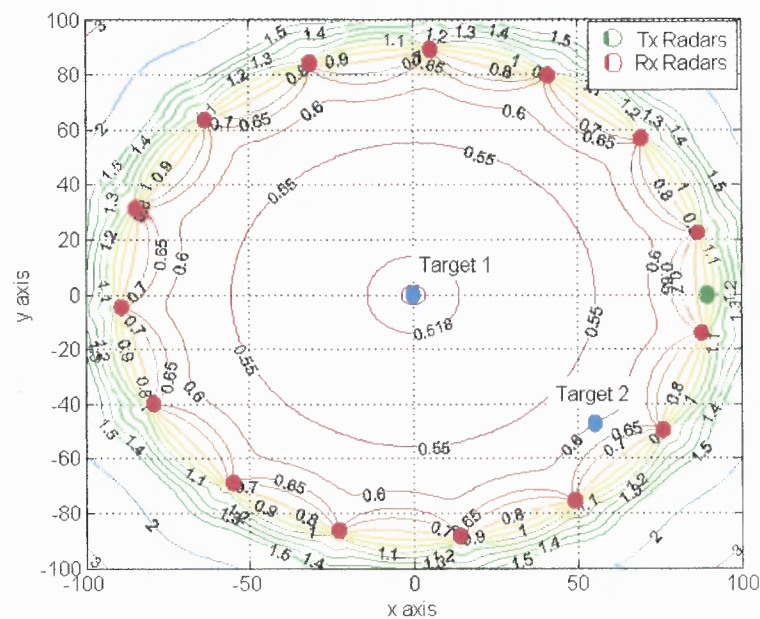
Figure 3.8 GDOP contour maps for coherent SIMO radar with $M = 1$ transmitter and $N = 15$ receivers - case I.

$K = MN = 15$ vertices of a polygon centered at the origin. These symmetrical placement around the axis origins is referred as case I. Target 1 in both Figures 3.7 and 3.8 is located optimally with respect to the sensors. Recalling the results in (3.32) and (3.39), the ratio $\frac{GDOP^2_{mimo}(t1)}{GDOP^2_{simo}(t1)} = \frac{(0.3652)^2}{(0.5164)^2} = 0.5$ is consistent with the results indicated in the previous section. Targets located inside the virtual $(N + M)$ (in Figure 3.7) or MN (in Figure 3.8) -sided polygon formed by the sensors locations demonstrate lower GDOP values than targets located outside the footprint of the polygon. In particular, the best localization is obtained for a target at the center of the system. The increase in GDOP values from the center to the polygon perimeter is slow. The ratio between the GDOPs for the MIMO and the SIMO cases demonstrates an increase from 0.5 at the center (for target 1) to about $\frac{GDOP^2_{mimo}(t2)}{GDOP^2_{simo}(t2)} = \frac{(0.55)^2}{(0.6)^2} = 0.84$ at target 2 location, closer to the polygon perimeter.
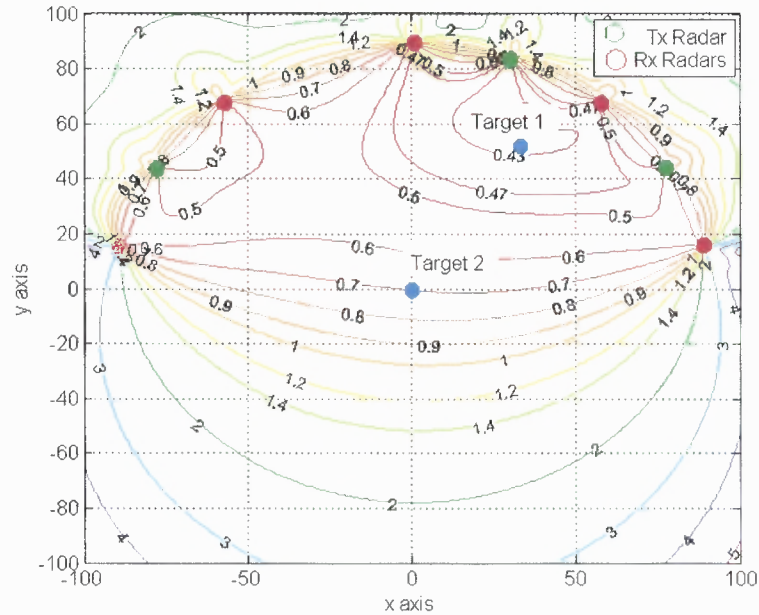
Figure 3.9 GDOP contour maps for coherent MIMO radar with $M = 3$ transmitters and $N = 5$ receivers - caseII.

In Figures 3.9 and 3.10 the sensors are deployed non-symmetrically with respect to the axis origins, hereafter referred to as case II. Contour plots of the GDOP values for a MIMO and SIMO with the same number of transmitters and receivers as in case I are given
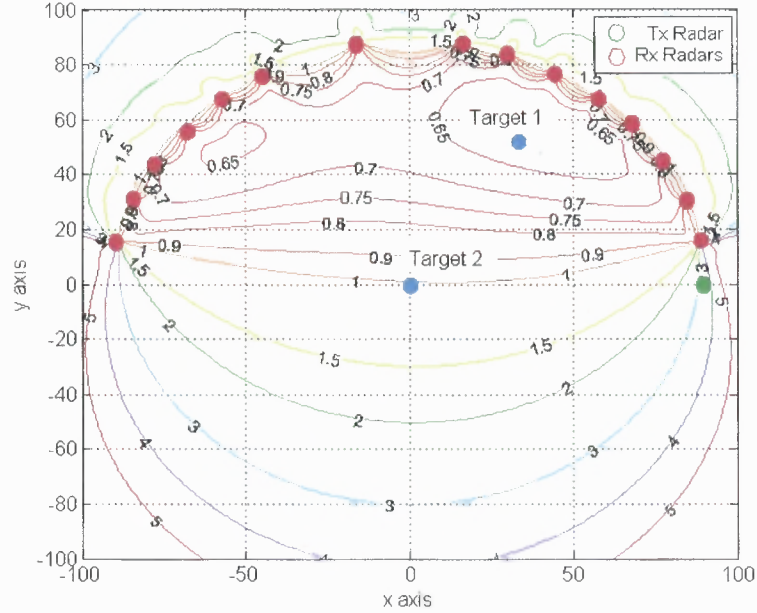
Figure 3.10 GDOP contour maps for coherent SIMO radar with $M = 1$ transmitter and $N = 15$ receivers - case II.

in these figures. For both, the spatial advantage does not reach the optimal value obtained in the symmetrical case. For target 1 in Figure 3.9 and 3.10, the ratio $\frac{GDOP^2_{mimo}(t1)}{GDOP^2_{simo}(t1)} = 0.466 <$ 0.5, i.e., the SIMO case experience a higher lose in performance compared with the MIMO scheme. This is further emphasized by target 2, where in the SIMO case $GDOP^2_{simo}(t2) > 1$ while $GDOP^2_{mimo}(t2) \simeq 0.5$. Case II indicates that for non-symmetrically deployments of sensors, a larger degradation in the coverage area benefiting from spatial advantage is observed with SIMO systems vs. MIMO systems.

3.4 Conclusions

Analytical expressions were derived for the MSE of the BLUE estimator for the cases of coherent MIMO and SIMO radar systems with widely distributed antenna. Both systems benefit from a spatial advantage imparted by the wide footprint of the multiple sensors. It turns out that when the sensors are placed optimally with respect to the target, the MIMO

configuration with M transmitters and N receiers (i.e., $M + N$ total sensors) has twice the spatial advantage of SIMO systems with 1 transmitter and MN receivers (i.e., $1 + MN$ total sensors). This advantage is inherent in the GDOP metric and is directly related to the layout of the sensors with respect to the target and the number of transmitting and receiving radars. The GDOP plots offer a clear insight into the relation between sensor configuration and localization accuracy. These plots demonstrate the superiority of MIMO systems over SIMO schemes in both spatial advantage and the resources required to achieve these performances.

CHAPTER 4

MULTIPLE TARGETS LOCALIZATION

The study of the single target case is extended to the case of multiple targets localization with coherent MIMO radar systems, dealing with the possible trade-offs that the increased number of targets impose on the localization accuracy performance. The CRLB is derived and evaluated for this case. Coherency and spatial advantages are identified and analyzed. As the spatial advantage is strongly reliant on the geographical setting of the radars with respect to the targets and on the geometric distribution of targets, an insight into the system inherent trade-offs is provided using numerical analysis.

4.1   System Model

Assume M transmitting radars and N receiving radars, widely distributed and time and phase synchronized. The receiving radars could be colocated with the transmitting ones or widely separated. The transmitting and receiving radars are located in a two dimensional plane (x, y). Consider Q point targets located at coordinates $X_q = (x_q, y_q)$, $q = 1, ..., Q$ (see Figure 4.1). A set of orthogonal waveforms is transmitted, with the lowpass equivalent $s_k(t)$, $k = 1, \ldots, M$. The power of the transmitted waveforms is normalized such that the aggregate power transmitted by the sensors is constant, irrespective of the number of transmit sensors. Let all transmitted waveforms be narrowband signals with individual effective bandwidth β_k defined as $\beta_k^2 = \left[\left(\int_{W_k} f^2 |S_k(f)|^2 df \right) / \left(\int_{W_k} |S_k(f)|^2 df \right) \right]$, where the integration is over the range of frequencies with non-zero signal content W_k [29]. The signals are narrowband in the sense that for a carrier frequency of f_c, the narrowband signal assumption implies $\beta_k^2 / f_c^2 \ll 1$. Assume the Q targets are located in a search cell of $\pm W/2$. The target model follows the one developed in [42], generalizing the complex target model in [29] to a near-field scenario and distributed sensors. In [42] it is shown

that a complex target located at $X_q = (x_q, y_q)$ may be equivalently defined as a point scatterer with complex amplitude $\zeta^q = \zeta_{re}^q + j\zeta_{im}^q$ and time delays $\tau_{\ell k}(X_q)$. To simplify the notation, the signal power term is embedded in the noise variance term such that the signal-to-noise ratio (SNR) at the transmitter, denoted SNR_t, and defined as the transmitted power by a sensors divided by the noise power at a receiving sensor, is set at a desired level. The following notation are defined for later use: $\tau_{\ell k}^q = \tau_{\ell k}(X_q)$, $\tau^q = [\tau_{11}^q, ..., \tau_{MN}^q]$, and $\zeta^q = [\zeta_{re}^q, \zeta_{im}^q]$.
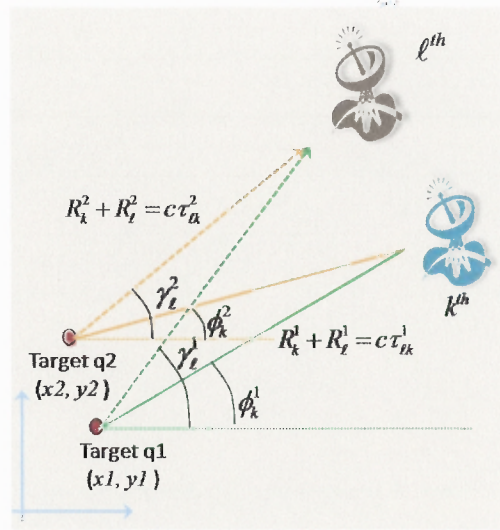
Figure 4.1 Multiplr targets signal model.

In the model developed below, path loss effects are neglected, i.e., the model accounts for the effect of the sensors/target localizations only through time delays (or phase shifts) of the signals. For convenience, a $4Q$ dimensioned vector θ is defined for of the unknown parameters:

$$\theta \stackrel{\text{def}}{=} \left[x_1, y_1, ..., x_Q, y_Q, \zeta^1, ..., \zeta^Q \right]^T. \tag{4.1}$$

The propagation time estimate of a signal transmitted by the k-th transmitting radar located at coordinates $T_k = (x_{tk}, y_{tk})$,reflected by a target located at $X_q = (x_q, y_q)$ and

received by a radar located at $R_\ell = (x_{r\ell}, y_{r\ell})$ can be expressed as:

$$\widehat{\tau}_{\ell k}^q = \tau_{\ell k}^q + \varepsilon_{\ell k}^q,$$

$$k = 1, .., M; \quad \ell = 1, .., N; \quad q = 1, .., Q \tag{4.2}$$

where $\tau_{\ell k}^q$, the propagation time, is the sum of the time delays from radar k to target q and from the target to radar ℓ:

$$\tau_{lk}^q = \frac{1}{c} \left(\sqrt{(x_{tk} - x^q)^2 + (y_{tk} - y^q)^2} \right.$$

$$\left. + \sqrt{(x_{r\ell} - x^q)^2 + (y_{r\ell} - y^q)^2} \right), \tag{4.3}$$

and $\varepsilon_{\ell k}^q$ is the estimation error. The speed of light is denoted by c.

Consider the case of a baseband representation of the signal observed at sensor ℓ due to a transmission from sensor k and reflection from Q scatterers, given by:

$$r_\ell(t) = \sum_{q=1}^{Q} \sum_{k=1}^{M} \zeta^q s_k \left(t - \tau_{\ell k}^q\right) \rho_{\ell k}^q + w_\ell(t), \tag{4.4}$$

where $\rho_{\ell k}^q$ accounts for the phase information and has the value of $\rho_{\ell k}^q = \exp\left(-j2\pi f_c \tau_{\ell k}^q\right)$. Others terms are the carrier frequency f_c , and $w_\ell(t)$ is circularly symmetric, zero-mean, complex Gaussian noise, spatially and temporally white with autocorrelation function $\sigma_w^2 \delta(\tau)$. Define the vectors $\mathbf{r} = [r_1(t), \ldots, r_N(t)]^T$ and $\psi = \left[\tau^1, \ldots, \tau^Q, \zeta^1, .., \zeta^Q\right]^T$ for later use. The received signal at each sensor is a mixture of the transmitted signals reflected by the targets. The mixture of signals is separated at the receiver end by exploiting the orthogonality between the transmitted waveforms.

4.2   The CRLB on Targets Location Estimation

The CRLB provides a lower bound for the mean square error (MSE) of any unbiased estimator for an unknown parameter(s). Given a vector parameter θ, its unbiased estimate $\widehat{\theta}$ satisfies the following inequality [26]:

$$E_\theta \left\{ \left(\widehat{\theta}_i - \theta_i \right) \left(\widehat{\theta}_i - \theta_i \right)^T \right\} \geq \left[\mathbf{J}^{-1}(\theta) \right]_{i,i}, \tag{4.5}$$

where $\mathbf{J}(\theta)$ is the Fisher Information matrix (FIM) given by:

$$\mathbf{J}(\theta) \overset{\text{def}}{=} E_\theta \left\{ \frac{\partial}{\partial \theta} \log p(\mathbf{r}|\theta) \left(\frac{\partial}{\partial \theta} \log p(\mathbf{r}|\theta) \right)^H \right\}, \tag{4.6}$$

where $p(\mathbf{r}|\theta)$ is the joint probability density function (pdf) of θ.

Let the CRLB matrix be defined as:

$$\mathbf{C}_{CRLB} = \left[\mathbf{J}(\theta) \right]^{-1}. \tag{4.7}$$

Since the received signal in (4.4) is defined as a function of the time of arrival, $\tau_{\ell k}^q$, and the reflectivity value $\zeta^q = \zeta_{re}^q + j\zeta_{im}^q$, with the use of the *chain rule*, $\mathbf{J}(\theta)$ could be decomposed to an alternative form [26] where the FIM is express as :

$$\mathbf{J}(\theta) = \begin{bmatrix} \mathbf{D} & \mathbf{0} \\ \mathbf{0} & \mathbf{I}_{2Q \times 2Q} \end{bmatrix} \cdot \mathbf{J}(\psi) \cdot \begin{bmatrix} \mathbf{D} & \mathbf{0} \\ \mathbf{0} & \mathbf{I}_{2Q \times 2Q} \end{bmatrix}^T, \tag{4.8}$$

where $\mathbf{J}(\psi)$ is the FIM for the unknown vector ψ, defines as:

$$\mathbf{J}(\psi) = E_\psi \left\{ \frac{\partial}{\partial \psi} \log p(\mathbf{r}|\psi) \left(\frac{\partial}{\partial \psi} \log p(\mathbf{r}|\psi) \right)^H \right\}. \tag{4.9}$$

The matrix **D** represents is of the form:

$$
\mathbf{D} = -\frac{1}{c}
\begin{bmatrix}
\mathbf{D}^1 & \cdots & \mathbf{0}_{2 \times MN} \\
\vdots & \ddots & \vdots \\
\mathbf{0}_{2 \times MN} & \cdots & \mathbf{D}^Q
\end{bmatrix}_{2Q \times MNQ}
, \tag{4.10}
$$

where the submatrix $\mathbf{D}^q$ is derived as:

$$
\mathbf{D}^q =
\begin{bmatrix}
\frac{\partial \tau_{11}^q}{\partial x^q} & \cdots & \frac{\partial \tau_{MN}^q}{\partial x^q} \\
\frac{\partial \tau_{11}^q}{\partial y^q} & \cdots & \frac{\partial \tau_{MN}^q}{\partial y^q}
\end{bmatrix}_{2 \times MN}
. \tag{4.11}
$$

By using the relation given in (4.3) in (4.11), the $\mathbf{D}^q$ matrix is calculated, resulting in:

$$
\mathbf{D}^q =
\begin{bmatrix}
a_{tx_1}^q + a_{rx_1}^q & a_{tx_1}^q + a_{rx_2}^q & \cdots & a_{tx_M}^q + a_{rx_N}^q \\
b_{tx_1}^q + b_{rx_1}^q & b_{tx_1}^q + b_{rx_2}^q & \cdots & b_{tx_M}^q + b_{rx_N}^q
\end{bmatrix}
, \tag{4.12}
$$

such that:

$$
\begin{aligned}
a_{tx_k}^q &= \cos\phi_k^q; \quad b_{tx_k}^q = \sin\phi_k^q; \quad k = 1, .., M, \quad q = 1, ..., Q \\
a_{rx_\ell}^q &= \cos\varphi_\ell^q; \quad b_{rx_\ell}^q = \sin\varphi_\ell^q; \qquad \ell = 1, .., N, \\
\phi_k^q &= \tan^{-1}\left(\frac{y^q - y_{tk}}{x^q - x_{tk}}\right); \quad \varphi_\ell^q = \tan^{-1}\left(\frac{y^q - y_{r\ell}}{x^q - x_{r\ell}}\right),
\end{aligned} \tag{4.13}
$$

where the phase ϕ_k^q is the bearing angle of the transmitting sensor k to target q measured with respect to the x axis; the phase φ_ℓ^q is the bearing angle of the receiving radar ℓ to target q measured with respect to the x axis. See illustration in Figure 4.1. Matrix $\mathbf{D}^q$ includes the geometric information of the radars location configuration relative to the position of the qth target.

In order to derive the FIM given in (4.9) the joint pdf $p\left(\mathbf{r}|\psi\right)$ is required. Given a set of known waveforms $s_k\left(t - \tau_{\ell k}^q\right)$ parameterized by the unknown time delays $\tau_{\ell k}^q$, which in turn are a function of the unknown targets locations $X_q = (x_q, y_q)$, for the signal

model (4.4), the joint pdf of the observations (time samples at multiple receive antennas) parameterized by the unknown parameters vector ψ, is then:

$$p\left(\mathbf{r}|\psi\right) \propto \exp \tag{4.14}$$

$$\left\{-\frac{1}{\sigma_w^2}\sum_{\ell=1}^{N}\int_T \left|r_\ell(t) - \sum_{q=1}^{Q}\sum_{k=1}^{M}\zeta^q s_k\left(t - \tau_{\ell k}^q\right)\rho_{\ell k}^q\right|^2 dt\right\}.$$

An expression for the FIM $\mathbf{J}\left(\psi\right)$, is derived in Appendix D, yielding:

$$\mathbf{J}_{multi}(\psi) = 8\pi^2 \operatorname{SNR} f_c^2 \begin{bmatrix} \boldsymbol{\Gamma}_\mathbf{x} & \mathbf{V}^T \\ \mathbf{V} & \boldsymbol{\Sigma}_\zeta \end{bmatrix}_{(2+MN)Q\times(2+MN)Q}, \tag{4.15}$$

with the block matrices $\boldsymbol{\Gamma}_\mathbf{x}$, $\boldsymbol{\Sigma}_\zeta$, and $\mathbf{V}$ defined in the Appendix D in (D.5), (D.9), and (D.11), respectively.

In order to determine the value of $\mathbf{J}\left(\theta\right)$, (4.15) and (4.10) are used in (4.8), to obtain the following FIM matrix:

$$\mathbf{J}_{multi}\left(\theta\right) = \frac{8\pi^2 \operatorname{SNR} f_c^2}{c^2} \begin{bmatrix} \mathbf{D}\boldsymbol{\Gamma}_\mathbf{x}\mathbf{D}^T & \mathbf{D}\mathbf{V}^T \\ \mathbf{V}\mathbf{D}^T & \boldsymbol{\Sigma}_\zeta \end{bmatrix}_{4Q\times 4Q}. \tag{4.16}$$

While the CRLB expresses the lower bound on the variance of the estimate of $\theta = \left[x_1, y_1, ..., x_Q, y_Q, \zeta^1, ..., \zeta^Q\right]^T$, only the estimation of the targets locations $X_q = \left(x_q, y_q\right)$ is of interest. The terms ζ^q serve as nuisance parameters. For the variances of the estimates of x_q and y_q, it is sufficient to derive the $2Q \times 2Q$ upper left submatrix $\left[\mathbf{C}_{CRLB_{multi}}\right]_{2Q\times 2Q} = \left[\mathbf{J}_{multi}\left(\theta\right)\right]_{2Q\times 2Q}^{-1}$ which can be expressed as:

$$\left[\mathbf{C}_{CRLB_{multi}}\right]_{2Q\times 2Q} = \eta\left(f_c\right)\left(\mathbf{D}\boldsymbol{\Gamma}\mathbf{D}^T - \mathbf{V}\mathbf{D}^T\boldsymbol{\Sigma}_\zeta^{-1}\mathbf{D}\mathbf{V}^T\right)^{-1}, \tag{4.17}$$

where $\eta\left(f_c\right) = \frac{c^2}{8\pi^2 \operatorname{SNR} f_c^2}$. The diagonal elements of the submatrix $\left[\mathbf{C}_{CRLB_{multi}}\right]_{2Q\times2Q}$ provide the lower bound on the localization mean squared error (MSE), $\sigma_{x_q}^2 \geq \sigma_{CRx_q}^2 = \left[\mathbf{C}_{CRLB_{multi}}\right]_{2q-1,2q-1}$ and $\sigma_{y_q}^2 \geq \sigma_{CRy_q}^2 = \left[\mathbf{C}_{CRLB_{multi}}\right]_{2q,2q}$, where these terms may be defined as:

$$\sigma_{CRx_q}^2 = \eta\left(f_c\right) \cdot \eta_{Spt}\left(x_q\right) \tag{4.18}$$

$$\sigma_{CRy_q}^2 = \eta\left(f_c\right) \cdot \eta_{Spt}\left(y_q\right), \tag{4.19}$$

and

$$\eta_{Spt}\left(x_q\right) = \left[\left(\mathbf{D}\mathbf{\Gamma_x}\mathbf{D}^T - \mathbf{V}\mathbf{D}^T\mathbf{\Sigma}_\zeta^{-1}\mathbf{D}\mathbf{V}^T\right)^{-1}\right]_{2q-1,2q-1} \tag{4.20}$$

$$\eta_{Spt}\left(y_q\right) = \left[\left(\mathbf{D}\mathbf{\Gamma_x}\mathbf{D}^T - \mathbf{V}\mathbf{D}^T\mathbf{\Sigma}_\zeta^{-1}\mathbf{D}\mathbf{V}^T\right)^{-1}\right]_{2q,2q},$$

The CRLB matrix is related to the sensors and targets locations through matrices $\mathbf{D}$, $\mathbf{\Gamma_x}$ and $\mathbf{V}$, while the latter two are also functions of the received waveforms correlation functions and its derivatives. This dependency is captured in the terms $\eta_{Spt}\left(x_q\right)$ and $\eta_{Spt}\left(y_q\right)$, where further analysis is required.

4.3 Discussion

The expression for the CRLB as given in (2.38), provides insight into the performance of multiple targets localization accuracy performance of MIMO radars systems with coherent processing.

Coherency advantage As in the single target case, the lower bound on the targets localization errors is inversely proportional to the carrier frequency f_c and independent of the signal individual effective bandwidth, due to the use of the phase information across the different paths. It is apparent that coherent processing offers a target localization precision gain of the order of f_c/β, referred to as *coherency advantage*.

The improvement in localization accuracy needs to be moderated with the observation that the CRLB is a bound of *small errors*. As such, it ignores effects that could lead to *large errors*. For example, MIMO radar with distributed sensors and coherent observations is subject to high sidelobes [1]. Additionally, a phase coherent system is sensitive to phase errors. These topics are outside the scope of this paper, but they should be kept in perspective.

Spatial advantage The CRLB submatrix terms are strongly reliant on the relative geographical spread of the radar sensors versus the targets locations. In MIMO radar, the targets play a similar role to the transmission channel in MIMO communication. As such, the elements in the CRLB, $\Gamma_x^{qq'}$ and $\mathbf{V}^{qq'}, q \neq q\prime$ may be viewed as overlapping multipath arrivals for a given ℓk propagation path. The trace of the CRLB provides an averaged spatial term $\eta_{Spt} = \frac{1}{Q}\sum_{q=1}^{Q} (\eta_{Spt}(x_q) + \eta_{Spt}(y_q))$, and may be written as:

$$\eta_{Spt} = \mathrm{tr} \left\{ \sum_{q=1}^{Q} \left[\mathbf{D}^q \Gamma^{qq} \mathbf{D}^{q^T} - \mathbf{V}^{qq} \mathbf{D}^{q^T} \Psi^{qq} \mathbf{D}^q \mathbf{V}^{qq^T} - \sum_{q'\neq q=1}^{Q} \mathbf{V}^{qq'} \mathbf{D}^{q'^T} \Psi^{q'q} \mathbf{D}^q \mathbf{V}^{qq'^T} \right] \right\}^{-1} \tag{4.21}$$

where $\Psi^{q'q} = \Sigma_\zeta^{-1}$. The first two terms in (4.21) are the auto-correlation terms, while the third term represents the cross-correlation between targets and therefore, serves as mutual interference. The elements of these cross-correlation matrices are products of the phase and amplitude elements, $\exp\left(-2\pi f_c \Delta \tau_{\ell k}^{qq'}\right)$ and $\int s_k \left(t - \Delta \tau_{\ell k}^{qq'}\right) s_k^*(t)\, dt$, where $\Delta \tau_{\ell k}^{qq'} = \tau_{\ell k}^q - \tau_{\ell k}^{q'}$, and its derivatives (see (D.5) and (D.11) in Appendix D). As the distance between the targets impacts the time delay differences, $\Delta \tau_{\ell k}^{qq'}$, the following might be gleaned by inspection of (4.21):

- Targets separated by distances larger than a c/β resolution cell are resolvable with negligible loss in performance relative to the single target case. This results from the decorrelation achieved by this scenario, where the third term in (4.21) approaches

zero. On the other end, distances smaller than the carrier wavelength λ are non-resolvable.

- The interference on paths ℓk for target q add in-phase with $\frac{c\Delta\tau_{\ell k}^{qq'}}{\lambda} \approx u, u = 0, 1, 2, ...,$ i.e. $\cos\left(-2\pi f_c\Delta\tau_{\ell k}^{qq'}\right) \simeq 1$. They add out-of-phase with $\frac{c\Delta\tau_{\ell k}^{qq'}}{4\lambda} \approx u, u = 1, 2, ...,$ i.e. $\cos\left(-2\pi f_c\Delta\tau_{\ell k}^{qq'}\right) \ll 1$. It is evident that the number of resolvable paths varies with the position of the radars with respect to the targets and the targets layout, where some may be more favorable than others. The number of resolvable propagation paths per target q and the geometric merit of these paths (integrated in matrix $\mathbf{D}^q$) determines the ability to localize target q and the localization accuracy quality. A minimum of 3 resolvable paths is required for the localization of a single target.

- Transmit and receive radar pairs, ℓk, with large aperture with respect to the targets layout are preferable due to the larger time delay differences they offer.

- Sensors placement needs to take into account the vertical and horizontal plane sensitivity needed for a given targets layout. For example, a horizontal targets layout requires better horizontal separation, achieved by broadside horizontal radar geometry.

To get a more intuitive understanding of the reliance of the spatial advantage on the geographical spread of the radars and targets, numerical analysis is employed in the next section for some special cases.

4.4 Numerical Analysis

The spatial advantage in the case of a single target is derived in [42]. It is shown to be equals $2/MN$ under optimal conditions, i.e. when the target is located at the center of a virtual circle created by the radars, and the radars are spread with equal angular spacing with respect to the center ($\frac{2\pi}{M}$ and $\frac{2\pi}{N}$) or any superposition of such symetrical placments. The value of the spatial advantage for any possiable target location with a given radar layout

was evaluated using a metric known as geometric dilution of precision (GDOP). In the case of multiple targets, the spatial advantage relies on the the number of targets and their layout in addition to the radar locations. For this reason, numerical analysis of the expresion in (4.20) for some special cases is employed in this section.

The value of the spatial advantage $\eta_{Spatial}$ is anaylazed for various radars/targets placements senarios. System parameters are set as follows: $\beta_k = \beta = 200\text{KHz}$, carrier frequency $f_c = 2\text{GHz}$ and therefore, the wavelength is $\lambda = 1.5\text{meter}$, SNR=20 and all reflectivity index values are assumed equal $|\zeta^q| = |\zeta| = 1$. In Figure (4.2) the spatial advantage value is drawn for the case of $M = 3$ transmit antennas employed with $N = 3, 4, 5$ receive antennas. Both transmit and receive antennas are located with angular spacing of $\frac{2\pi}{M}$ and $\frac{2\pi}{N}$ with respect the the axis origin. Targets are located in a linear array with the first target located at $(0, 0)$ and the rest located at $(x_q = x_{q-1} + 10, y_q = 0)$. At $Q = 1$, the resulting spatial advantage in Figure (4.2) follow the results for a single target where the values of $\frac{2}{9}$, $\frac{2}{12}$, and $\frac{2}{15}$ are obtained. It is observed that an increas in the number of targets results in a decrease in the spatial advantage and therefore, in the accuracy. This decreas may be moderated by increasing the number of transmit and receive radars, MN. In the case of $M = N = 3$ three targets enjoy spatial advantage while with $M = 3$ and $N = 5$ six targets still benefit from spatial advantage. For the later case, up to four targets are located with high accuracy. In Figure (4.3) the spatial advantage of the x and y axis is draw separtly for the same senario as in Figure (4.2). It conveys the way in which each of the axis performs. It demonstrates that the axis accurecies might vary significantly for the x and y axis. Moreover, the performance gap shrinks as the number of transmit and reveice radar increases, due to the aditional, spatially spread, view points. As mentioned previously, the spatial advantage for the case of a single target is $MN/2$ under optimal conditions, i.e. when the target is located at the center of a virtual circle created by uniformly spaced sensors. In the case of multiple targets, the spatial advantage relies on the number of targets and their layout relative to the sensors locations.
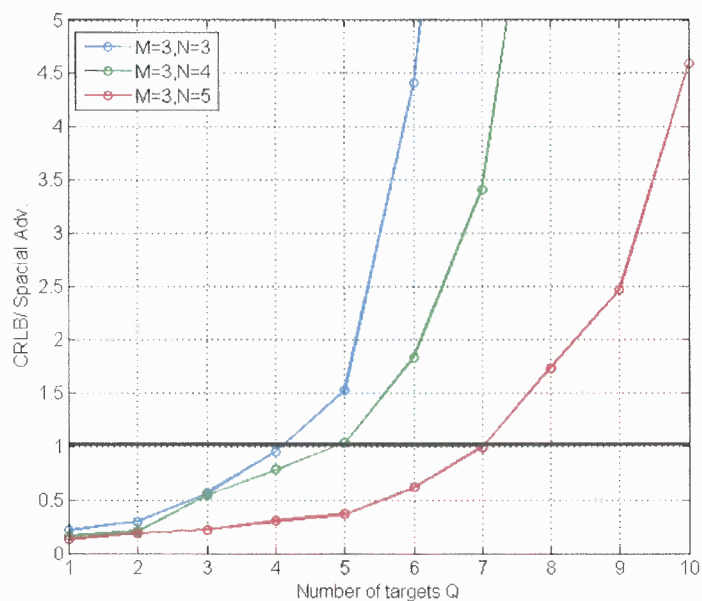
Figure 4.2 Spatial advantage values for the case of M=3 transmitter and N=3, 4, and 5 receivers, symmetrically positioned around the axis origin.
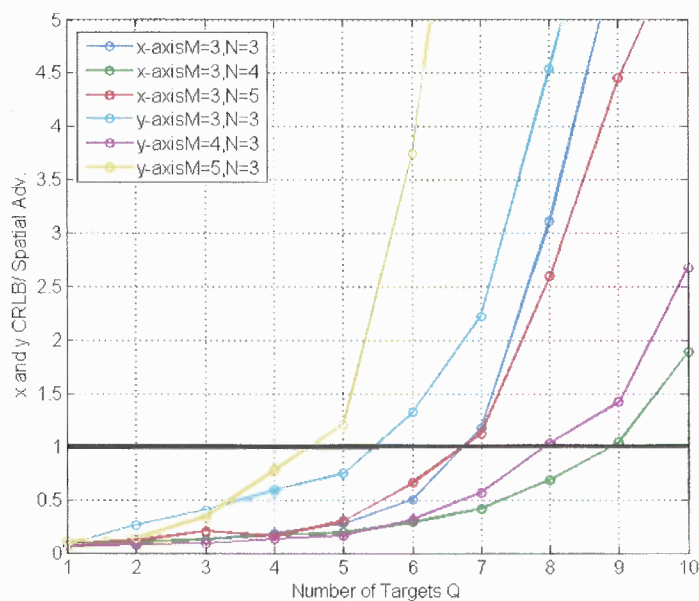
Figure 4.3 Spatial advantage values in x and y for the case of M=3 transmitter and N=3, 4, and 5 receivers, symmetrically positioned around the axis origin.
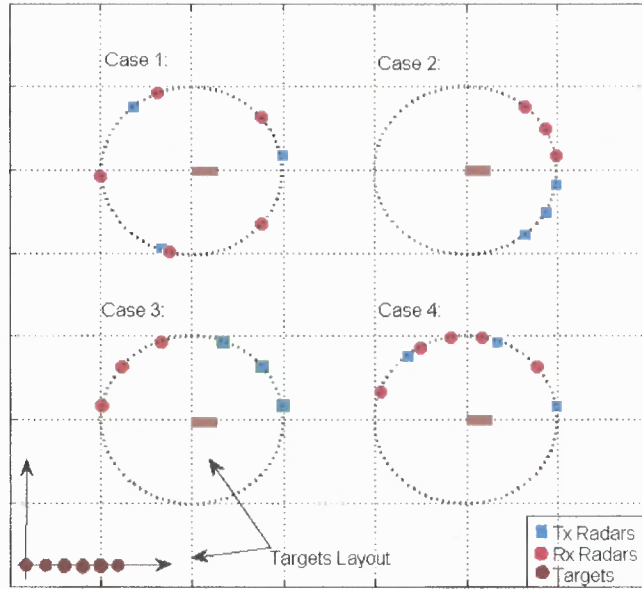
Figure 4.4 System layout for cases 1 to 4.

To identify favorable radars locations with respect to the targets layout, four special cases, demonstrated in Figure (4.4), are analyzed.

The averaged value of η_{Spt} versus the number of targets is drawn in Figure (4.5). Following the discussion in previous section, one needs to avoid $\Delta\tau_{\ell k}^{qq'} \simeq 0$ and keep $\Delta\tau_{\ell k}^{qq'}$ as large as possible. It is observed in the figure that a symmetrical placement, as shown in Case 1, is not an optimal one. Rearranging the radars, in the more favorable setting (as in Case 4) demonstrates a performance gain, in terms of the number of targets and the spatial advantage, achieved without any change in the number of antennas. This is a result of the larger transmit/receive aperture sets contributing to larger delays. Placing the radars in a broadside horizontal spread (as in Case 3) provides better spatial advantage and moderate performance loss rate when compared with Case 2, where a vertical radar setting is used. This is a combined effect of the larger time delays and the impact of matrix $\mathbf{D}$, which provide better horizontal separation in Case 3 [68]. Increasing the number of radars, as can
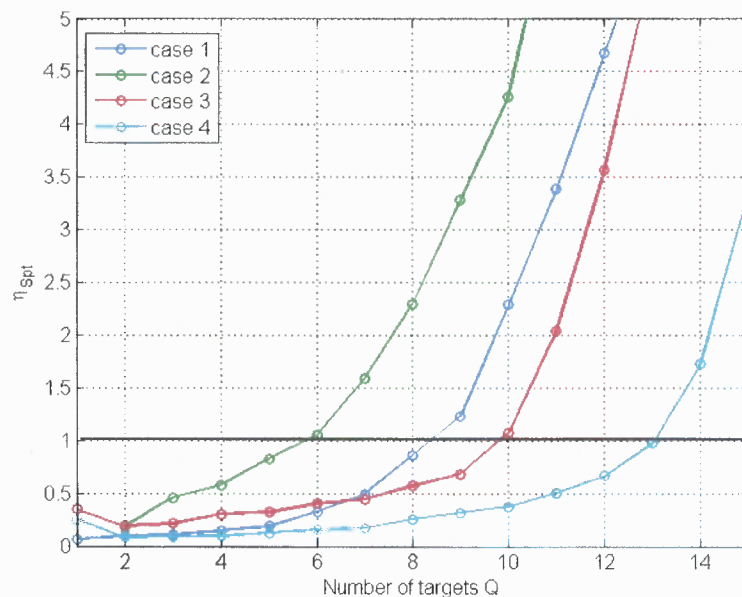
Figure 4.5 Spatial advantage values for cases 1 to 4.

be noticed from comparing Case 3 and Case 4, allows for localization of more targets with higher spatial advantage and restrained performance loss rate.

4.5   Conclusions

The analytical expression for the CRLB for the case of multiple targets localization in coherent MIMO radar systems with widely distributed antenna is derived, demonstrating both coherency advantage and spatial advantage.   Nonetheless, there is a tradeoff between the ability to localize multiple targets and the accuracy with which it can be done, introduced by the mutual interference between the targets' reflected paths. These cross-correlation terms may be controlled by choosing propitious radars locations.   The relation between different sensor schemes and targets layouts on the performance was examined using numerical analysis. It demonstrates the tradeoff between spatial advantage and the number of targets.   It is shown that performance loss may be compensated by increasing the number of transmit and/or receive radars or by rearranging the sensors

locations. As the CRLB provides a good bound at high SNR, a more rigid bound needs to be found for the low SNR case, where the ambiguities predominate the estimation capabilities.

CHAPTER 5

SENSITIVITY ANALYSIS TO PHASE SYNCHRONIZATION MISMATCH

Improvement in target parameter estimation capabilities is among the advantage of MIMO radar systems [1, 42]. In particular, target localization with coherent MIMO radar systems, utilizing widely distributed antennas, offers significant advantages [42]. Typically, performance analysis of system parameter estimation problems is based on the derivation of the Cramer-Rao bound (CRB), which sets a lower bound on the estimation MSE for unbiased estimators. Such an evaluation is provided in Chapter 2 for coherent MIMO radar systems, demonstrating a localization accuracy advantage, inversely proportional to the signal carrier frequency. In addition, a spatial advantage of the order of the product of the number of transmit and receive radars is also incorporated in the CRB.

This performance gain comes with the challenge of attaining phase synchronization in a distributed system. Errors introduced to the system parameters by phase synchronization mismatch, will result in parameter estimation mean-square error (MSE) degradation and bias. In this work, the *hybrid* CRB (HCRB) is used to test the sensitivity of the target localization MSE to phase errors. The HCRB takes into account deterministic unknown parameters, such as the target location, as well as random parameters, phase calibration errors, in this case. This method has been applied to passive source localization [69], [70] for the problem of source bearing and range estimation with uncertainty in the sensors' locations or phase synchronization errors.

In this chapter, the HCRB is derived for coherent MIMO radars, with phase synchronization errors. A closed-form expression for the HCRB for the target's location (x, y) is derived, providing the means to assess the effects of phase errors on the localization accuracy. The effect of the number of radars, their geometric layout, and the phase mismatch MSE is incorporated in the HCRB terms.

In this study, the hybrid Cramer-Rao bound (CRB) is developed for target localization, to establish the sensitivity of the estimation mean-square error (MSE) to the level of phase synchronization mismatch in coherent Multiple-Input Multiple-Output (MIMO) radar systems with widely distributed antennas. The lower bound on the MSE is derived for the joint estimation of the vector of unknown parameters, consisting of the target location and the mismatch of the allegedly known system parameters, i.e., phase offsets at the radars. Synchronization errors are modeled as being random and Gaussian. A closed-form expression for the hybrid CRB is derived for the case of orthogonal waveforms. The bound on the target localization MSE is expressed as the sum of two terms - the first represents the CRB with no phase mismatch, and the second captures the mismatch effect. The latter is shown to depend on the phase error variance, the number of mismatched transmitting and receiving sensors and the system's geometry. For a given phase synchronization error variance, this expression offers the means to analyze the achievable localization accuracy. Alternatively, for a predetermined localization MSE target value, the derived expression may be used to determine the necessary phase synchronization level in the distributed system.

5.1 Background

The hybrid CRB provides a low bound on the MSE of any unbiased estimator for an unknown parameter(s), where the parameters are partially deterministic and partially random [28]. Given a vector parameter $\theta = [\theta_{nr}, \theta_r]^T$, where θ_{nr} stands for the nonrandom parameter vector and θ_r for a random parameter vector, its unbiased estimate $\widehat{\theta}$ satisfies the following inequality [28]:

$$E_{\theta_{nr},\theta_r} \left\{ \left(\widehat{\theta}_i - \theta_i \right) \left(\widehat{\theta}_i - \theta_i \right)^T \right\} \geq \left[\mathbf{J}_H^{-1} \left(\theta_{nr}, \theta_r \right) \right]_{i,i}, \tag{5.1}$$

where $\mathbf{J}_H (\theta)$ is the hybrid Fisher Information matrix (HFIM) expressed as

$$\mathbf{J}_H (\theta_{nr}, \theta_r) = \mathbf{J}_D + \mathbf{J}_P. \tag{5.2}$$

The elements of the matrices $\mathbf{J}_D$ and $\mathbf{J}_P$ given by

$$[\mathbf{J}_D]_{i,j} = -E_{\theta_r|\theta_{nr}}\left\{E_{\mathbf{r}|\theta_{nr},\theta_r}\left\{\frac{\partial \ln p\left(\mathbf{r}|\theta_{nr},\theta_r\right)}{\partial\theta_i\partial\theta_j}\right\}\right\}, \tag{5.3}$$

and

$$[\mathbf{J}_P]_{i,j} = -E_{\theta_r|\theta_{nr}}\left\{\frac{\partial^2 \ln p\left(\theta_r|\theta_{nr}\right)}{\partial\theta_i\partial\theta_j}\right\},$$

where $p\left(\mathbf{r}|\theta_{nr},\theta_r\right)$ is the conditional, joint probability density function (pdf) of the observations and $p\left(\theta_r|\theta_{nr}\right)$ the conditional joint pdf of θ_r. The matrix $\mathbf{J}_D$ represents the contribution of the data and the matrix $\mathbf{J}_P$ represents the contribution of prior information.

The HCRB matrix is defined as

$$\mathbf{HCRB} = \left[\mathbf{J}_H\left(\theta_{nr},\theta_r\right)\right]^{-1}. \tag{5.4}$$

In cases in which the observation statistic is expressed in terms of $p\left(\mathbf{r}|\kappa_{nr},\kappa_r\right)$, and the relationship between the unknown parameters θ_{nr}, θ_r and κ_{nr}, κ_r is given by $\kappa_j = f_j(\theta)$, the *chain rule*, can be used to express $\mathbf{J}_H\left(\theta_{nr},\theta_r\right)$ in an alternative form [26]:

$$\mathbf{J}_H\left(\theta_{nr},\theta_r\right) = \mathbf{P}\left(\mathbf{J}_H\left(\kappa_{nr},\kappa_r\right)\right)\mathbf{P}^T, \tag{5.5}$$

where the elements of the matrix $\mathbf{P}$ are given by $[\mathbf{P}]_{i,j} = \frac{\partial\kappa_j}{\partial\theta_i}$.

5.2 HCRB with Phase Mismatch

In this section, the HCRB is developed for target localization. A point target is assumed with complex reflectivity $\vartheta = \vartheta_{\text{Re}} + j\vartheta_{\text{Im}}$, located in a two dimensional plane at coordinates $X = (x,y)$. Consider a set of M transmitting stations and N receiving stations, widely distributed over a given geographical area, and time and phase synchronized. A set of orthogonal waveforms is transmitted, with the lowpass equivalents $s_k\left(t\right)$, $k = 1,\ldots,M$, and effective bandwidths β [29]. The signals are narrowband in the sense that for a carrier frequency of f_c, the narrowband signal assumption implies $\beta^2/f_c^2 \ll 1$

In [42], perfect phase synchronization was assumed. In practice, synchronization errors exists, modeled here as zero mean Gaussian random variables with standard deviation σ_Δ^2 and denoted by $\Delta\phi = [\Delta\phi_{t_1}, \Delta\phi_{t_2}, ..., \Delta\phi_{t_M}, \Delta\phi_{r_1}, \Delta\phi_{r_2}, ..., \Delta\phi_{r_N}]^T$, where $\Delta\phi_{t_k}$ and $\Delta\phi_{r_\ell}$ are phase errors at transmitting radar k and receiving radar ℓ, respectively. The phase errors introduced by the different stations are assumed to be statistically independent. The vector of unknown parameters is defined by

$$\theta = [\theta_{nr}, \theta_r]^T , \tag{5.6}$$

where $\theta_{nr} = [x, y, \vartheta_{\mathrm{Re}}, \vartheta_{\mathrm{Im}}]$ denotes the deterministic unknowns and $\theta_r = \Delta\phi^T$ denotes the random unknowns.

The estimation process is based on the signals observed at the receiving sensors. The signal received at sensor ℓ is a superposition of the transmitted signals, reflected from the target, and given by:

$$r_\ell(t) = \sum_{k=1}^{M} \vartheta s_k (t - \tau_{\ell k}) \eta_{\ell k} + n_\ell(t), \tag{5.7}$$

where $\eta_{\ell k}$ accounts for the phase information and has the value of $\eta_{\ell k} = \exp(-j2\pi f_c \tau_{\ell k}) \exp(-j(\Delta\phi_{t_k} + \Delta\phi_{r_\ell}))$. The noise $n_\ell(t)$ is assumed to be circularly symmetric, zero-mean, complex Gaussian, spatially and temporally white with autocorrelation function $\sigma_n^2 \delta(\tau)$. The propagation time, $\tau_{\ell k}$, is a sum of the time delays from station k to the target and from the target to station ℓ, and may be expressed as

$$\tau_{\ell k} = \frac{1}{c} \left(\sqrt{(x_{tk} - x)^2 + (y_{tk} - y)^2} \right. \tag{5.8}$$
$$\left. + \sqrt{(x_{r\ell} - x)^2 + (y_{r\ell} - y)^2} \right),$$

where c denotes the speed of light, (x_{tk}, y_{tk}) denotes the location of transmitting radar k and $(x_{r\ell}, y_{r\ell})$ denotes the location of receiving radar ℓ. The following vector notation is introduced: $\tau = [\tau_{11}, \tau_{12}, ..., \tau_{\ell k}, ..., \tau_{NM}]^T$.

The received signals are separated at the receiver by exploiting the orthogonality between the transmitted waveforms. The signal in (5.7) is defined as a function of the time of arrival, $\tau_{\ell k}$, the reflectivity value ϑ, and the phase mismatch $\Delta\phi$. The vector of unknown parameters for the observations $r_\ell(t)$ is expressed as a function of the time delays τ rather than a function of the unknown location (x, y) (as seen in (5.8)); i.e., the vector of unknown parameters is denoted by $\kappa = [\kappa_{nr}, \kappa]^T$, with $\kappa_{nr} = [\tau^T, \vartheta_{\text{Re}}, \vartheta_{\text{Im}}]$ and $\kappa_r = \Delta\phi^T$. The following notation is defined for later use: $\mathbf{r} = [r_1(t), \ldots, r_N(t)]^T$, $Q = MN$, $L = M + N$.

In order to derive the HFIM given in (5.2) and (5.3), the conditional joint pdf $p(\mathbf{r}|\kappa)$ is required. For the signal model given in (5.7), the conditional joint pdf of the observations (time samples at multiple receive antennas) parametrized by the unknown parameters vector κ, is then

$$p(\mathbf{r}|\kappa) \propto \exp \tag{5.9}$$

$$\left\{ -\frac{1}{\sigma_n^2} \sum_{\ell=1}^{N} \int_T \left| r_\ell(t) - \sum_{k=1}^{M} \vartheta s_k(t - \tau_{\ell k}) \eta_{\ell k} \right|^2 dt \right\}.$$

The observation is given as a function of κ. Therefore, the matrix $\mathbf{P}$, defined following (5.5), needs to be derived. The relation given in (5.8) is used, resulting in

$$\mathbf{P} = \begin{bmatrix} \mathbf{D}_{2\times Q}^T & \mathbf{0} \\ \mathbf{0} & \mathbf{I}_{(2+L)\times(2+L)} \end{bmatrix}, \tag{5.10}$$

with

$$\mathbf{D} = -\frac{1}{c} \begin{bmatrix} \cos\alpha_1 + \cos\gamma_2 & \sin\alpha_2 + \sin\gamma_2 \\ \vdots & \vdots \\ \cos\alpha_M + \cos\gamma_N & \sin\alpha_M + \sin\gamma_N \end{bmatrix}^T, \tag{5.11}$$

where α_k is the bearing angle of the transmitting sensor k to the target, measured with respect to the x axis, and γ_ℓ is the bearing angle of the receiving radar ℓ to the target, measured with respect to the x axis.

Using the conditional pdf $p\left(\mathbf{r}|\kappa\right)$ in (5.9) and the Gaussian distribution of the phase errors, the HFIM $\mathbf{J}_H\left(\kappa\right)$, defined by (5.2) and (5.3), is derived in Appendix E, resulting in

$$\mathbf{J}_H\left(\kappa_{nr}, \kappa_r\right) = \begin{bmatrix} \mathbf{R}_\tau & \mathbf{G} \\ \mathbf{G}^T & \mathbf{H} \end{bmatrix}, \tag{5.12}$$

where matrices $\mathbf{G}$ and $\mathbf{H}$ are defined by

$$\mathbf{G} = \begin{bmatrix} \mathbf{F}_{\tau\vartheta} & \mathbf{F}_{\tau\Delta} \end{bmatrix}_{Q\times(2+L)}, \tag{5.13}$$

and

$$\mathbf{H} = \begin{bmatrix} \mathbf{\Sigma}_\vartheta & \mathbf{F}_{\vartheta\Delta} \\ \mathbf{F}_{\vartheta\Delta}^T & \mathbf{\Sigma}_\Delta + \frac{1}{\sigma_\Delta^2}\mathbf{I} \end{bmatrix}_{(2+L)\times(2+L)}, \tag{5.14}$$

and the other submatrices in (5.12), (5.13) and (5.14) are defined and derived in Appendix E (see (E.1), (E.3), (E.4) and (E.5)). Applying (5.10) and (5.12) in (5.5) yields

$$\mathbf{J}_H\left(\theta\right) = \begin{bmatrix} \mathbf{DR}_\tau\mathbf{D}^T & \mathbf{DG} \\ \mathbf{G}^T\mathbf{D}^T & \mathbf{H} \end{bmatrix}. \tag{5.15}$$

The HCRB for the unknown parameters (x, y) may be derived from (5.15), applying the relation given in (5.4) :

$$\text{HCRB}\left(x, y\right) = \left[\mathbf{DR}_\tau\mathbf{D}^T - \mathbf{DGH}^{-1}\mathbf{G}^T\mathbf{D}^T\right]_{2\times2}^{-1}. \tag{5.16}$$

To find the closed-form solution to $\mathbf{HCRB}\,(x, y)$, the matrix $\mathbf{H}^{-1}$ is expressed using the formula for the inverse of a partitioned matrix [71]:

$$\left[\mathbf{H}^{-1}\right]_{11} = \left[\boldsymbol{\Sigma}_{\vartheta} - \mathbf{F}_{\vartheta\Delta}\mathbf{A}_{\Delta}^{-1}\mathbf{F}_{\vartheta\Delta}^{T}\right]^{-1} \tag{5.17}$$

$$\left[\mathbf{H}^{-1}\right]_{22} = -\left[\mathbf{F}_{\vartheta\Delta}^{T}\boldsymbol{\Sigma}_{\vartheta}^{-1}\mathbf{F}_{\vartheta\Delta}^{T} - \mathbf{A}_{\Delta}\right]^{-1} \tag{5.18}$$

and

$$\left[\mathbf{H}^{-1}\right]_{12} = \left[\mathbf{H}^{-1}\right]_{21}^{T} = \boldsymbol{\Sigma}_{\vartheta}^{-1}\mathbf{F}_{\vartheta\Delta}\left[\mathbf{F}_{\vartheta\Delta}^{T}\boldsymbol{\Sigma}_{\vartheta}^{-1}\mathbf{F}_{\vartheta\Delta} - \mathbf{A}_{\Delta}\right]^{-1} \tag{5.19}$$

where $\mathbf{A}_{\Delta} = \left(\boldsymbol{\Sigma}_{\Delta} + \frac{1}{\sigma_{\Delta}^{2}}\mathbf{I}\right)$. The term $\left[\boldsymbol{\Sigma}_{\vartheta} - \mathbf{F}_{\vartheta\Delta}^{-1}\mathbf{A}_{\Delta}^{-1}\mathbf{F}_{\vartheta\Delta}^{T}\right]^{-1}$ in (5.17), is transformed based on the formula for the inverse of a matrix $\mathbf{B}$ of the form $\mathbf{B} = \mathbf{A} + \mathbf{XRY}$, given in [71]. Following some additional matrix manipulations, the HCRB for the location MSE can be expressed as

$$\mathbf{HCRB}\,(x, y) = \mathbf{J}_{F}^{-1} + \left[\mathbf{J}_{F}\mathbf{P}_{\Delta}^{-1}\mathbf{J}_{F} - \mathbf{J}_{F}\right]^{-1} \tag{5.20}$$

$$= \mathbf{CRB}_{o}\,(x, y) + \Delta\mathbf{CRB},$$

where $\mathbf{CRB}_{o}\,(x, y) = \mathbf{J}_{F}^{-1}$ is the CRB with no phase mismatch, and $\Delta\mathbf{CRB} = \left[\mathbf{J}_{F}\mathbf{P}_{\Delta}^{-1}\mathbf{J}_{F} - \mathbf{J}_{F}\right]^{-1}$ represents the increment in the bound due to phase synchronization errors. The matrices $\mathbf{J}_{F}$ and $\mathbf{P}_{\Delta}$ are defined by

$$\mathbf{J}_{F} = \mathbf{D}\mathbf{R}_{\tau}\mathbf{D}^{T} - \mathbf{D}\mathbf{F}_{\tau\vartheta}\boldsymbol{\Sigma}_{\vartheta}^{-1}\mathbf{F}_{\tau\vartheta}^{\mathbf{T}}\mathbf{D}^{T},$$

and

$$\mathbf{P}_{\Delta} = \mathbf{D}\mathbf{F}_{\tau\vartheta}\boldsymbol{\Sigma}_{\vartheta}^{-1}\mathbf{F}_{\vartheta\Delta}\mathbf{R}_{\Delta}^{-1}\mathbf{F}_{\vartheta\Delta}^{T}\boldsymbol{\Sigma}_{\vartheta}^{-1}\mathbf{F}_{\tau\vartheta}^{\mathbf{T}}\mathbf{D}^{T} \tag{5.21}$$

$$- 2\,\mathrm{Re}\left\{\mathbf{D}\mathbf{F}_{\tau\Delta}\mathbf{R}_{\Delta}^{-1}\mathbf{F}_{\vartheta\Delta}^{T}\boldsymbol{\Sigma}_{\vartheta}^{-1}\mathbf{F}_{\tau\vartheta}^{\mathbf{T}}\mathbf{D}^{T}\right\}$$

$$+ \mathbf{D}\mathbf{F}_{\tau\Delta}\mathbf{R}_{\Delta}^{-1}\mathbf{F}_{\tau\Delta}^{\mathbf{T}}\mathbf{D}^{T},$$

and the matrix $\mathbf{R}_\Delta^{-1}$ can be calculated recursively using the formula for the inverse of the sum of matrices [72], resulting in

$$\mathbf{R}_\Delta^{-1} = \begin{bmatrix} \lambda_1 \mathbf{I}_{M \times M} + \frac{N\lambda_1^2}{M(1-N\lambda_1)}\mathbf{1}\mathbf{1}^T & \mathbf{0} \\ \mathbf{0} & \lambda_2 \mathbf{I}_{N \times N} + \frac{M\lambda_2^2}{N(1-M\lambda_2)}\mathbf{1}\mathbf{1}^T \end{bmatrix}, \qquad (5.22)$$

where $\mathbf{1} = [1, 1, , ..., 1]^T$ and the terms λ_1 and λ_2 are

$$\lambda_1 = \frac{2\,\mathrm{snr}\,\sigma_\Delta^2}{1+2\,\mathrm{snr}\,N\sigma_\Delta^2} \quad \text{and} \quad \lambda_2 = \frac{2\,\mathrm{snr}\,\sigma_\Delta^2}{1+2\,\mathrm{snr}\,M\sigma_\Delta^2}. \qquad (5.23)$$

Calculating the explicit value of $\Delta\mathbf{CRB}$, one gets

$$\Delta\mathbf{CRB} = \left[\mathbf{J}_F \left(\sum_{m=1}^{3} k_m \mathbf{B}_m \right)^{-1} \mathbf{J}_F - \mathbf{J}_F \right]^{-1}_{2\times2}, \qquad (5.24)$$

where the constants k_m, $m = 1, 2, 3$ are functions of the phase synchronization error variance σ_Δ^2 (through λ_1 and λ_2, defined in (5.23)) and the number of transmitting and receiving radars M and N, as follows:

$$k_1 = k\left(\lambda_1/M + \lambda_2/N\right), \qquad (5.25)$$

$$k_2 = k\lambda_1\left(N^2/M\right),$$

$$k_3 = k\lambda_2\left(M^2/N\right),$$

$$k = \frac{8\pi^2\left(f_c^2 + \beta^2\right)\mathrm{snr}}{c^2}.$$

The matrices $\mathbf{B}_m$, $m = 1, 2, 3$ depend on the geographical layout of the radars with respect to the target location:

$$\mathbf{B}_m = \begin{bmatrix} [\mathbf{D}_m\mathbf{1}]_{1,1}^2 & [\mathbf{D}_m\mathbf{1}]_{1,1}[\mathbf{D}_m\mathbf{1}]_{2,1} \\ [\mathbf{D}_m\mathbf{1}]_{1,1}[\mathbf{D}_m\mathbf{1}]_{2,1} & [\mathbf{D}_m\mathbf{1}]_{2,1}^2 \end{bmatrix},$$

using the following $\mathbf{D}_m$ matrices:

$$\mathbf{D}_1 = c\mathbf{D} \tag{5.26}$$

$$\mathbf{D}_2 = \begin{bmatrix} \cos\alpha_1 & \sin\alpha_2 \\ \vdots & \vdots \\ \cos\alpha_M & \sin\alpha_M \end{bmatrix}^T_{M\times 2} \,,$$

and

$$\mathbf{D}_3 = \begin{bmatrix} \cos\gamma_2 & \sin\gamma_2 \\ \vdots & \vdots \\ \cos\gamma_N & \sin\gamma_N \end{bmatrix}^T_{N\times 2} \,.$$

The expression for the HCRB as given in (5.20), offers an interesting observation on the effects of phase errors on the target localization MSE. First, it is apparent that the HCRB may be expressed as the sum of the CRB with no phase error and a term dependent on the statistics of the phase errors. This term is a function of the sensors location with respect to the target, through the matrices $\mathbf{B}_m$, and the system parameters (SNR, phase errors variance σ_Δ^2 and the number of mismatched transmitting and receiving radars) through the coefficients μ_m. The manner in which the number of radars, their spread and the phase synchronization error variance affect the performance is not readily understood from (5.24). For this reason, numerical examples are employed in the next section to gain some insight into the relationships between system parameters and performance degradation.

5.3 Numerical Analysis

The HCRB expression given in (5.20) is numerically evaluated using the following example: $M = 11$, $N = 9$ and $\sigma_\Delta^2 = [0, 0.0001, 0.0005, 0.001, 0.005, 0.01, 0.05]$, where σ_Δ^2 is expressed in (rad^2). The HCRB (x_o, y_o) is drawn in Figure 5.11. As σ_Δ^2 increases beyond a specific value, the additional CRB term ΔCRB dominates the performance and the curve. For high phase error levels, the performance degradation starts at lower SNRs.
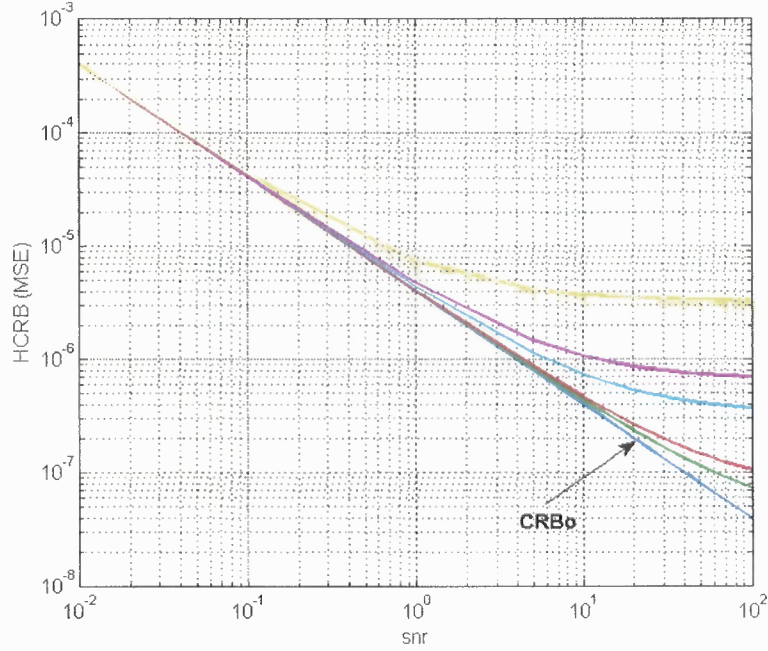
Figure 5.1 HCRB for M=11 and N=9. The blue line represent the CRB value with no phase errors.

For small phase errors, localization accuracy is not undermined by the phase mismatch, and the HCRB (x_o, y_o) curve follows the $\mathrm{CRB}_o (x_o, y_o)$ closely.

For a given system, the tolerated $[\sigma^2_\Delta]_{\max}$ may be determined by solving $\Delta\mathrm{CRB}\left([\sigma^2_\Delta]_{\max}\right) \preceq \mathrm{CRB}_o (x_o, y_o)$. This value can serve as a design goal in the system phase calibration. For a given phase synchronization error variance σ^2_Δ, the expression $\Delta\mathrm{CRB}\left(\sigma^2_\Delta\right)$ gives the localization accuracy penalty.

5.4 Conclusions

MIMO radar with coherent processing exploits the signal phase measured at the receive antennas to generate high resolution target location estimation. To take advantage of this scheme, full phase synchronization is required among all participating radars. In practice, inevitable phase synchronization errors reflect on the system localization performance. In this paper, a closed-form expression of the HCRB of target localization has been

derived, capturing the impact of the phase synchronization errors on the achievable target localization accuracy. In particularly it has been shown that the HCRB can be expressed as a sum of the CRB with no phase error and a term that represents the phase error penalty. The latter has been shown to be a function of the sensors geometry, SNR, and the number of transmitting and receiving radars in addition to the phase error MSE. As phase synchronization over distributed platform is a complex operation and phase errors are unavoidable, the HCRB offers valuable information at the system design level. For a given phase error MSE, the HCRB may be used to derive the attainable target localization accuracy. Otherwise, for a given system performance goal on localization accuracy, the HCRB provides with an upper bound on the necessary phase error MSE values.

CHAPTER 6

TARGET TRACKING IN MIMO RADAR SYSTEMS

Target tracking as it is an essential requirement for surveillance systems [73–75]. Herein, target tracking performances of MIMO radar systems are evaluated. The joint Bayesian Cramer-Rao bound (BCRB) [28] is formulated, and a recursive bound on the state variables (target location and velocity) is derived based on the nonlinear filtering bound developed in [76]. A BCRB based analysis for multi-static radar systems is provided in [77]. The system model assumes one transmitter and multiple receivers. Target position estimation performance is demonstrated for a given target path, yet limited insight is provided as to the dependency of this bound on system parameters. In this study, the effect of system parameters on target tracking performance is presented. Based on this study, two tracking schemes are proposed. The first is a centralized architecture, based on joint processing of either raw or partially processed (compressed) data at a fusion center. This approach provides highly accurate target tracking and takes full advantage of the MIMO configuration. The second is a decentralized scheme, based on a hybrid combination of local processing at the receiving radars and joint tracking at a fusion center. The latter approach supports resource aware system operation. Reduced communication requirements and processing load may be achieved with relatively low performance cost with the proposed decentralized method.

In this Chapter, the study of target localization in MIMO radar systems with distributed antennas and noncoherent processing is extended to target tracking. The BCRB on target location and velocity is derived, and insight is gained into the effect of the radars geometric layout and the target location on tracking accuracy. The relation between estimation error and the number of radars is examined and the contribution of target reflectivity and path loss to tracking performance is evaluated. Adaptive tracking tactics are

proposed, accounting for the target parameters estimation accuracy and the radar sensors spread.

6.1 System Model

Assume M transmitting radars and N receiving radars, widely distributed, and time and phase synchronized. The receiving radars could be collocated with the transmitting elements or widely separated. The transmitting and receiving radars are located in a two dimensional plane (x, y). Consider a single moving complex target with an initial location (x_o, y_o) and velocity $(\dot{x}_o, \dot{y}_o)$. At state n, defines as the time interval $n\Delta t$, where Δt is the observation interval, the target is located at coordinates (x_n, y_n) (see Figure 6.1). A set of orthogonal waveforms is transmitted, with the lowpass equivalent $s_k(t)$, $k = 1, \ldots, M$. The power of the transmitted waveforms is normalized such that the aggregate power transmitted by the sensors is constant, irrespective of the number of transmit sensors. Let all transmitted waveforms be narrowband signals with individual effective bandwidth β_k defined as $\beta_k^2 = \left[\left(\int_{W_k} f^2 \, |S_k(f)|^2 \, df \right) / \left(\int_{W_k} |S_k(f)|^2 \, df \right) \right]$, and an effective time duration T_{b_k} defined as $T_{b_k}^2 = \left[\left(\int_{T_k} t^2 \, |s_k(t)|^2 \, dt \right) / \left(\int_{T_k} |S_k(t)|^2 \, dt \right) \right]$, where the integration is over the range of frequencies with non-zero signal content W_k [29]. The signals are narrowband in the sense that for a carrier frequency f_c, the narrowband signal assumption implies $\beta_k^2 / f_c^2 \ll 1$ and $\beta^2 / f_c^2 \ll 1$, where $\beta = \frac{1}{M} \sum_{k=1}^{M} \beta_k$.

The propagation time estimate of a signal transmitted by the k-th transmitting radar located at coordinates $T_k = (x_{tk}, y_{tk})$, reflected by a target located at (x_n, y_n), and received by a radar located at $R_\ell = (x_{r\ell}, y_{r\ell})$ can be approximated as:

$$\widehat{\tau}_{\ell k_n} = \tau_{\ell k_n} + \varepsilon_{\tau_{\ell k_n}},$$
$$k = 1, .., M; \; \ell = 1, .., N$$

(6.1)

where $\tau_{\ell k_n}$, the propagation time, is the sum of the time delays from radar k to the target and from the target to radar ℓ in state n:

$$\tau_{\ell k_n} = \frac{1}{c} \left(\sqrt{(x_{tk} - x_n)^2 + (y_{tk} - y_n)^2} \right. \tag{6.2}$$
$$\left. + \sqrt{(x_{r\ell} - x_n)^2 + (y_{r\ell} - y_n)^2} \right),$$

and $\varepsilon_{\tau_{\ell k_n}}$ is the time delay estimation error. The speed of light is denoted by c.

The Doppler shift estimate of a signal transmitted on the ℓk-th path can be approximated as:

$$\widehat{\omega}_{\ell k_n} = \omega_{\ell k_n} + \varepsilon_{\omega_{\ell k_n}}, \tag{6.3}$$

where $\omega_{\ell k_n}$, the Doppler shift on the ℓk-th path due to the target velocity in state n

$$\omega_{\ell k_n} = -\frac{2\pi}{\lambda} \left[\frac{(x_n - x_{tk})\dot{x}_n + (y_n - y_{tk})\dot{y}_n}{\sqrt{(x_n - x_{tk})^2 + (y_n - y_{tk})^2}} + \frac{(x_n - x_{r\ell})\dot{x}_n + (y_n - y_{r\ell})\dot{y}_n}{+\sqrt{(x_n - x_{r\ell})^2 + (y_n - y_{r\ell})^2}} \right] \tag{6.4}$$
$$= -\frac{2\pi}{\lambda} \left[\dot{x}_n \left(\cos \phi_{k_n} + \cos \varphi_{\ell_n} \right) + \dot{y}_n \left(\sin \phi_{k_n} + \sin \varphi_{\ell_n} \right) \right],$$

and $\varepsilon_{\omega_{\ell k_n}}$ is the Doppler shift estimation error. The term $\dot{x}_n$ stands for the target velocity in direction x and $\dot{y}_n$ for the target velocity in direction y at the nth state. The phase ϕ_{k_n} is the bearing angle of the target to transmitting sensor k with respect to the x axis; the phase φ_{ℓ_n} is the bearing angle of the target receiving radar ℓ measures with respect to the x axis. See illustration in Figure 6.1.

Consider the case of a baseband representation of the signal observed at sensor ℓ due to a transmission from sensor k and reflection from the scatterer at coordinates (x_n, y_n), given by:

$$r_{\ell_n}(t) = \sum_{k=1}^{M} \alpha_{\ell k_n} s_{k_n} \left(t - \tau_{\ell k_n} \right) \exp^{-j\omega_{\ell k_n} t} + w_{\ell_n}(t), \tag{6.5}$$

where $\alpha_{\ell k_n}$ represent the combined effect of path loss, targets' reflectivity along the ℓk-th path and the phase shift equivalent to the time delay along the path, the noise $w_{\ell_n}(t)$ is circularly symmetric, zero-mean, complex Gaussian noise, spatially and temporally white with temporal autocorrelation function $\sigma_w^2 \delta(\tau)$, and $k = 1, ..., M$, $\ell = 1, ..., N$. The observation vector $\mathbf{r}$ at state n is:

$$\mathbf{r}_n = [r_1(t), r_2(t), ..., r_N(t)].\tag{6.6}$$

The signal received at each sensor is a mixture of the transmitted signals reflected by the target. The mixture of signals is separated at the receiver end by exploiting the orthogonality between the transmitted waveforms.

The state vector $\mathbf{x}_n$, representing the target location and velocity at state n, is:

$$\mathbf{x}_n = [x_n, y_n, \dot{x}_n, \dot{y}_n]^T.\tag{6.7}$$

In the analysis, the state vector $\mathbf{x}_n$ is treated as unknown random, while α_n is assumed unknown deterministic.
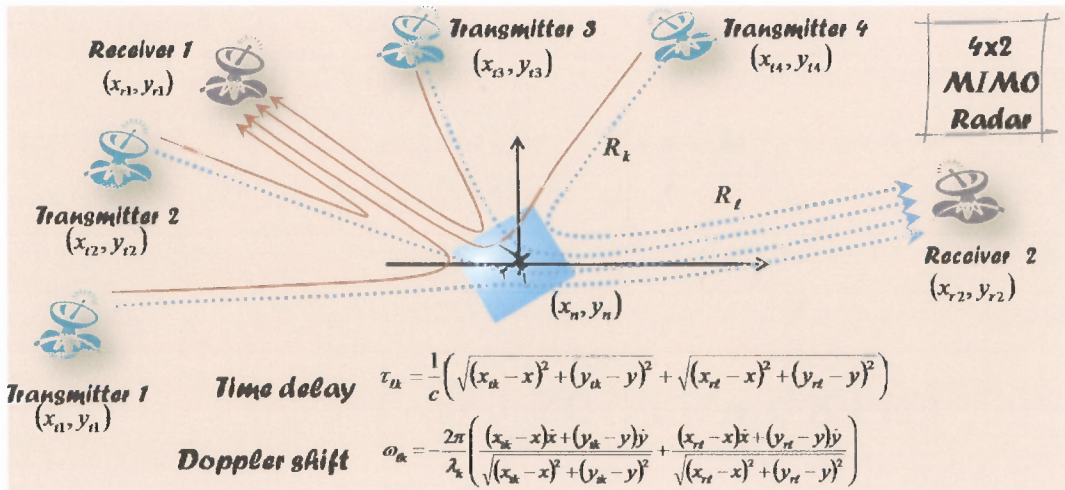

Figure 6.1 Tracking system layout.

The state model is a linear motion model, represented as ([78], [73]):

$$\mathbf{x}_{n+1} = \mathbf{F}\mathbf{x}_n + \mathbf{v}_n, \tag{6.8}$$

$$\mathbf{F} = \begin{bmatrix} 1 & \Delta t & 0 & 0 \\ 0 & 1 & 0 & 0 \\ 0 & 0 & 1 & \Delta t \\ 0 & 0 & 0 & 1 \end{bmatrix},$$

where $\mathbf{v}_n$ is modeled as white Gaussian process noise with covariance matrix $\mathbf{Q}_\mathbf{v}$ of the form:

$$\mathbf{Q_v} = \begin{bmatrix} \frac{1}{3}\Delta t^3 \mathbf{I} & \frac{1}{2}\Delta t^2 \mathbf{I} \\ \frac{1}{2}\Delta t^2 \mathbf{I} & \Delta t \mathbf{I} \end{bmatrix}. \tag{6.9}$$

The observation model is a nonlinear function of the vector of unknown parameters, ψ_n:

$$\mathbf{z}_n = \mathbf{d}\left(\psi_n\right) + \mathbf{w}_n, \tag{6.10}$$

where $\mathbf{d}$ stands for the observation, that in the MIMO radar case is the set of signals observed at the receiving radars, expressed by 6.5 as a nonlinear function of a vector of unknown parameters ψ_n defined as:

$$\psi_n = \begin{bmatrix} \tau_n \\ \omega_n \\ \alpha_n \end{bmatrix}, \tag{6.11}$$

$$\tau_n = \left[\tau_{1_n}, \tau_{2_n}, \dots \tau_{L_n} \right]^T,$$

$$\omega_n = \left[\omega_{1_n}, \omega_{2_n}, \dots \omega_{L_n} \right]^T,$$

$$\alpha_n = \left[\alpha_{1_n}, \alpha_{2_n}, \dots \alpha_{L_n} \right]^T,$$

where $L = MN$.

6.2 The Bayesian Cramer-Rao Bound (BCRB)

In [76], a recursive, multiple dimensional, generalized Bayesian Cramer-Rao Bound (BCRB) is developed. In general, the BCRB for an unknown vector parameter $\theta \in R^{n \times 1}$, estimated using an observation vector $\mathbf{r}$, is of the form:

$$E_{\mathbf{r},\theta} \left\{ \left[\widehat{\theta}(\mathbf{r}) - \theta \right] \left[\widehat{\theta}(\mathbf{r}) - \theta \right]^T \right\} \geq \mathbf{J}_B^{-1} = \mathbf{C}_B. \qquad (6.12)$$

where $\mathbf{J}_B$ is the Bayesian information matrix (BIM), and $\mathbf{C}_B$ is the BCRB matrix. The BIM is calculated using the joint probability density function (pdf), as follows:

$$\mathbf{J}_B = E \left\{ -\frac{\partial^2}{\partial \theta^2} \log p_{\mathbf{r},\theta}(\mathbf{r}, \theta) \right\}. \qquad (6.13)$$

Based on the relation $p_{\mathbf{r},\theta}(\mathbf{r}, \theta) = p_{\mathbf{r}|\theta}(\mathbf{r}|\theta) \cdot p_\theta(\theta)$, it is shown in [76] that the BIM may be expressed as a linear combination of two matrices:

$$\mathbf{J}_B = \mathbf{J}_D + \mathbf{J}_P, \qquad (6.14)$$

where $\mathbf{J}_D$ is the Fisher information matrix (FIM) and represents the information coming from the data and $\mathbf{J}_P$ represents the a priori information, named hereafter as PIM. The FIM and PIM are derived using:

$$\mathbf{J}_D = E_\theta \left\{ -\frac{\partial^2}{\partial \theta^2} \log p_{\mathbf{r}|\theta}(\mathbf{r}|\theta) \right\} \qquad (6.15)$$

$$\mathbf{J}_P = E_\theta \left\{ -\frac{\partial^2}{\partial \theta^2} \log p_\theta(\theta) \right\} \qquad (6.16)$$

The BCRB sets the lower bound on the estimation MSE for the unknown vector parameter $\mathbf{x}_{n+1} = [x_{n+1}, y_{n+1}, \dot{x}_{n+1}, \dot{y}_{n+1}]$

$$E_{\mathbf{x}_{n+1}} \left\{ ([\widehat{\mathbf{x}}_{n+1}]_i - [\mathbf{x}_{n+1}]_i) ([\widehat{\mathbf{x}}_{n+1}]_i - [\mathbf{x}_{n+1}]_i)^T \right\} \geq \mathbf{J}_{\mathbf{B}_{n+1}}^{-1} (\mathbf{x}_{n+1}) \qquad (6.17)$$

where "$\widehat{()}$" denotes estimated quantities and $\mathbf{J}_{\mathbf{B}_{n+1}}$ is the BIM of the system at state $n + 1$, defined in (6.13). The recursive BCRB is of the form [76] :

$$\mathbf{J}_{\mathbf{B}_{n+1}} = \left[\mathbf{Q}_\mathbf{v} + \mathbf{F} \mathbf{J}_{\mathbf{B}_{n+1}}^{-1} \mathbf{F}^T \right]^{-1} + E_{\mathbf{x}_{n+1}} \left[\mathbf{J}_{\mathbf{D}_{n+1}} \right] \qquad (6.18)$$

where $\mathbf{J}_{\mathbf{D}_{n+1}}$ is the FIM of the system at state $n + 1$, defined in (6.15), and $E_{\mathbf{x}_{n+1}} [\cdot]$ is the expectation with respect to the joint probability density function (pdf) of the state vector $\mathbf{x}_{n+1}$. The FIM $\mathbf{J}_{\mathbf{D}_{n+1}}$ is derived using the conditional pdf:

$$p(\mathbf{r}|\psi) \propto \exp \qquad\qquad\qquad\qquad\qquad\qquad\qquad (6.19)$$

$$\left\{ -\frac{1}{\sigma_w^2} \sum_{\ell=1}^{N} \int_T \left| r_\ell(t) - \sum_{k=1}^{M} \alpha_{\ell k} s_k (t - \tau_{\ell k}) \exp^{(-j\omega_{\ell k} t)} \right|^2 dt \right\}.$$

and by applying the chain rule [26] for :

$$\mathbf{J}_{\mathbf{D}_{n+1}} (\mathbf{x}_{n+1}) = \begin{bmatrix} \mathbf{H}_{n_1,\tau} & \mathbf{H}_{n_1,\omega} \\ \mathbf{H}_{n_2,\tau} & \mathbf{H}_{n_2,\omega} \end{bmatrix} \cdot \mathbf{J}_{\mathbf{D}_{n+1}} (\psi_{n+1}) \cdot \begin{bmatrix} \mathbf{H}_{n_1,\tau} & \mathbf{H}_{n_1,\omega} \\ \mathbf{H}_{n_2,\tau} & \mathbf{H}_{n_2,\omega} \end{bmatrix}^T. \qquad (6.20)$$

where matrices $\mathbf{H}$ are defined below and matrix $\mathbf{J}_{\mathbf{D}_{n+1}} (\psi_{n+1})$ is the FIM for the unknown vector ψ_{n+1}, derived based on the same process developed in Appendix C, and may be shown to be:

$$\mathbf{J}_{D_{n+1}} (\psi_{n+1}) = \begin{bmatrix} \mathbf{J}_{\tau\tau_{n+1}} & 0 \\ 0 & \mathbf{J}_{\omega\omega_{n+1}} \end{bmatrix}, \qquad (6.21)$$

where matrix $\mathbf{J}_{\tau\tau_{n+1}}$ is

$$\mathbf{J}_{\tau\tau_{n+1}} = 8\pi^2 diag \left(\frac{|\alpha_{\ell k}|^2}{\sigma_w^2} \beta_k^2 \right), \tag{6.22}$$

and matrix $\mathbf{J}_{\omega\omega_{n+1}}$ follows,

$$\mathbf{J}_{\omega\omega_{n+1}} = 8\pi^2 diag \left(\frac{|\alpha_{\ell k}|^2}{\sigma_w^2} T_{b_k}^2 \right). \tag{6.23}$$

Elements of matrices $\mathbf{H}$ are provided by the derivative of the expressions in (6.2) and (6.4) with respect to the state vector in (6.7). It can be shown that:

$$\left[\mathbf{H}_{n1,\tau} \right]_{col(j=\ell k)} = \frac{1}{c} \begin{bmatrix} \cos\phi_{n_k} + \cos\varphi_{n_\ell} \\ \sin\phi_{n_k} + \sin\varphi_{n_\ell} \end{bmatrix}, \tag{6.24}$$

$$\left[\mathbf{H}_{n2,\tau} \right]_{col(j=\ell k)} = \begin{bmatrix} 0 \\ 0 \end{bmatrix},$$

$$\left[\mathbf{H}_{n2,\omega} \right]_{col(j=\ell k)} = -2\pi \begin{bmatrix} \lambda_k^{-1} \left(\cos\phi_{n_k} + \cos\varphi_{n_\ell} \right) \\ \lambda_k^{-1} \left(\sin\phi_{n_k} + \sin\varphi_{n_\ell} \right) \end{bmatrix},$$

$$\left[\mathbf{H}_{n1,\omega} \right]_{col(j=\ell k)} = -2\pi \begin{bmatrix} \lambda_k^{-1} \left[\dot{x}_{n\ell k} \left(\frac{\sin^2\phi_{n_k}}{R_{tk_n}} + \frac{\sin^2\varphi_{n_\ell}}{R_{r\ell_n}} \right) - \dot{y}_{n\ell k} \left(\frac{\sin 2\phi_{n_k}}{R_{tk_n}} + \frac{\sin 2\varphi_{n_\ell}}{R_{r\ell_n}} \right) \right] \\ \lambda_k^{-1} \left[\dot{y}_{n\ell k} \left(\frac{\cos^2\phi_{n_k}}{R_{tk_n}} + \frac{\cos^2\varphi_{n_\ell}}{R_{r\ell_n}} \right) - \dot{x}_{n\ell k} \left(\frac{\sin 2\phi_{n_k}}{R_{tk_n}} + \frac{\sin 2\varphi_{n_\ell}}{R_{r\ell_n}} \right) \right] \end{bmatrix}.$$

Using (6.24) and (6.21) in (6.20), yields:

$$\mathbf{J}_{\mathbf{D}_{n+1}} (\mathbf{x}_{n+1}) = \begin{bmatrix} \mathbf{H}_{n1,\tau} \mathbf{J}_{\tau\tau_{n+1}} \mathbf{H}_{n1,\tau}^T + \mathbf{H}_{n1,\omega} \mathbf{J}_{\omega\omega_{n+1}} \mathbf{H}_{n1,\omega}^T & \mathbf{H}_{n1,\omega} \mathbf{J}_{\omega\omega_{n+1}} \mathbf{H}_{n2,\omega}^T \\ \mathbf{H}_{n2,\omega} \mathbf{J}_{\omega\omega_{n+1}} \mathbf{H}_{n1,\omega}^T & \mathbf{H}_{n2,\omega} \mathbf{J}_{\omega\omega_{n+1}} \mathbf{H}_{n2,\omega}^T \end{bmatrix}, \tag{6.25}$$

The lower bound on the state vector estimation error in state $n + 1$, is provided by the expression in (6.18), integrating the FIM derived in (6.25). Next, numerical analysis of the BCRB, integrating (6.25) in (6.18) is provided, establishing an understanding of the tracking performance of MIMO radar systems.

6.3 Numerical Analysis

It is apparent from (6.18) that the performance of the BCRB in (6.25) depends on the geometric layout of the MIMO radar system and the track of the target. To get an understanding of these relations, a few schemes are evaluated. First, the sensitivity of the performance to radars spread with respect to the target location is analyzed through the evaluation of four system layouts, illustrated in Figure 6.2. A wide angular spread of the radars with respect to the target position (Cases 1 and 4 in Figures 6.2-Figure 6.4) supports higher accuracies than when the radars are spread in a narrower angle (see Cases 2 and 3 in Figures 6.2-6.4). Furthermore, when the target motion direction is opposed to the radar locations, the performances degrades.
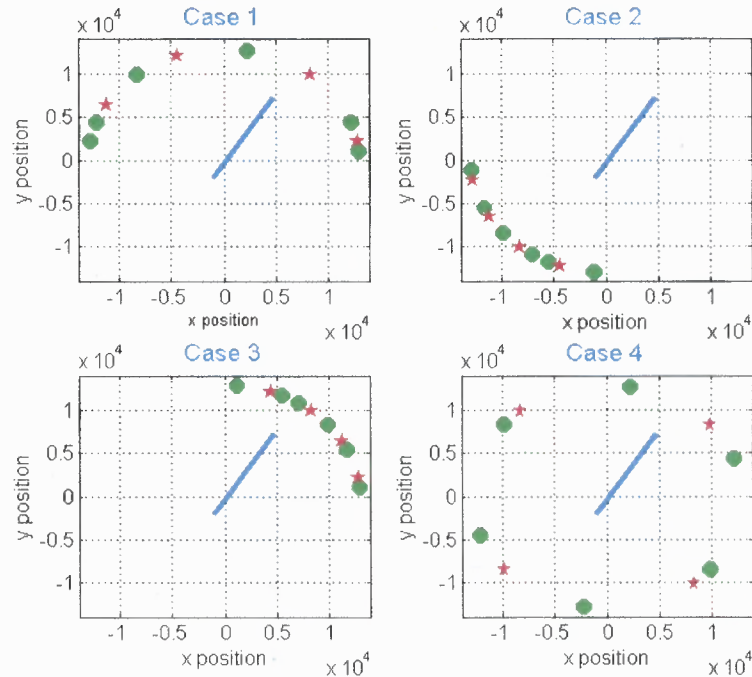
Figure 6.2 Scenario I: 6x4 MIMO radar system with different angular spreads.

The effect of the number of transmitting and receiving radars on tracking performance is examined through the use of MIMO radar configurations shown in Figure 6.5. The four test cases are: 3x4, 6x4, 12x4 and 18x4 MIMO radar systems. It is
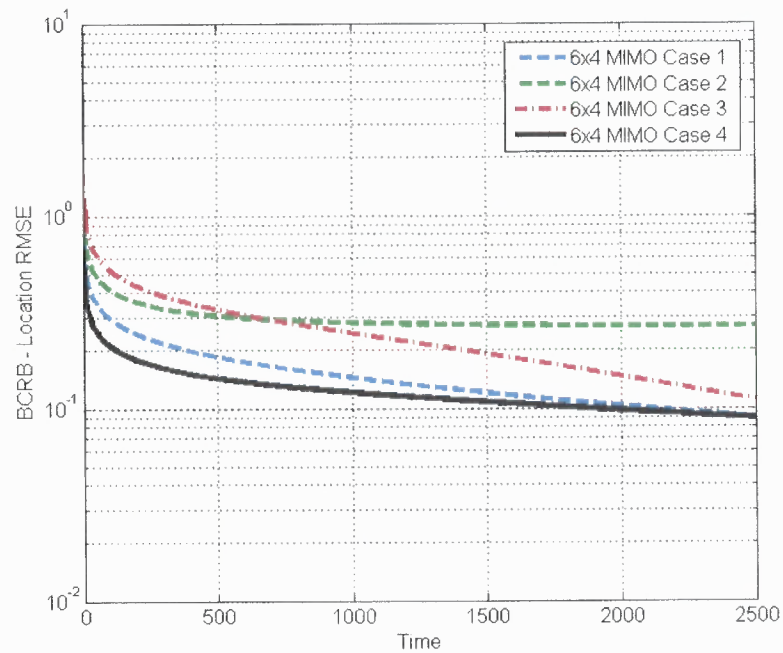
Figure 6.3 BCRB on target location tracking for scenario I.
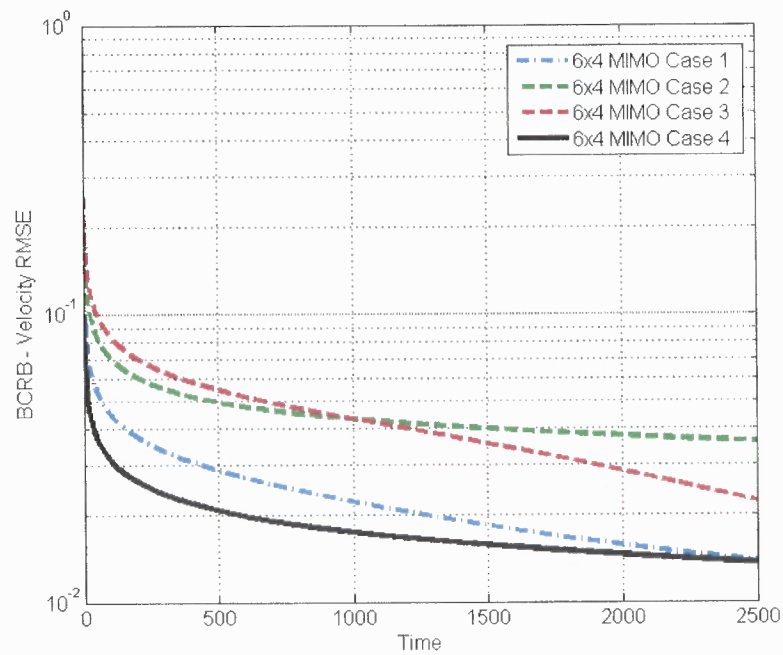

Figure 6.4 BCRB on target velocity tracking for scenario I.

observed that the product of the number of transmitting and receiving radars MN is 12, 24, 48 and 72, for Cases 1-4, respectively. Therefore, the ratio of the products MN is $\frac{MN(\text{Case 2})}{MN(\text{Case 1})} = \frac{MN(\text{Case 3})}{MN(\text{Case 2})} = 2$ and $\frac{MN(\text{Case 4})}{MN(\text{Case 3})} = 1.5$. It is clear from Figures 6.6 and 6.7 that the tracking mean-square error (MSE) decreases for both position and velocity as M and N increase, i.e., as the product MN increases. The performance gain, defined as the ratio between the MSE bound of two given MIMO radar systems, is proportional to the increase in the product MN. The position accuracy performances shown in Figure 6.6 and velocity accuracies provided in Figure 6.7, demonstrate that.
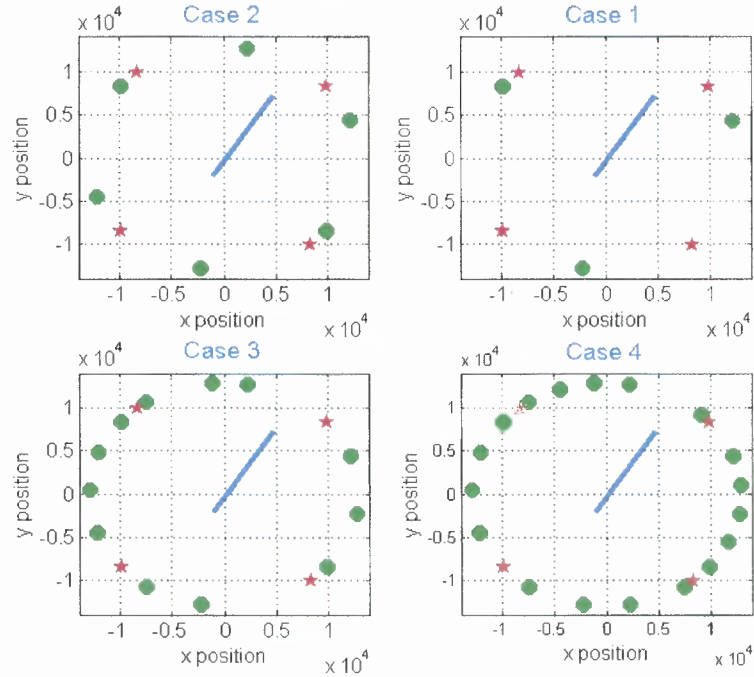
Figure 6.5 Scenario II: Various symmetrical MIMO radar configurations: (1) 3x4. (2) 6x4. (3) 12x4 (4) 18x4.

In practical situation, each propagation path between a set of transmitting and receiving radar has different characteristic, depending on path loss, target reflectivity and phase errors. To assess the effect of the propagation paths on tracking performance, MIMO radar layouts given in Figure 6.2 are used. Different paths propagation coefficients are modeled. It is shown in Figure 6.8 that receivers with increasing path loss show worse
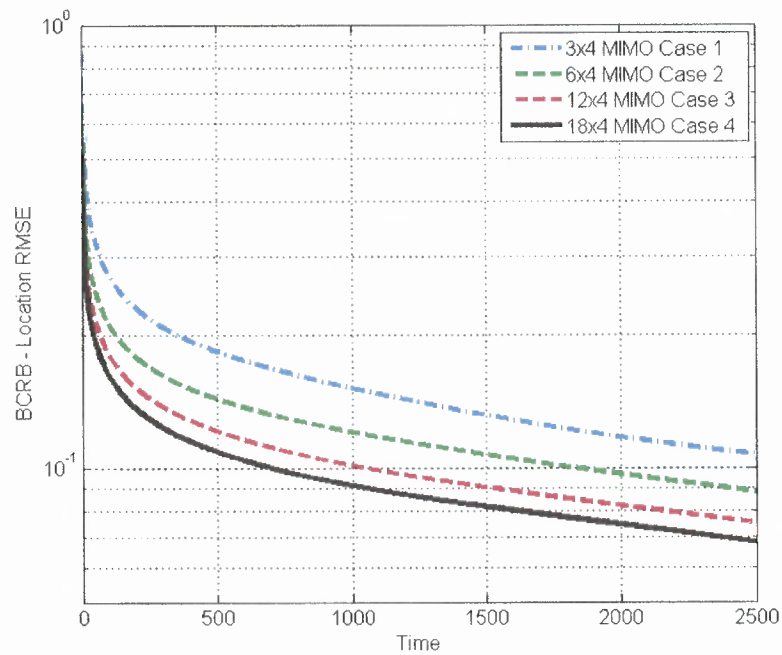
Figure 6.6 BCRB on target location tracking for scenario II.
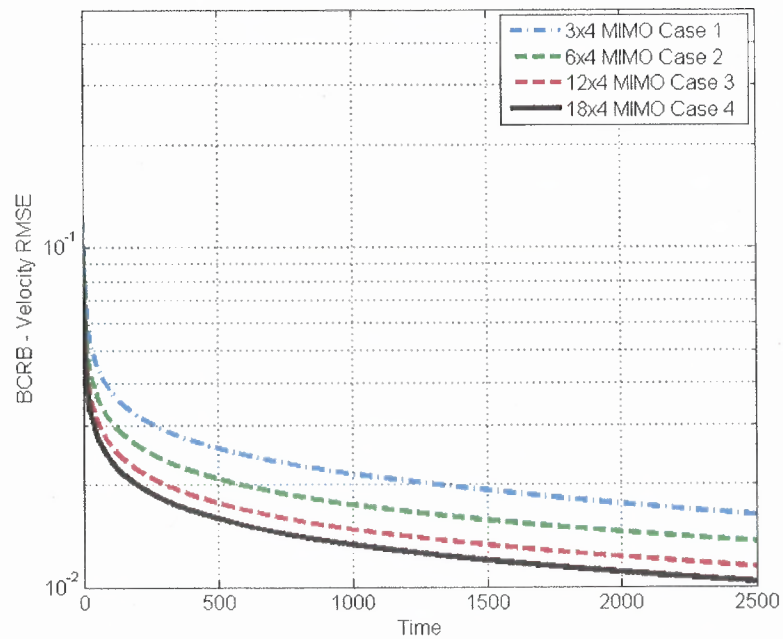
Figure 6.7 BCRB on target location tracking for scenario I.

estimation capabilities when comapred with receivers with little path loss. The joint MIMO radar tracking with path loss experience some performance degradation, when compared with the case of no path loss, given in Figure 6.3. The advantage of MIMO radars system over SIMO (single-input multiple-output) or MISO (multiple-input single-output) is also demonstrated in Figure 6.8.
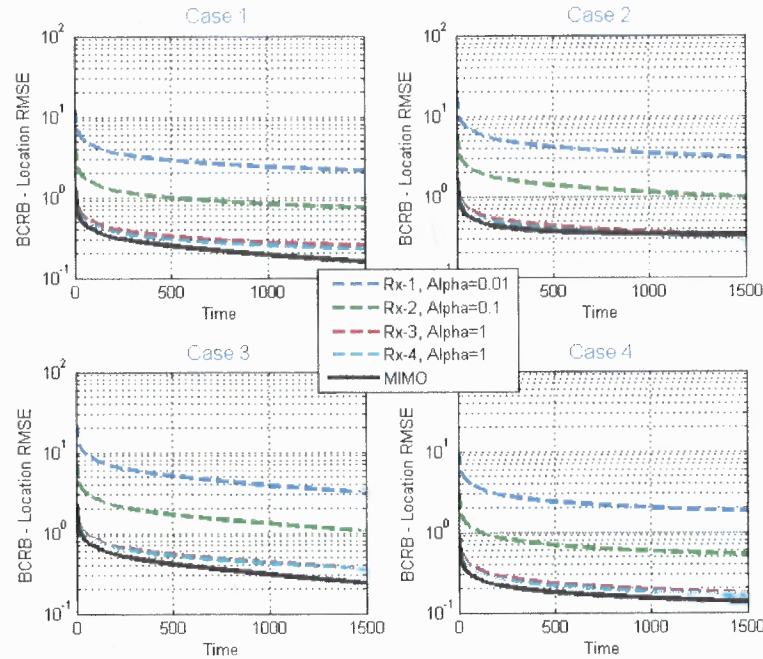
Figure 6.8 BCRB on target location tracking for scenario I, with receivers one and two experiencing different levels of path loss.

6.4 Tracking Algorithms

As established in the previous section, MIMO radar systems provide tracking accuracy advantages that grow proportionally with the number of transmitting and receiving radars. Increasing the number of transmitting and receiving radars leads to increased communication needs and computation load. These are reliant on the specific tracker employed.

Target position and velocity may be tracked based on a centralized or a decentralized approach. In a centralized tracking approach, the observations are jointly measured in a fusion center to produce target location and velocity estimates. The decentralized approach takes advantage of observations obtained at a receiver from signals of M transmitting radars, and generates a local estimate of the target location and velocity. These estimates are then sent to a fusion center to be fused based on a local cost function. MIMO radar systems with at least three transmitters support decentralized target position and velocity estimation, as each receiver may act as a MISO radar system. Processing in a MIMO radar system may be distributed among N MISO subsystems, each with an $M \times 1$ structure. It is expected that the individual subsystems will provided lower performances, when compared with the MIMO system (as illustrated in the BCRB of Figure 6.8)). Choice of an adequate fusion algorithm, for which the separate estimates are combined effectively, may overcome the destructive contribution of weaker propagation paths.

6.4.1 Centralized Tracking

Centralized tracking may use direct or indirect estimation techniques. The multiple propagation paths, created by multiple transmitted waveforms from multiple widely spread antennas and echoes from scatterers received at multiple widely separated antennas, support target parameters estimation, such as location and velocity, through either direct or indirect estimation. With direct estimation, the observations collected by the sensors are jointly processed to produce target location and/or velocity estimates. With indirect estimation, the TOAs and Doppler shifts are estimated first, and target location and/or velocity are subsequently estimated based on the relations given in (6.2) and (6.4). The advantage of using direct estimation is in the estimation MSE, while the indirect estimation technique offers data compression.

In direct estimation, raw data is transmitted to a fusion center for joint estimation of target location and velocity. The observations collected by the radars are jointly processed

using maximum likelihood estimator (MLE) at the central fusion center to produce the localization estimate,

$$\widehat{\mathbf{x}}_{n+1} = \arg\max_{\check{\mathbf{x}}_{n+1}} \left[\sum_{k=1}^{M}\sum_{\ell=1}^{N} \int r_\ell(t)\, s_k^*\left(t - \varsigma_{\ell k}\left(\check{\mathbf{x}}_{n+1}\right)\right) \exp\left(-j v_{\ell k}\left(\check{\mathbf{x}}_{n+1}\right) t\right) dt \right]. \quad (6.26)$$

In this case, a search cell is defined and a maximum is obtained by evaluating the ML value for each location on a given grid $\check{\mathbf{x}}_{n+1}$.

Indirect techniques are involved with a preliminary stage where TOAs and Doppler frequencies are first estimated at the receiving radars and transmitted to the fusion center for joint estimation, where localization is subsequently estimated by multilateration. This estimation approach incorporates an intermediate step of estimating the unknown parameter vector as follows,

$$\widehat{\eta}_{n+1} = \arg\max_{\varsigma, v} \left[\sum_{k=1}^{M}\sum_{\ell=1}^{N} \int r_\ell(t)\, s_k^*\left(t - \varsigma_{\ell k}\right) \exp\left(-j v_{\ell k} t\right) dt \right]. \quad (6.27)$$

Indirect localization enables data compression and reduced complexity while potentially dealing with higher sidelobes.

Following, a centralized tracker with indirect estimation is proposed. The extended Kalman filter (EKF) is used for the model given in (6.8) and (6.10) in the fusion center. The initial target position and velocity $\widehat{\mathbf{x}}_0 = [x_o, y_o, \dot{x}_o, \dot{y}_o]^T$ are chosen based on a preliminary MLE obtained following target detection. The initial pdf $\mathbf{P}_{0|0}$ is determined based on the CRLB. The centralized algorithm is described in Table 6.1.

Table 6.1 Centralized Tracking

Centralized Tracking Algorithm:

1. Initial conditions: $\begin{cases} \widehat{\mathbf{x}}_0 = \mathbf{x}_0 \\ \mathbf{P}_{0|0} = \mathbf{R}_{\mathbf{x}_0} \end{cases}$

2. Project the state ahead: $\begin{cases} \widehat{\mathbf{x}}_{n+1|n} = \mathbf{F}\mathbf{x}_{n|n} \\ \mathbf{D}_{n+1} = \left\{ \nabla_{\mathbf{x}_{n+1}} \left[\mathbf{d}_{n+1}^T (\mathbf{x}_{n+1}) \right] \right\}^T \Big|_{\mathbf{x}_{n+1}=\widehat{\mathbf{x}}_{n+1|n}} \end{cases}$

3. *Locally at the ℓth receiver:*

Perform time delay and Doppler shift estimates at the N receivers:

3.1   Perform time delay $\widehat{\tau}_{\ell k_{n+1}}$ and Doppler shift $\widehat{\omega}_{\ell k_{n+1}}$ MLEs and the MSEs $\mathbf{R}_{\eta\ell_{n+1}}$.
3.2   Transmit to fusion center: $\begin{cases} \widehat{\eta}_{\ell_{n+1}} = \left[\widehat{\tau}_{\ell 1_{n+1}}, ..., \widehat{\tau}_{\ell M_{n+1}}, \widehat{\omega}_{\ell 1_{n+1}}, ..., \widehat{\omega}_{\ell M_{n+1}} \right] \\ \mathbf{R}_{\eta\ell_{n+1}} \end{cases}$

At fusion center:

4. Join estimations $\widehat{\eta}_{n+1}$ and MSEs $\mathbf{R}_{\eta_{n+1}}$ at fusion center:

$$\begin{cases} \widehat{\eta}_{n+1} = \left[\widehat{\eta}_{1_{n+1}}, .., \widehat{\eta}_{N_{n+1}} \right]^T \\ \mathbf{R}_{\eta_{n+1}} = diag \left(\mathbf{R}_{\eta 1_{n+1}}, \mathbf{R}_{\eta 2_{n+1}}, ..., \mathbf{R}_{\eta N_{n+1}} \right) \end{cases}$$

5. Project the covariance $\mathbf{P}_{n+1|n}$ and gain $\mathbf{G}_{n+1}$ for the EKF:

$$\mathbf{P}_{n+1|n} = \mathbf{F}\mathbf{P}_{n|n}\mathbf{F}^T + \mathbf{Q}_v$$

$$\mathbf{G}_{n+1} = \mathbf{P}_{n+1|n}\mathbf{D}_{n+1}^T \left(\mathbf{D}_{n+1}\mathbf{P}_{n+1|n}\mathbf{D}_{n+1}^T + \mathbf{R}_{\eta_{n+1}} \right)^{-1}$$

6. Update *estimator equation* $\widehat{\mathbf{x}}_{n+1|n+1}$ with measurement and the MSE $\mathbf{P}_{n+1|n+1}$:

$$\widehat{\mathbf{x}}_{n+1|n+1} = \widehat{\mathbf{x}}_{n+1|n} + \mathbf{G}_{n+1} \left(\widehat{\eta}_{n+1} - \mathbf{d}_{n+1} \left(\widehat{\mathbf{x}}_{n+1|n} \right) \right)$$

$$\mathbf{P}_{n+1|n+1} = \mathbf{P}_{n+1|n} + \mathbf{G}_{n+1} \left(\mathbf{D}_{n+1}\mathbf{P}_{n+1|n}\mathbf{D}_{n+1}^T + \mathbf{R}_{\eta_{n+1}} \right) \mathbf{G}_{n+1}^T$$

7. Send to all receivers $\widehat{\mathbf{x}}_{n+1|n+1}$.

8. go to step 2.

6.4.2 Decentralized Tracking

In decentralized tracking each receiving radars performs local estimates of the target location and velocity using either direct MLE-based estimation of $\widehat{x}_{\ell_{n+1}}$ or indirect estimation, i.e., first estimate $\widehat{\eta}_{\ell_{n+1}} = \left[\widehat{\tau}_{\ell 1_{n+1}}, ..., \widehat{\tau}_{\ell M_{n+1}}, \widehat{\omega}_{\ell 1_{n+1}}, ..., \widehat{\omega}_{\ell M_{n+1}} \right]$ and then estimate $\widehat{x}_{\ell_{n+1}}$ using linearizion techniques. The projected or last updated target location and velocity are used as a reference point in the linearizion process. The local estimates are sent to a central fusion center, where they are combined based on a predetermined cost function. The estimates are chosen such that path with significant fading or low reflectivity will be either discarded of introduce with very high cost coefficients. By doing so, the overall estimation MSE is kept as close as possible to the centralized performance. The centralized algorithm is described in Table 6.2.

The centralized and decentralized algorithms performance are provided in Figure 6.9. The proposed decentralized algorithm achieves accuracies very close to the centralized one. The cost-based decentralized tracking method is shown to perform better than when all paths a combined without any weighing coefficients (see Figure 6.10).
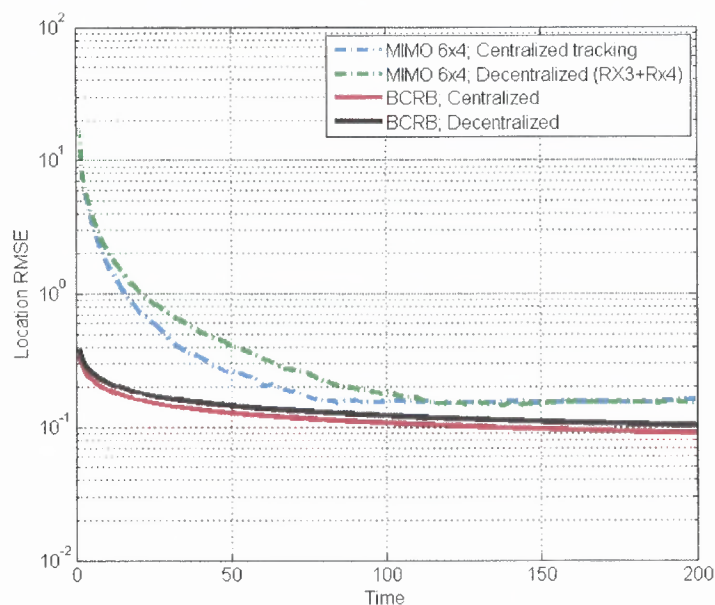
Figure 6.9 BCRB on target location tracking for centralized and decentralized tracking and the EKF and *hybrid* KF performance.
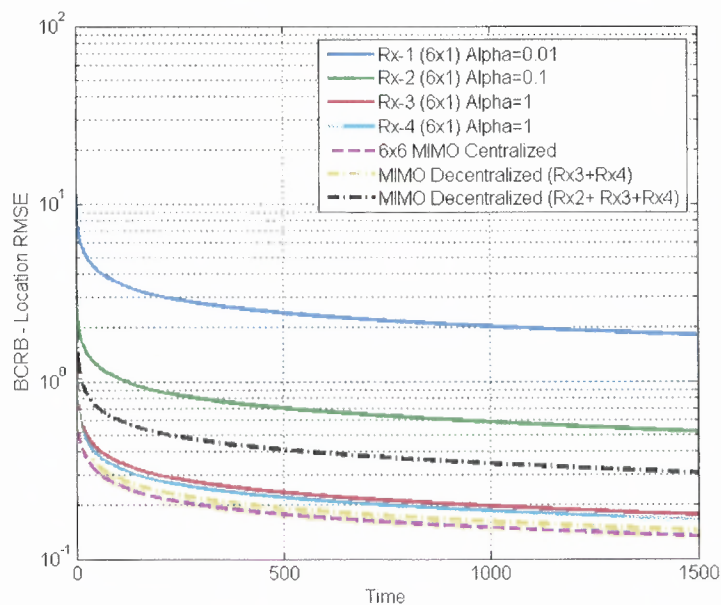
Figure 6.10 BCRB on target location tracking for centralized and decentralized tracking with different decentralized algorithms.

Table 6.2 Decentralized Tracking Algorithm

Decentralized Tracking:

1. Initial conditions:
$$\begin{cases} \widehat{\mathbf{x}}_0 = \mathbf{x}_0 \\ \mathbf{P}_{0|0} = \mathbf{R}_{\mathbf{x}_0} \end{cases}$$

2. Project the state ahead: $\left\{ \widehat{\mathbf{x}}_{n+1|n} = \mathbf{F}\mathbf{x}_n \right.$

3. *Locally at the ℓth receiver:*

   Perform target location $\left(\tilde{x}_{\ell_{n+1}}, \tilde{y}_{\ell_{n+1}} \right)$ and velocity $\left(\tilde{\dot{x}}_{\ell_{n+1}}, \tilde{\dot{y}}_{\ell_{n+1}} \right)$ estimates.

   3.1 Perform time delay and Doppler shift MLEs.

   3.2 $\mathbf{D}_{\ell_{n+1}} = \left\{ \nabla_{\mathbf{x}_{n+1}} \left[\mathbf{d}^T_{\ell_{n+1}} \left(\mathbf{x}_{n+1} \right) \right] \right\}^T \Big|_{\mathbf{x}_{n+1} = \widehat{\mathbf{x}}_{n+1|n}}$

   3.3 Estimate target location and velocity based on local EKF.

   3.4 To central fusion center: $\tilde{\mathbf{x}}_{\ell_{n+1}} = \left[\tilde{x}_{\ell_{n+1}}, \tilde{y}_{\ell_{n+1}}, \tilde{\dot{x}}_{\ell_{n+1}}, \tilde{\dot{y}}_{\ell_{n+1}} \right]$

   $$\mathbf{R}_{\tilde{\mathbf{x}}_{\ell_{n+1}}}$$

   At fusion center:

4. Perform target location $\left(\tilde{x}_{n+1}, \tilde{y}_{n+1} \right)$ and velocity $\left(\tilde{\dot{x}}_{n+1}, \tilde{\dot{y}}_{n+1} \right)$ estimates.:

   4.1 Choose the best estimates by evaluating the covariance matrix

   For a predetermined threshold, choose $\ell \in \{A_r\}$ if $trace \left(\mathbf{R}_{\tilde{\mathbf{x}}_{\ell_{n+1}}} \right) \leq \chi$

   4.2 Final estimation:

   $$\tilde{\mathbf{x}}_{n+1} = \frac{1}{\mu_o} \sum_{\ell \in \{A_r\}} \mu_\ell \tilde{\mathbf{x}}_{\ell_{n+1}}$$

   $$\mathbf{R}_{\tilde{\mathbf{x}}_{n+1}} = \frac{1}{\mu_o} \sum_{\ell \in \{A_r\}} \mu_\ell \mathbf{R}_{\tilde{\mathbf{x}}_{\ell_{n+1}}}$$

   $$\mu_o = \sum_{\ell \in \{A_r\}} \mu_\ell$$

   where μ_ℓ are the cost functions applied in combining the estimates,

   and χ is a threshold function, set to exclude the estimates with high MSEs.

5. Project the covariance $\mathbf{P}_{n+1|n}$ and gain $\mathbf{G}_{n+1}$ for the Kalman filter:

   $$\mathbf{P}_{n+1|n} = \mathbf{F}\mathbf{P}_{n|n}\mathbf{F}^T + \mathbf{Q}_{\mathbf{v}}$$

   $$\mathbf{G}_{n+1} = \mathbf{P}_{n+1|n} \left(\mathbf{P}_{n+1|n} + \mathbf{R}_{\tilde{\mathbf{x}}_{n+1}} \right)^{-1}$$

Decentralized Tracking:

---

6. Update estimate $\widehat{\mathbf{x}}_{n+1|n+1}$ with measurement and the MSE $\mathbf{P}_{n+1|n+1}$:

$$\widehat{\mathbf{x}}_{n+1|n+1} = \widehat{\mathbf{x}}_{n+1|n} + \mathbf{G}_{n+1}\left(\widetilde{\mathbf{x}}_{n+1} - \widehat{\mathbf{x}}_{n+1|n}\right)$$

$$\mathbf{P}_{n+1|n+1} = (\mathbf{I} - \mathbf{G}_{n+1})\,\mathbf{P}_{n+1|n}$$

7. Send to all receivers $\widehat{\mathbf{x}}_{n+1|n+1}$ and $\mathbf{P}_{n+1|n+1}$.

8. go back to step 2.

6.5 Conclusions

Study of moving target tracking capabilities is offered through the use of the BCRB for the estimation of both target location and velocity in non-coherent MIMO radar systems with widely distributed antennas. It is shown that increasing the number of transmitting and receiving radars provides better tracking performances in terms of higher accuracy gains for target location and velocity estimation. The performance gain is proportional to the increase in the product of the number of transmitting and receiving radars. Wider spread of the radars results in better accuracies. The MIMO radar architecture support both centralized and decentralized tracking techniques, inherit to the system nature. Each receiver may contribute to central processing by providing either raw data or partially/fully processed data. It is demonstrated that communication requirements and processing load may be reduced at a relatively low performance cost. Based on mission needs, the system may use either modes of operation: centralized for high accuracy or decentralized resource-aware tracking.

CHAPTER 7

CONCLUSION AND FUTURE WORK

In the framework of this dissertation work, concepts of target localization in MIMO radar systems with noncoherent and coherent processing were developed. Generally speaking, MIMO radars with widely distributed transmit and receive antennas are addressed. The main results discussed in the dissertation can be summarized as follows:

- The analytical expressions of the CRLB for noncoherent and coherent processing were derived. For both noncoherent and coherent processing, an improvement in target localization accuracy, proportional to the product of the number of transmitting and receiving radars, MN, is obtained. This is referred to as *spatial advantage*.

- Location estimation based on noncoherent observations is shown to be inversely proportional to the signals averaged effective bandwidth. Dramatically higher accuracy can be obtained from processing coherent observations. In this case, the estimation error is inversely proportional to the carrier frequency. This gain, in the order of $\frac{f_c^2}{\beta^2}$, is due to the exploitation of phase information, and is referred to as *coherency advantage*.

- Formulating a convex optimization problem, it is shown that symmetric deployment of transmitting and receiving sensors around a target is optimal with respect to minimizing the location estimation error on both x and y axis.

- Closed-form solution for the best linear unbiased estimator (BLUE) of target localization is obtained for noncoherent and coherent MIMO radars. It supports the use of the GDOP metric as a tool for target localization accuracy analysis. This metric is shown to represent the spatial advantage of the system. Contour maps of

the GDOP, provide an insight of the mutual relation between a given deployment of sensors and the achievable accuracy at various target locations.

- Comparative evaluation of target localization performances for MIMO and SIMO radar systems, based on the BLUE is established. The advantage of the MIMO radar scheme over SIMO is evident when considering that the achievable accuracy for MIMO radar systems with M transmitters and N receivers is proportional to MN and an equivalent SIMO radar systems with the same number of antennas, i.e. 1 transmitter and $M + N - 1$ receivers, is proportional to $(M + N - 1)$, especially for $MN \gg (M + N)$.

- Multiple targets localization, using coherent processing, is shown to benefit from coherency advantage. The trade-off between target localization accuracy and the number of targets that can be localized is incorporated in the spatial advantage term. Increase in the number of targets exposes the system to elevated mutual interferences. This trade-off depends on the geometric footprint of both the sensors and the targets, and the relative positions of the two.

- Coherent processing advantage might be significant, for the ratio of the signal carrier frequency to the signal effective bandwidth is commonly in the order of hundreds. The reliance of coherent processing on phase synchronization initiated an analysis that will evaluate the sensitivity of coherent localization to phase synchronization errors. The bound on the target localization estimation error is shown to be a sum of two terms – the first represents the CRB with no phase mismatch, and the second captures the mismatch effect. The latter is shown to depend on the phase error variance, the number of mismatched transmitting and receiving and the system geometry. This expression provides the means to establish, for a given phase synchronization error variance, if an advantage is still achievable for coherent processing over noncoherent one. Alternatively, when system requirement

determined a specific localization accuracies, the derived expression may be used to determine the necessary phase synchronization level in the distributed system.

- Study of moving target tracking capabilities of noncoherent MIMO radar systems is performed through the use of the BCRB for the estimation of both target location and velocity. It is shown that increasing the number of transmitting and receiving radars provides alleviates tracking performances in terms of accuracy gains for both location and velocity estimates. Performance gain is proportional to the increase in the product of the number of transmitting and receiving radars. Wider spread of the radars results in better accuracies.

- MIMO radar architecture support both centralized and decentralized tracking techniques, inherit to the system nature. Each receiver may contribute to central processing by providing either raw data or partially/fully processed data. It is demonstrated that communication requirements and processing load may be reduced at a relatively low performance cost. Based on mission needs, the system may use either modes of operation: centralized for high accuracy or decentralized resource-aware tracking.

To fully gain from these systems some research and engineering challenges need to be addressed. Among theses:

- Synchronization of the transmitting and receiving radars is of significant importance to mapping performance. For non-coherent processing, time synchronization is necessary while for coherent processing phase synchronization is required as well.

- Centralized coordination of sensor transmissions and waveforms design.

- Synchronized communication among radars and with a central processing center.

- Analysis of target RCS phenomena.

Traditionally, radar stations are grid-powered elements, incorporating transmitters, receivers and fusion center on site, based on a fixed communication infrastructure. Over the years, radar applications that include mobile deployment of stations were introduced, such as anti-missiles defense radars. These systems are powered off-grid by diesel generators. Other military applications require similar deployment of mobile stations for surveillance of a given area, such as radars mounted on vehicles that have limited energy resources. This type of systems utilizes secured wireless communication. In this case, the notion of power aware design is very important.

APPENDIX A

CRLB FOR NON-COHERENT PROCESSING

In this appendix, we develop the submatrices of the FIM for the unknown parameter vector ψ_{nc}, based on the conditional pdf in (2.19). The first derivative of $p(\mathbf{r}|\psi_{nc})$ with respect to the elements of τ is:

$$
\frac{\partial [\log p(\mathbf{r}|\psi_{nc})]}{\partial \tau_{\ell k}} = \frac{1}{\sigma_w^2} \left\{ \left[r_\ell(t) - \sum_{k'=1}^{M} \alpha_{\ell k'} s_{k'}(t - \tau_{\ell k'}) \right] \cdot \alpha_{\ell k}^* \frac{\partial [s_k^*(t - \tau_{\ell k})]}{\partial \tau_{\ell k}} \right.
$$
$$
\left. + \left[r_\ell(t) - \sum_{k'=1}^{M} \alpha_{\ell k'} s_{k'}(t - \tau_{\ell k'}) \right]^* \cdot \alpha_{\ell k} \frac{\partial [s_k(t - \tau_{\ell k})]}{\partial \tau_{\ell k}} \right\} dt. \qquad \text{(A.1)}
$$

Applying the second derivative to (A.1), defines a matrix $\mathbf{S}_{nc}$ with the following elements:

$$
[\mathbf{S}_{nc}]_{ii'} = \begin{cases} Re \left\{ \alpha_{\ell k} \alpha_{\ell k'}^* \left[\int \dot{s}_k(t - \tau_{\ell k}) \dot{s}_{k'}^*(t - \tau_{\ell k'}) dt \right] \right\} & \ell = \ell' \\ 0 & \ell \neq \ell' \end{cases}, \qquad \text{(A.2)}
$$

where indexing used is

$$
i = (\ell - 1) * M + k, \quad i' = (\ell' - 1) * M + k',
$$
$$
\ell, \ell' = 1, .., N; \qquad k, k' = 1, .., M;
$$

and the notation $\dot{s}(t - \tau_{\ell k}) = \frac{\partial}{\partial \tau_{\ell k}} s_k(t - \tau_{\ell k})$.

Elements of matrix Λ_α are defined as follows:

$$
[\Lambda_\alpha]_{ii'} = [\Lambda_\alpha]_{(MN+i),(MN+i')} = \begin{cases} Re \left\{ \int s_k(t - \tau_{\ell k}) s_{k'}^*(t - \tau_{\ell k'}) dt \right\} & \ell = \ell' \\ 0 & \ell \neq \ell' \end{cases}, \qquad \text{(A.3)}
$$

and

$$[\mathbf{\Lambda}_\alpha]_{i,(MN+i')} = [\mathbf{\Lambda}_\alpha]_{(MN+i),i'} = \begin{cases} -Im\left\{\int s_k\left(t - \tau_{\ell k}\right) s_{k'}^*\left(t - \tau_{\ell k'}\right) dt\right\} & \ell = \ell' \\ 0 & \ell \neq \ell' \end{cases}.$$

$$\text{(A.4)}$$

Elements of matrix $\mathbf{V}_{nc}$ are defined as follows:

$$[\mathbf{V}_{nc}]_{ii'} = \begin{cases} Re\left\{\alpha_{\ell k}\int \dot{s}_k\left(t - \tau_{\ell k}\right) s_{k'}^*\left(t - \tau_{\ell k'}\right) dt\right\} & \ell = \ell' \\ 0 & \ell \neq \ell' \end{cases}, \qquad \text{(A.5)}$$

and

$$[\mathbf{V}_{nc}]_{i,(MN+i')} = \begin{cases} -Im\left\{\alpha_{\ell k}\int_k \dot{s}\left(t - \tau_{\ell k}\right) s_{k'}^*\left(t - \tau_{\ell k'}\right) dt\right\} & \ell = \ell' \\ 0 & \ell \neq \ell' \end{cases}. \qquad \text{(A.6)}$$

Orthogonal Waveforms

Orthogonality implies that all cross elements $\int s_k\left(t - \tau_{\ell k}\right) s_{k'}^*\left(t - \tau_{\ell' k'}\right) dt = 0$, for $\ell \neq \ell'$ and $k \neq k'$, and after some algebra, the matrices defined by (A.2)-(A.6) take the following form:

$$[\mathbf{S}_{nc}]_{ii'} = \begin{cases} 4\pi^2\beta^2\left[|\alpha_{\ell k}|^2\beta_{R_k}^2\right] & i = i' \\ 0 & i \neq i' \end{cases}$$

$$[\mathbf{\Lambda}_\alpha]_{ii'} = [\mathbf{\Lambda}_\alpha]_{(MN+i),(MN+i')} = \begin{cases} 1 & i = i' \\ 0 & i \neq i' \end{cases} \qquad \text{(A.7)}$$

$$[\mathbf{\Lambda}_\alpha]_{i,(MN+i')} = [\mathbf{\Lambda}_\alpha]_{(MN+i),i'} = 0$$

$$[\mathbf{V}_{nc}]_{ii'} = 0$$

$$[\mathbf{V}_{nc}]_{i,(MN+i')} = 0.$$

CRLB FOR COHERENT PROCESSING

In this appendix, we develop the submatrices of the FIM for the unknown parameter vector ψ_c, based on the conditional pdf in (2.34). The first derivative of $p(\mathbf{r}|\psi_c)$ with respect to the elements of τ is:

$$\frac{\partial\left[\log p(\mathbf{r}|\psi_c)\right]}{\partial\tau_{\ell k}} = \frac{1}{\sigma_w^2}\left\{\left[r_\ell(t)-\sum_{k'=1}^M \zeta \exp^{-j2\pi f_c\tau_{\ell k'}} s_{k'}(t-\tau_{\ell k'})\right]\right. \tag{B.1}$$

$$\cdot\zeta^*\frac{\partial\left[\exp^{j2\pi f_c\tau_{\ell k}} s_k^*(t-\tau_{\ell k})\right]}{\partial\tau_{\ell k}}$$

$$+\left[r_\ell(t)-\sum_{k'=1}^M \zeta \exp^{-j2\pi f_c\tau_{\ell k'}} s_{k'}(t-\tau_{\ell k'})\right]^* \tag{B.2}$$

$$\left.\cdot\zeta\frac{\partial\left[\exp^{-j2\pi f_c\tau_{\ell k}} s_k(t-\tau_{\ell k})\right]}{\partial\tau_{\ell k}}\right\}dt. \tag{B.3}$$

Applying the second derivative to (B.1) define a matrix $\mathbf{S}_{nc}$ with the following elements:

$$[\mathbf{S}_c]_{ii'} = \tag{B.4}$$

$$\begin{cases} Re\left\{|\zeta|^2\exp^{-j2\pi f_c(\tau_{\ell k}-\tau_{\ell k'})}\left[\int 4\pi^2 f_c^2 s_k(t-\tau_{\ell k}) s_{k'}^*(t-\tau_{\ell k'})\,dv\right.\right. \\ \left.+\int j2\pi f_c\left[\dot{s}_k(t-\tau_{\ell k}) s_{k'}^*(t-\tau_{\ell k'})-s_k(t-\tau_{\ell k})\dot{s}_{k'}^*(t-\tau_{\ell k'})\right]dt\right]\right\} \quad \ell=\ell' \\ \left.+\int \dot{s}_k(t-\tau_{\ell k})\dot{s}_{k'}^*(t-\tau_{\ell k'})\,dv\right]\right\} \\ \qquad\qquad\qquad 0 \qquad\qquad\qquad\qquad\qquad \ell\neq\ell' \end{cases}$$

where $\dot{s}_k(t-\tau_{\ell k}) = \frac{\partial}{\partial\tau_{\ell k}}[s_k(t-\tau_{\ell k})]$.

Elements of matrix $\mathbf{\Lambda}_{\alpha c}$ are defined as follows:

$$[\mathbf{\Lambda}_{\alpha c}]_{11} = [\mathbf{\Lambda}_{\alpha c}]_{22} = \tag{B.5}$$

$$= Re\left\{\sum_{\ell=1}^N\sum_{k=1}^M\sum_{k'=1}^M\left[\exp\left(-j2\pi f_c(\tau_{\ell k}-\tau_{\ell k'})\right)\int s_k(t-\tau_{\ell k}) s_{k'}^*(t-\tau_{\ell k'})\,dt\right]\right\},$$

and

$$[\boldsymbol{\Lambda}_{\alpha c}]_{12} = [\boldsymbol{\Lambda}_{\alpha c}]_{21} = \tag{B.6}$$

$$= -Im\left\{\sum_{\ell=1}^{N}\sum_{k=1}^{M}\sum_{k'=1}^{M}\left[\exp\left(-j2\pi f_c\left(\tau_{\ell k}-\tau_{\ell k'}\right)\right)\int s_k\left(t-\tau_{\ell k}\right)s_{k'}^*\left(t-\tau_{\ell k'}\right)dt\right]\right\}.$$

Elements of matrix $\mathbf{V}_c$ are defined as follows:

$$[\mathbf{V}_c]_{i1} = Re\left\{\sum_{k'=1}^{M}\zeta\exp^{-j2\pi f_c(\tau_{\ell k}-\tau_{\ell k'})}\right. \tag{B.7}$$

$$\cdot\left[\int \dot{s}_k\left(t-\tau_{\ell k}\right)s_{k'}^*\left(t-\tau_{\ell k'}\right)dt\right.$$

$$\left.\left.-\int j2\pi f_c s_k\left(t-\tau_{\ell k}\right)s_{k'}^*\left(t-\tau_{\ell k'}\right)dt\right]\right\}, \tag{B.8}$$

and

$$[\mathbf{V}_c]_{i2} = -Im\left\{\sum_{k'=1}^{M}\zeta\exp^{-j2\pi f_c(\tau_{\ell k}-\tau_{\ell k'})}\right. \tag{B.9}$$

$$\cdot\left[\int \dot{s}_k\left(t-\tau_{\ell k}\right)s_{k'}^*\left(t-\tau_{\ell k'}\right)dt\right.$$

$$\left.\left.-\int j2\pi f_c s_k\left(t-\tau_{\ell k}\right)s_{k'}^*\left(t-\tau_{\ell k'}\right)dt\right]\right\}. \tag{B.10}$$

Orthogonal Waveforms

Orthogonality implies that all cross elements $\int s_k \left(t - \tau_{\ell k}\right) s_{k'}^* \left(t - \tau_{\ell' k'}\right) dt = o$ for $\ell \neq \ell'$ and $k \neq k'$. Therefore, the matrices defined by (B.4)-(B.9) take the following form:

$$[\mathbf{S}_{c_{or}}]_{ii'} = \begin{cases} 4\pi^2 |\zeta|^2 f_c^2 f_{R_k} & i = i' \\ 0 & i \neq i' \end{cases}$$

$$[\mathbf{\Lambda}_{\alpha c_{or}}]_{11} = [\mathbf{\Lambda}_{\alpha_{or}}]_{22} = \begin{cases} MN & i = i' \\ 0 & i \neq i' \end{cases} \tag{B.11}$$

$$[\mathbf{\Lambda}_{\alpha c_{or}}]_{21} = [\mathbf{\Lambda}_{\alpha_{or}}]_{12} = 0$$

$$[\mathbf{V}_{c_{or}}]_{i1} = 2\pi \zeta^I f_c$$

$$[\mathbf{V}_{c_{or}}]_{i2} = -2\pi \zeta^R f_c.$$

where $f_{R_k} = \left(1 + \frac{\beta_k^2}{f_c^2}\right)$. When we invoke the narrowband assumption $\beta_k^2/f_c^2 \ll 1$ it follows that $f_{R_k} \simeq 1$.

APPENDIX C

DERIVATION OF ERROR COVARIANCE MATRIX FOR TIME OBSERVATIONS

C.1 Noncoherent Processing:

For a set of received waveforms $r_\ell(t)$, $1 \leq \ell \leq N$, in (2.10), the time delay estimates $\mu_{nc} = [\mu_{nc_{11}}, \mu_{nc_{12}}, ..., \mu_{nc_{MN}}]^T$ are determined by maximizing the following statistic:

$$\mu_{nc_{\ell k}} = \arg\max_v \left| \int_T r_\ell(t) s_k^*(t - v) \, dt \right|, \tag{C.1}$$

by redefining the time notation $t \to t - \tau_{\ell k}^c$, where $\tau_{\ell k}^c$ denotes the propagation time on the ℓk^{th} path for the nominal point (x_c, y_c). Equivalently,

$$\left[\int_T \frac{d}{dv} \left[\alpha_{\ell k} s_k(t - \widetilde{\tau}_{\ell k}) + w_\ell(t) \right] s_k^*(t - v) \, dt \right]_{v = \mu_{nc_{\ell k}}} = 0. \tag{C.2}$$

The time delay estimates are expressed in (3.3). It is not difficult to show that the following relation holds:

$$\frac{dg_{nc}(v)}{dv} \bigg|_{v = \mu_{nc_{\ell k}}} + n_{nc_{\ell k}} = 0, \tag{C.3}$$

where

$$g_{nc}(v) = \alpha_{lk} \int_T s_k(t - \widetilde{\tau}_{\ell k}) s_k^*(t - v) \, dt, \tag{C.4}$$

and

$$n_{nc_{\ell k}} = \int_T \frac{d}{dv} w_\ell(t) s_k^*(t - v) \, dt. \tag{C.5}$$

We wish to write (C.3) in the form of (3.3). With a few algebraic manipulations, including expanding $g_{nc}(v)$ in a Taylor series around $\widetilde{\tau}_{\ell k}$, and neglecting terms $o\left[(\widetilde{\tau}_{\ell k} - \mu_{nc_{\ell k}})^3 \right]$, it can be shown that

$$\widehat{\tau}_{\ell k} = \widetilde{\tau}_{\ell k} + \frac{n_{nc_{\ell k}} \alpha_{lk}}{4\pi^2 \beta_k^2 |\alpha_{lk}|^2}. \tag{C.6}$$

Comparing this with (3.3), we have for the error term

$$\epsilon_{nc_{\ell k}} \simeq \frac{n_{nc_{\ell k}} \alpha_{lk}}{4\pi^2 \beta_k^2 |\alpha_{lk}|^2}.$$ (C.7)

To find the first and second order statistics of $\epsilon_{nc_{\ell k}}$, we need the statistical characterization of $n_{\ell k}$. As previously stated, we assume the receiver noise $w_\ell(t)$ is a Gaussian random process with zero mean and autocorrelation function $\sigma_w^2 \delta(\tilde{\tau})$. Since $n_{\ell k}$ is a linear transformation of the process $w_\ell(t)$, since the mean $w_\ell(t)$ is zero, $E[n_{\ell k}] = 0$. Similarly, it can be shown that

$$E[n_{nc_{\ell k}} n_{nc_{nm}}] = \begin{cases} 0 & \forall \ell k \neq nm \\ 2\pi^2 \sigma_w^2 \beta_k^2 & \forall \ell k = nm \end{cases}.$$ (C.8)

Using these results, we finally get

$$E[\epsilon_{nc_{\ell k}} \epsilon_{nc_{nm}}] = \frac{E[n_{nc_{\ell k}} n_{nc_{nm}}]}{16\pi^4 \beta_k^4 |\alpha_{lk}|^2}$$ (C.9)

$$= \begin{cases} 0 & \forall \ell k \neq nm \\ \frac{1}{8\pi^2 \beta_k^2 (|\alpha_{lk}|^2/\sigma_w^2)} & \forall \ell k = nm \end{cases},$$

concluding that the covariance matrix of the terms $\epsilon_{nc_{\ell k}}$ is given by:

$$\mathbf{C}_{\epsilon_{nc}} = \frac{1}{8\pi^2} diag \left(\frac{1}{\beta_1^2 SNR_{11}}, \frac{1}{\beta_1^2 SNR_{12}}, ..., \frac{1}{\beta_M^2 SNR_{MN}} \right)_{MN \times MN}.$$ (C.10)

where $SNR_{\ell k} = \frac{|\alpha_{lk}|^2}{\sigma_w^2}$.

C.2 Coherent Processing

For a set of received waveforms $r_\ell(t)$, $1 \le \ell \le N$, in (2.8), the time delay estimates $\mu_c = [\mu_{c_{11}}, \mu_{c_{12}}, ..., \mu_{c_{MN}}]^T$ are determined by maximizing the following statistic:

$$\mu_{c_{\ell k}} = \arg\max_v \left| \exp(j2\pi f_c v) \int_T r_\ell(t) s_k^*(t - v)\, dt \right|. \tag{C.11}$$

by redefining the time notation $t \to t - \tau_{\ell k}^c$, where $\tau_{\ell k}^c$ denotes the propagation time on the ℓk^{th} path for the nominal point (x_c, y_c). Equivalently,

$$\left[\int_T \frac{d}{dv} \zeta \exp(j2\pi f_c v) \left[\exp(-j2\pi f_c \widetilde{\tau}_{\ell k}) s_k(t - \widetilde{\tau}_{\ell k}) + w_\ell(t) \right] s_k^*(t - v)\, dt \right]_{v = \mu_{c_{\ell k}}} = 0. \tag{C.12}$$

The time delay estimates are expressed in (3.3). It is not difficult to show that the following relation holds:

$$\left. \frac{dg_c(v)}{dv} \right|_{v = \mu_{c_{\ell k}}} + n_{c_{\ell k}} = 0, \tag{C.13}$$

where

$$g_c(v) = \zeta \int_T \exp\left[j2\pi f_c(v - \widetilde{\tau}_{\ell k}) \right] s_k(t - \widetilde{\tau}_{\ell k}) s_k^*(t - v)\, dt, \tag{C.14}$$

and

$$n_{c_{\ell k}} = \int_T \frac{d}{dv} w_\ell(t) s_k^*(t - v) \exp(j2\pi f_c v)\, dt. \tag{C.15}$$

With a few algebraic manipulations, including expanding $g_c(v)$ in a Taylor series around $\widetilde{\tau}_{\ell k}$, and neglecting terms $o\left[(\widetilde{\tau}_{\ell k} - \mu_{c_{\ell k}})^3 \right]$, it can be shown that

$$\mu_{c_{\ell k}} = \tau_{\ell k} + \frac{n_{c_{\ell k}} \zeta}{4\pi^2 f_c^2 \left(1 + \frac{\beta_k^2}{f_c^2} \right) |\zeta|^2}. \tag{C.16}$$

Comparing this with (3.3), and invoking the narrowband assumption $\beta_k^2 / f_c^2 \ll 1$, we have for the error term

$$\epsilon_{c_{\ell k}} \simeq \frac{n_{c_{\ell k}}}{4\pi^2 f_c^2 |\zeta|^2 f_{R_k}}. \tag{C.17}$$

To find the first and second order statistics of $\epsilon_{c_{\ell k}}$, we need the statistical characterization of $n_{\ell k}$. As previously stated, we assume the receiver noise $w_\ell(t)$ is a Gaussian random process with zero mean and autocorrelation function $\sigma_w^2 \delta(\tau)$. Since $n_{\ell k}$ is a linear transformation of the process $w_\ell(t)$, since the mean $w_\ell(t)$ is zero, $E\left[n_{c_{\ell k}}\right] = 0$. Similarly, it can be shown that

$$
E\left[n_{c_{\ell k}} n_{c_{nm}}\right] = \begin{cases} 0 & \forall \ell k \neq nm \\ 2\pi^2 \sigma_w^2 f_c^2 & \forall \ell k = nm \end{cases} . \tag{C.18}
$$

Using these results, we finally get

$$
E\left[\epsilon_{c_{\ell k}} \epsilon_{c_{nm}}\right] = \frac{E\left[n_{c_{\ell k}} n_{c_{nm}}\right]}{16\pi^4 |\zeta|^2 f_c^4} \tag{C.19}
$$

$$
= \begin{cases} 0 & \forall \ell k \neq nm \\ \frac{1}{8\pi^2 f_c^2 \left(|\zeta|^2 / \sigma_w^2\right)} & \forall \ell k = nm \end{cases} ,
$$

concluding that the covariance matrix of the terms $\epsilon_{c_{\ell k}}$ is given by:

$$
\mathbf{C}_{\epsilon_c} = \frac{1}{8\pi^2 f_c^2 SNR_\zeta} \mathbf{I}_{MN \times MN}. \tag{C.20}
$$

where $SNR_\zeta = \frac{|\zeta|^2}{\sigma_w^2}$.

APPENDIX D

DERIVATION OF FIM MATRIX FOR PHASE SENSATIVITY ANALYSIS

In this appendix, we develop the FIM for the unknown parameter vector ψ, based on the conditional pdf in (4.14). The submatrices that define $\mathbf{J}(\psi) = E\left\{\nabla_\psi \log p(\mathbf{r}|\psi)(\nabla_\psi \log p(\mathbf{r}|\psi))^H\right\} = -E\left[\frac{\partial^2 \log p(\mathbf{r}|\psi)}{\partial^2 \psi}\right]$ are derived hereafter.

The submatrix $\mathbf{\Gamma_x}$, $\mathbf{\Sigma}$, and $\mathbf{V}$ have the following general form:

$$
\mathbf{A} = \begin{bmatrix} \mathbf{A}^{11} & \cdots & \mathbf{A}^{1Q} \\ \vdots & \ddots & \vdots \\ \mathbf{A}^{Q1} & \cdots & \mathbf{A}^{QQ} \end{bmatrix}.
\tag{D.1}
$$

The first derivative of $p(\mathbf{r}|\psi)$ in (4.14) with respect to the elements of τ^q is:

$$
\frac{\partial[\log p(\mathbf{r}|\psi)]}{\partial \tau_{\ell k}^q} = \int \left\{ \left[r_\ell(t) - \sum_{q'=1}^{Q}\sum_{k'=1}^{M} \zeta^{q'} \rho_{\ell' k'}^{q'} s_{k'}\left(t - \tau_{\ell k'}^{q'}\right) \right] \right.
$$
$$
\cdot \frac{(\zeta^q)^*}{\sigma_w^2} \frac{\partial[\rho_{\ell k}^q s_k(t - \tau_{\ell k}^q)]^*}{\partial \tau_{\ell k}^q}
$$
$$
+ \left[r_\ell(t) - \sum_{q'=1}^{Q}\sum_{k'=1}^{M} \zeta^{q'} \rho_{\ell' k'}^{q'} s_{k'}\left(t - \tau_{\ell k'}^{q'}\right) \right]^*
$$
$$
\left. \cdot \frac{\zeta^q}{\sigma_w^2} \frac{\partial[\rho_{\ell k}^q s_k(t - \tau_{\ell k}^q)]}{\partial \tau_{\ell k}^q} dt \right\}.
\tag{D.2}
$$

The following indexing notations are used throughout:

$$
i = (q-1)j, \qquad i' = (q'-1)j',
$$
$$
j = [(\ell-1)*M + k], \quad j' = [(\ell'-1)*M + k'],
$$
$$
k, k' = 1,..,M, \qquad \ell, \ell' = 1,..,N,
$$
$$
q, q' = 1,..,Q.
\tag{D.3}
$$

Applying the second derivative to (D.2) define the matrix $\boldsymbol{\Gamma}^{qq'}$ with the following elements:

$$[\boldsymbol{\Gamma}^{qq'}]_{jj'} = \frac{1}{\eta_o}[\mathbf{J}(\psi)]_{ii'} = -\frac{1}{\eta_o}E\left[\frac{\partial^2 \log p(\mathbf{r}|\psi)}{\partial \tau_{\ell k}^q \partial \tau_{\ell' k'}^{q'}}\right]. \tag{D.4}$$

where $\eta_o = 8\pi^2\, \mathrm{SNR}\, f_c^2$ .In matrix form,

$$\boldsymbol{\Gamma}^{qq'} = \begin{cases} |\zeta^q|^2\, f_{R_k}\mathbf{I}_{MN \times MN} & q = q' \\ \frac{\zeta^q(\zeta^{q'})}{\eta_o}\,\mathrm{Re}\left\{\frac{\partial^2}{\partial\tau^2}\left[\boldsymbol{\Lambda}^q\mathbf{R}_s^{qq'}(\boldsymbol{\Lambda}^{q'})^H\right]\right\} & q \neq q' \end{cases}, \tag{D.5}$$

where we define $\boldsymbol{\Lambda}^q = \mathrm{diag}(\mathbf{e}^q)$. The notation $\mathrm{diag}(\cdot)$ is used to represent a diagonal matrix with elements of vector $(\cdot)$ on its diagonal, $\mathbf{e}^q$ is defined as $\mathbf{e}^q = [\exp(-2\pi f_c\tau_{11}^q), \exp(-2\pi f_c\tau_{12}^q), ..., \exp(-2\pi f_c\tau_{MN}^q)]^T$, and we abuse the notation and let

$$\left[\frac{\partial^2}{\partial\tau^2}\mathbf{A}\right]_{jj'} \equiv \frac{\partial}{\partial\tau_{\ell k}^q \partial\tau_{\ell' k'}^{q'}}[\mathbf{A}]_{jj'}. \tag{D.6}$$

The frequency ratio f_{R_k} is defined as $f_{R_k} = \left(1 + \frac{\beta_k^2}{f_c^2}\right)$. When we invoke the narrowband assumption $\beta_k^2/f_c^2 \ll 1$ it follows that $f_{R_k} \simeq 1$.

The elements of matrix $\mathbf{R}_s$ are defined as:

$$\left[\mathbf{R}_s^{qq'}\right]_{jj'} \equiv \begin{cases} \int s_k(t - \tau_{\ell k}^q)\, s_k^*\left(t - \tau_{\ell k}^{q'}\right)dt & \ell = \ell'; k = k' \\ 0 & \ell \neq \ell'; k \neq k' \end{cases}. \tag{D.7}$$

The second matrix $\boldsymbol{\Sigma}$ in (4.8) is defined by a set of matrices $\boldsymbol{\Sigma}^{qq'}$ with the following elements:

$$[\boldsymbol{\Sigma}^{qq'}]_{1,1} = [\boldsymbol{\Sigma}^{qq'}]_{2,2} = -\frac{1}{\eta_o}E\left[\frac{\partial^2 \log p(\mathbf{r}|\psi)}{\partial\zeta_{re}^q \partial\zeta_{re}^{q'}}\right]$$

$$[\boldsymbol{\Sigma}^{qq'}]_{1,2} = [\boldsymbol{\Sigma}^{qq'}]_{2,1} = -\frac{1}{\eta_o}E\left[\frac{\partial^2 \log p(\mathbf{r}|\psi)}{\partial\zeta_{re}^q \partial\zeta_{im}^{q'}}\right]. \tag{D.8}$$

In matrix form,

$$\mathbf{\Sigma}^{qq'} = \begin{cases} \dfrac{2}{\eta_o} M N \mathbf{I}_{2\times 2} & q = q' \\[2mm] \dfrac{1}{\eta_o} \begin{bmatrix} \mathrm{Re}\,[\vartheta] & -\mathrm{Im}\,[\vartheta] \\[2mm] -\mathrm{Im}\,[\vartheta] & \mathrm{Re}\,[\vartheta] \end{bmatrix} & q \neq q' \end{cases}, \qquad (\text{D.9})$$

where we use the notation $\vartheta = (\mathbf{e}^q)^T \mathbf{R}_s^{qq'} \left(\mathbf{e}^{q'}\right)^*$.

The third matrix $\mathbf{V}$ is defined by a set of matrices $\mathbf{V}^{qq'}$ with the following elements:

$$[\mathbf{V}^{qq'}]_{i1} = -\frac{1}{\eta_o} E \left[\frac{\partial^2 \log p\,(\mathbf{r}|\psi)}{\partial \tau_{\ell k}^q \, \partial \zeta_{re}^{q'}} \right] \qquad (\text{D.10})$$

$$[\mathbf{V}^{qq'}]_{i2} = -\frac{1}{\eta_o} E \left[\frac{\partial^2 \log p\,(\mathbf{r}|\psi)}{\partial \tau_{\ell k}^q \, \partial \zeta_{im}^{q'}} \right],$$

In matrix form,

$$\mathbf{V}^{qq'} = \begin{cases} \sqrt{\dfrac{2}{\eta_o}} \begin{bmatrix} -\zeta_{im}^q \\[2mm] \zeta_{re}^q \end{bmatrix} & q = q' \\[4mm] \dfrac{1}{\eta_o} \begin{bmatrix} \mathrm{Re}\left\{ \zeta \frac{\partial}{\partial \tau} \left[\mathbf{\Lambda}^q \mathbf{R}_s \left(\mathbf{e}^{q'}\right)^* \right] \right\} \\[2mm] -\mathrm{Im}\left\{ \zeta \frac{\partial}{\partial \tau} \left[\mathbf{\Lambda}^q \mathbf{R}_s \left(\mathbf{e}^{q'}\right)^* \right] \right\} \end{bmatrix} & q \neq q' \end{cases}. \qquad (\text{D.11})$$

APPENDIX E

DERIVATION OF FIM MATRIX FOR THE BCRB

In this appendix, we develop the elements of the matrix $\mathbf{J}_D(\kappa)$, i.e. $[\mathbf{J}_D(\kappa)]_{i,,j} = -E_{\kappa_r|\kappa_{nr}} \left\{ E_{\mathbf{r}|\kappa} \left[\frac{\partial^2 \ln(p(\mathbf{r}|\kappa))}{\partial \kappa_i \partial \kappa_j} \right] \right\}$, based on the conditional pdf in (5.9).The diagonal submatrix $\mathbf{R}_\tau$ is derived as follows:

$$[\mathbf{R}_\tau]_{i,j} = -E_{\kappa_r|\kappa_{nr}} \left\{ E_{\mathbf{r}|\kappa} \left[\frac{\partial^2 \ln(p(\mathbf{r}|\kappa))}{\partial \tau_{\ell k} \partial \tau_{\ell' k'}} \right] \right\} \tag{E.1}$$

$$= \sigma_n^2 Re \left\{ |\vartheta|^2 \left[\begin{array}{c} \frac{\partial^2}{\partial \tau_{\ell k} \partial \tau_{\ell' k'}} \int \rho(\ell k) \rho^*(\ell' k') \\ \cdot s_k(t - \tau_{\ell k}) s_{k'}^*(t - \tau_{\ell' k}') \end{array} \right] \right\},$$

and

$$\mathbf{R}_\tau = 8\pi^2 \left(f_c^2 + \beta^2 \right) snr \mathbf{I}_{Q \times Q},$$

where $snr = |\vartheta|^2 / \sigma_n^2$, and the following notation is used:

$$i = [(\ell - 1) * M + k] \quad \text{and} \quad j = [(\ell' - 1) * M + k'],$$
$$k, k' = 1, .., M, \qquad \qquad \ell, \ell' = 1, .., N, \tag{E.2}$$

The elements of the matrix Σ_ϑ are given by

$$[\Sigma_\vartheta]_{1,1} = \frac{2MN snr}{|\vartheta|^2} = [\Sigma_\vartheta]_{2,2}, \tag{E.3}$$

and

$$[\Sigma_\vartheta]_{1,2} = 0 = [\Sigma]_{2,1},$$

and the elements of the matrix Σ_Δ are given by

$$\Sigma_\Delta = 2snr \left[\begin{array}{cc} N\mathbf{I}_{M \times M} & \left(\mathbf{1}\mathbf{1}^T \right)_{M \times N} \\ \left(\mathbf{1}\mathbf{1}^T \right)_{N \times M} & M\mathbf{I}_{N \times N} \end{array} \right]_{L \times L}. \tag{E.4}$$

The off-diagonal submatrices are as follows:

$$\mathbf{F}_{\tau\vartheta_{Q\times 2}} = \frac{4\pi f_c}{\sigma_n^2} \left[\begin{array}{cc} \vartheta_{Im}\mathbf{1}_{Q\times 1} & -\vartheta_{Re}\mathbf{1}_{Q\times 1} \end{array} \right],$$

$$\mathbf{F}_{\tau\Delta_{Q\times L}} = 4\pi f_c snr \left[\begin{array}{c|c} \mathbf{I}_{M\times M} & \Pi(1) \\ \vdots & \vdots \\ \mathbf{I}_{M\times M} & \Pi(N) \end{array} \right]_{Q\times L},$$

$$\Pi(\ell) = \left[\begin{array}{ccc} \mathbf{0}_{N\times(\ell-1)} & \mathbf{1}_{N\times 1} & \mathbf{0}_{N\times(N-\ell-1)} \end{array} \right]_{N\times N}$$

(E.5)

and

$$\mathbf{F}_{\vartheta\Delta_{2\times L}} = \frac{2snr}{|\vartheta|^2} \left[\begin{array}{cc} \vartheta_{Im}N\mathbf{1}_{1\times M}^T & \vartheta_{Im}M\mathbf{1}_{1\times N}^T \\ -\vartheta_{Re}N\mathbf{1}_{1\times M}^T & -\vartheta_{Re}M\mathbf{1}_{1\times N}^T \end{array} \right].$$

(E.6)

REFERENCES

[1] A. Haimovich, R. Blum, and L. Cimini, "MIMO radar with widely separated antennas," *IEEE Signal Proc. Magazine*, January 2008.

[2] E. Fishler, A. M. Haimovich, R. S. Blum, L. Cimini, D. Chizhik, and R. Valenzuela, "MIMO radar: An idea whose time has come," *Processing of the 2004 IEEE International Conference on Radar*, pp. 71–78, April 2004.

[3] H. Godrich, A. M. Haimovich, and R. S. Blum, *Concepts and Applications of a MIMO Radar System with Widely Separated Antennas*. John Wiley, 2009.

[4] J. Li and P. Stoica, "MIMO radar with colocated antennas," *IEEE Signal Proc. Magazine*, pp. 106–114, September 2007.

[5] ——, "MIMO radar- diversity means superiority," *Proc. 14th Annu. Workshop Adaptive Sensor Array Processing*, pp. 123–127, June 2006.

[6] E. Fishler, A. Haimovich, R. Blum, L. Cimini, D. Chizhik, and R. Valenzuela, "Performance of MIMO radar systems: Advantages of angular diversity," *Proc. 38th Asilomar Conf. Signals, Syst. Comput.*, pp. 305–309, November 2004.

[7] D. W. Bliss and K. W. Forsythe, "Multiple-input multiple-output (MIMO) radar and imaging: degrees of freedom and resolution," *Proc. 37th Asilomar Conf. Signals, Syst. Comput.*, pp. 54–59, November 2003.

[8] J. Li, P. Stoica, and Y. Xie, "On probing signal design for MIMO radar," *Proc. 40th Asilomar Conf. Signals, Syst. Comput.*, pp. 31–35, November 2006.

[9] F. C. Robey, S. Coutts, D. Weikle, J. C. McHarg, and K.Cuomo, "MIMO radar theory and experimental results," *Proc. 38th Asilomar Conf. Signals, Syst. Comput.*, pp. 300–304, November 2004.

[10] J. Tabrikian, "Barankin bounds for target localization by MIMO radars," *Proc. 14th IEEE Workshop on Sensor Array and Multi-Channel Processing*, pp. 278–281, July 2006.

[11] I. Bekkerman and J. Tabrikian, "Target detection and localization using MIMO radars and sonars," *IEEE Trans. on Sig. Proc.*, vol. 54, pp. 3873–3883, October 2006.

[12] J. Li, P. Stoica, L. Xu, and W. Roberts, "On parameter identifiability of MIMO radar," *IEEE Signal Processing Lett.*, vol. 14, December 2007.

[13] L. Xu, J. Li, and d P. Stoica, "Adaptive techniques for MIMO radar," *Proc. 14th IEEE Workshop on Sensor Array and Multi-Channel Processing*, pp. 278–281, July 2006.

[14] E. Fishler, A. Haimovich, R. Blum, L. Cimini, D. Chizhik, and R. Valenzuela, "Spatial diversity in radars - models and detection performance," *IEEE Trans. on Sig. Proc.*, vol. 54, pp. 823–838, March 2006.

[15] K. Forsythe and D. Bliss, "Waveform correlation and optimization issues for MIMO radar," *Proc. 39th Asilomar Conf. Signals, Syst. Comput.*, pp. 1306–1310, November 2005.

[16] L. Xu, J. Li, P. Stoica, K. Forsythe, and D. Bliss, "Waveform optimization for MIMO radar: A cramer-rao bound based study," *Proc. 2007 IEEE Int. Conf. Acoustics, Speech, and Signal Processing*, April 2007.

[17] N. Lehmann, A. M. Haimovich, R. S. Blum, and L. Cimini, "MIMO radar application to moving target detection in homogenous clutter," *Proc. 14th IEEE Workshop on Sensor Array and Multi-Channel Processing*, July 2006.

[18] ——, "High resolution capabilities of MIMO radar," *Proc. of 40th Asilomar Conf. on Signals, Systems and Computers*, pp. II–917–920, November 2006.

[19] D. Fuhrmann and G. S. Antonio, "Transmit beamforming for MIMO radar systems using partial signal correlations," *Proc. of 38th Asilomar Conf. on Signals, Systems and Computers*, pp. 295–299, November 2004.

[20] A. Leshem, O. Naparstek, and A. Nehorai, "Information theoretic adaptive radar waveform design for multiple extended targets," *IEEE Journal of Selected Topics in Signal Processing*, vol. 1, June 2007.

[21] C. Chun-Yang and P. Vaidyanathan, "MIMO radar ambiguity properties and optimization using frequency-hopping waveforms," *IEEE Trans. on Signal Processing*, vol. 56, pp. 5926–5936, December 2008.

[22] B. J. Donnet and I. D. Longstaff, "Combining mimo radar with ofdm communications," September 2006.

[23] B. Friedlander, "Waveform design forMIMO radars," *IEEE Trans. on Aerospace and Electronic Systems*, vol. 43, pp. 1227–1238, July 2007.

[24] C. Chun-Yang and P. Vaidyanathan, "Properties of the mimo radar ambiguity function," March 2008, pp. 2309–2312.

[25] G. S. Antonio, D. Fuhrmann, and F. C. Robey, "MIMO radar ambiguity functions," *IEEE Journal of Selected Topics in Signal Processing*, vol. 1, no. 1, pp. 167–177, June 2007.

[26] S. M. Kay, *Fundamentals of Statistical Signal Processing: Estimation Theory.* New Jersey: Prentice Hall PTR, 1993.

[27] F. Gini and R. Reggiannini, "The modified cramer rao bound in vector parameter estimation," *IEEE Trans. on Communications*, vol. 46, no. 1, pp. 52–60, January 1998.

[28] H. L. V. Trees and K. L. Bell, *Bayesian Bounds for Parameter Estimation and Nonlinear Filtering.* Wiley-Interscience, 2007.

[29] M. Skolnik, *Introduction to Radar Systems.* New York: McGraw-Hill, 2001.

[30] N. Levanon, *Radar Principles.* New York: John Wiley and Sons Inc, 1988.

[31] M. A. Richards, *Fundementals of Radar Signal Processing*. New York: McGraw-Hill, 2005.

[32] P. M. Woodward, *Probability and Information Theory with Application to Radar*. Norwood, MA: Artech House, 1953.

[33] N. Levanon, *Radar Signals*. New York: John Wiley and Sons Inc, 2004.

[34] V. S. Chernyak, *Fundemental of Multisite Radar Syatems: Multistatic Radars and Multiradar systems*. OPA, 1998.

[35] H. L. V. Trees, K. L. Bell, and Y. Wang, "Bayesian cramer rao bounds for multistatic radar," January 2006.

[36] Y. Qi, H. Kobayashi, and H. Suda, "Analysis of wireless geolocation in non-line-of-sight environment," *IEEE Trans. on Wireless Communications*, vol. 5, pp. 672–681, March 2006.

[37] A. Dogandzic and A. Nehorai, "Cramer-rao bounds for estimating range, velocity, and direction with an active array," *IEEE Trans. on Sig. Proc.*, vol. 49, no. 6, June 2001.

[38] P. M. Schultheiss and E. Weinstein, "Lower bounds on the localization errors of a moving source observed by a passive array," *IEEE Trans. on Acoustics, Speech and Signal Processing*, vol. ASSP-29, no. 3, June 1981.

[39] H. B. Lee, "A novel procedure for assessing the accuracy of the hyperbolic multilateration systems," *IEEE Trans. on Aerospace and Electronic Systems*, vol. 11, no. 3, pp. 2–15, January 1975.

[40] N. Levanon, "Lowest GDOP in 2-D scenarios," *IEE Proc.-Radar, Sonar, Navig.*, vol. 147, pp. 149–155, June 2000.

[41] R. Yarlagadda, I. Ali, N. AlDhahir, and J. Hershey, "Gps gdop metric," *IEE Proc. Radar Sonar Navig.*, vol. 147, no. 5, pp. 259–264, October 2000.

[42] H. Godrich, A. M. Haimovich, and R. S. Blum, "Target localization accuracy gain in MIMO radar based system," *IEEE Trans. on Information Theory*.

[43] ——, "Cramer rao bound on target localization estimation in MIMO radar systems," *Proc. of CISS Conf.*, pp. 134–139, March 2008.

[44] ——, "Target localisation techniques and tools for MIMO radar," *IEEE Radar Conf*, pp. 1–6, March 2008.

[45] ——, "Target localisation techniques and tools for MIMO radar," *IET Radar, Sonar and Navigation*, pp. 314–327, August 2009.

[46] ——, "A comparative study of target localization in MIMO radar systems," *IEEE Intl. Waveform Diversity and Design Conf.*, pp. 123–127, March 2009.

[47] ——, "Target localization accuracy and multiple target localization: Tradeoff in MIMO radars," *Proc. of 42th Asilomar Conf. Signals, Syst. Comput.*, pp. 614–618, October 2008.

[48] H. Godrich, A. M. Haimovich, and H. V. Poor, "An analysis of phase synchronization mismatch sensitivity for coherent MIMO radar systems," *To appear in Proc. of the Third International Workshop on Computational Advances in Multi-Sensor Adaptive Processing (CAMSAP)*, December 2009.

[49] Q. He, R. S. Blum, H. Godrich, and A. M. Haimovich, "Cramer-rao bound for target velocity estimation in MIMO radar with widely separated antennas," *Proc. of 42nd Annual Conference on Information Sciences and Systems (CISS)*, pp. 123–127, March 2008.

[50] ——, "Target velocity estimation and antenna placement for mimo radar with widely separated antennas," *IEEE Journal of Selected Topics in Signal Processing*.

[51] H. Godrich, A. M. Haimovich, and R. S. Blum, "A MIMO radar system approach to target tracking," *To appear in Proc. of 43th Asilomar Conf. Signals, Syst. Comput.*, November 2009.

[52] ——, "Target tracking in MIMO radar systems: Techniques and performance analysis radar," *submitted to IEEE Radar Conf.*, May 2010.

[53] J. Minkoff, *Signal Processing Fundamentals and Applications for Communications and Sensing Systems.* Artech House, 2002.

[54] D. R. B. III, G. B. Prince, and J. A. McNeill, "Time-slotted round-trip aarrier synchronization for distributed beamforming," *IEEE Trans. on Signal Processing*, vol. 56, no. 11, pp. 5630–5643, November 2008.

[55] Y. S. Tu and G. J. Pottie, "Coherent cooperative transmission from multiple adjacent antennas to a distant stationary antenna through AWGN channels," *Proc. IEEE VTC 02*, pp. 130–134, 2002.

[56] G. Barriac, R. Mudumbai, and U. Madhow, "Distributed beamforming for information transfer in sensor networks," *Proc. of the Third International Symposium on Information Processing in Sensor Networks*, pp. 81–88, 2004.

[57] S. Berger and A. Wittneben, "Carrier phase synchronization of multiple distributed nodes in a wireless network," *8th IEEE Workshop on Signal Processing Advances for Wireless Communications (SPAWC)s*, June 2007.

[58] W. Wang, C. B. Ding, and X. D. Liangl, "Time and phase synchronisation via direct-path signal for bistatic synthetic aperture radar systems," *IET Radar, Sonar and Navigation*, vol. 2, pp. 1–11, February 2008.

[59] P. Napier, A. R. Thompson, and R. D. Ekers, "The very large array: Design and performance of a modern synthesis radio telescope," *IEEE Proc.*, vol. 71, no. 11, pp. 1295–1320, November 1983.

[60] B. D. Steinberg, "Phase synchronizing a nonrigid, distributed, transmit-receive radar antenna array," *IEEE Trans. on Aero. and Elect. Systems*, vol. AES-18, pp. 609–620, September 1982.

[61] B. D. Steinberg, W. Whistler, and D. Carlson, "Two-dimensional imaging with a radio camera," *IEEE Proc*, vol. 71, pp. 1325–1326, November 1983.

[62] B. M. Keel and T. H. Heath, "A comprehensive review of quasi-orthogonal waveforms," *Proc. of 38th Asilomar Conf. on Signals, Systems and Computers*, pp. 122–127, April 2007.

[63] S. Boyd and L. Vandenberghe, *Convex Optimization*. Cambridge Press, 2004.

[64] V. D. Blondel, S. Boyd, and H. Kimurae, *Recent Advances in Learning and Control*. Springer, 2008.

[65] H. V. Poor, *An Introduction to Signal Detection and Estimation*, 2nd ed. New York: Springer, 1994.

[66] E. Weinstein and A. Weiss, "Fundemental limitation in passive time-delay estimation-part ii: wide -band systems," *IEEE Trans. on Acoustics, Speech and Signal Proc.*, vol. ASSP-32, no. 5, pp. 1064–1078, October 1984.

[67] A. Zeira and P. M. Schultheiss, "Realizable lower bounds for time delay estimation," *IEEE Trans. on Signal Processing*, vol. 41, no. 11, November 1993.

[68] M. Hamilton and P. M. Schultheiss, "Passive ranging in mulyipath dominant environment, part i: Known multipath parameters," *IEEE. trans on Signal Proc.*, vol. 40, no. 1, January 1992.

[69] Y. Rockah and P. M. Schultheiss, "Array shape calibration using sources in unknown locations - part i: Far-field sources," *IEEE Trans. Acoust., Speech, Signal Proc.*, vol. Vol. ASSP-35, pp. 286–299, March 1987.

[70] Y. Rockah, H. Messer, and P. M. Schultheiss, "Localization performance of arrays subject to phase errors," *IEEE Trans. Acoust., Speech, Signal Proc.*, vol. ASSP-35, no. 8, pp. 286–299, March 1987.

[71] R. A. Horn and C. R. Johnson, *Matrix Analysis*. Cambridge UK: Cambridge University Press,, 1990.

[72] K. S. Miller, "On the inverse of the sum of matrices," *Mathematics Magazine*, vol. 54, no. 2, pp. 67–72, 1981.

[73] Y. Bar-Shalom, X. R. Li, and T. Kirubarajan, *Estimation with Applications to Tracking and Navigation*. NewYork, NY: John Wiley and sons, 2001.

[74] L. D. Stone, C. A. Barlow, and T. L. Corwin, *Bayesian Multiple Target Tracking*. Norwood, MA: Artech House, Inc, 1999.

[75] a. P. S. Blackman, *Modern Tracking Systems*. Norwood, MA: Artech Hounse, 1999.

[76] P. Tichavsky, C. H. Muravchik, and A. Nehorai, "Posterior cramer-rao bounds for discrete-time nonlinear filtering," *IEEE Trans. Signal Processing*, vol. 46, no. 5, pp. 1386–1396, May 1998.

[77] H. L. V. Trees, K. L. Bell, and Y. Wang, "Bayesian cramer-rao bounds for multistatic radar," *Proc. Of IEEE WDD Conf.*, May 2006.

[78] R. E. Zarnich, K. L. Bell, and H. L. V. Trees, "A unified method for measurement and tracking of contacts from an array of sensors," *IEEE Trans. Signal Processing*, vol. 49, no. 12, pp. 2950–2961, December 2001.